

2007

Exploring the binding of amine and sulfonamide ligands in Rhenium(I) Tricarbonyl and Platinum(II) complexes

Anna Maria Christoforou

Louisiana State University and Agricultural and Mechanical College

Follow this and additional works at: https://digitalcommons.lsu.edu/gradschool_dissertations



Part of the [Chemistry Commons](#)

Recommended Citation

Christoforou, Anna Maria, "Exploring the binding of amine and sulfonamide ligands in Rhenium(I) Tricarbonyl and Platinum(II) complexes" (2007). *LSU Doctoral Dissertations*. 1436.

https://digitalcommons.lsu.edu/gradschool_dissertations/1436

This Dissertation is brought to you for free and open access by the Graduate School at LSU Digital Commons. It has been accepted for inclusion in LSU Doctoral Dissertations by an authorized graduate school editor of LSU Digital Commons. For more information, please contact gradetd@lsu.edu.

**EXPLORING THE BINDING OF AMINE AND SULFONAMIDE LIGANDS IN
RHENIUM(I) TRICARBONYL AND PLATINUM(II) COMPLEXES**

A Dissertation

**Submitted to the Graduate Faculty of the
Louisiana State University and
Agricultural and Mechanical College
in partial fulfillment of the
requirements for the degree of
Doctor of Philosophy**

in

The Department of Chemistry

**by
Anna Maria Christoforou
B.S., University of Cyprus, 2001
August 2007**

DEDICATION

To my parents
Prokopis and Theodora Christoforou

ACKNOWLEDGEMENTS

I would like to thank the following:

My advisor, **Dr. Luigi G. Marzilli**, for his guidance during the last five years, for teaching me not to believe, but to research and to be patient. **Dr. Patricia A. Marzilli**, for the invaluable discussions, chemistry related and non. **Dr. Frank Fronczek** and **Dr. Dale Treleaven** for their technical help. My committee members, **Dr. Andrew Maverick**, **Dr. Jayne Garno**, **Dr. Anne Grove**, and **Dr. Philip Elzer**, for their constructive advice when needed. My “Marzilli Sisters”, **Janet Manono**, **Kristie Adams**, **Vidhi Maheswari**, and **Theshini Perera**, for their friendship, the discussions, the stress, the fights, the fun, the laughter and everything else we shared together. Our former post-doc **Dr. Maria Carlone**, and visiting researchers **Dr. Rosita Ranaldo**, and **Dr. Patrizia Siega**. Also, **Cecilia McGregor** and **Aissatou Sylla** for their friendship. Last but not least, my parents **Prokopis** and **Theodora**, my sister **Constantina** and my brother **Marios**, as well as my extended family.

TABLE OF CONTENTS

| | |
|--|-----|
| DEDICATION..... | ii |
| ACKNOWLEDGEMENTS..... | iii |
| ABSTRACT..... | vi |
| CHAPTER 1. INTRODUCTION..... | 1 |
| 1.1 <i>cis</i> -[Pt(NH ₃) ₂ Cl ₂]..... | 1 |
| 1.2 <i>fac</i> -[M(CO) ₃ (H ₂ O) ₃] ⁺ (M = Tc or Re)..... | 2 |
| 1.3 Sulfonamide Ligands..... | 3 |
| 1.4 References..... | 4 |
| CHAPTER 2. THE NEGLECTED Pt–N(SULFONAMIDO) BOND IN PLATINUM CHEMISTRY. NEW FLUOROPHORE-CONTAINING PLATINUM COMPLEXES USEFUL FOR ASSESSING PLATINUM INTERACTIONS WITH BIOMOLECULES..... | 7 |
| 2.1 Introduction..... | 7 |
| 2.2 Experimental Section..... | 10 |
| 2.3 Results..... | 14 |
| 2.4 Discussion..... | 26 |
| 2.5 Conclusions..... | 36 |
| 2.6 References..... | 37 |
| CHAPTER 3. <i>fac</i> -Re(CO) ₃ L COMPLEXES CONTAINING TRIDENTATE MONOANIONIC LIGANDS (L ⁻) WITH A SELDOM-STUDIED SULFONAMIDO GROUP AS ONE TERMINAL LIGATING GROUP..... | 40 |
| 3.1 Introduction..... | 40 |
| 3.2 Experimental Section..... | 43 |
| 3.3 Results and Discussion..... | 46 |
| 3.4 Conclusions..... | 58 |
| 3.5 References..... | 58 |
| CHAPTER 4. <i>fac</i> -[Re(CO) ₃ L] ⁺ COMPLEXES WITH N-CH ₂ -CH ₂ -X-CH ₂ -CH ₂ -N TRIDENTATE LIGANDS. SYNTHETIC, X-RAY CRYSTALLOGRAPHIC AND NMR SPECTROSCOPIC INVESTIGATIONS..... | 62 |
| 4.1 Introduction..... | 62 |
| 4.2 Experimental Section..... | 65 |
| 4.3 Results and Discussion..... | 68 |
| 4.4 Conclusions..... | 86 |
| 4.5 References..... | 87 |
| CHAPTER 5. CONCLUSIONS..... | 90 |

| | |
|--|-----|
| APPENDIX A. <i>fac</i> -[Re(CO) ₃ L] COMPLEXES CONTAINING TRIDENTATE MONOANIONIC LIGANDS (L ⁻) HAVING A TERMINAL AMIDO AND TWO AMINE LIGATING GROUPS..... | 91 |
| APPENDIX B. SUPPLEMENTARY MATERIAL FOR CHAPTER 3 | 107 |
| APPENDIX C. SUPPLEMENTARY MATERIAL FOR CHAPTER 4 | 112 |
| APPENDIX D. CRYSTALLOGRAPHIC AND SPECTROSCOPIC DATA FOR MISCELLANIOUS PLATINUM(II)-SULFONAMIDO COMPLEXES | 116 |
| APPENDIX E. PERMISSION LETTERS | 126 |
| VITA..... | 128 |

ABSTRACT

Platinum is the metal present in various classes of inorganic medicinal agents directed at important diseases such as cancer or viral infections. Several new Pt(II) complexes of polyamine ligands bearing a dansyl moiety linked by a sulfonamide group were prepared; in some cases the sulfonamide nitrogen formed a bond to Pt. The sulfonamido group donates strongly to Pt and places the dansyl group close to a vacant coordination position, allowing it to stack with bound guanine base (**G**) when **G** binds. The emission of the fluorophore decreases with decreasing distance to Pt.

Metal nuclide radiopharmaceuticals contain a metal core and an inner ligating unit, usually having chelate rings. The development of the advantageous $fac-[^{99m}\text{Tc}(\text{CO})_3(\text{H}_2\text{O})_3]^+$ precursor has opened new directions for radiolabeling. The non-radioactive $fac-[\text{Re}(\text{CO})_3(\text{H}_2\text{O})_3]^+$ analogue is useful in understanding the chemistry of agents derived from the $[^{99m}\text{Tc}(\text{CO})_3(\text{H}_2\text{O})_3]^+$ species. To achieve a net neutral coordination unit in radiopharmaceuticals with a $fac\text{-M}(\text{CO})_3^+$ core ($\text{M} = \text{Tc}, \text{Re}$), facially coordinated monoanionic tridentate ligands (L^-) are needed. Several $fac\text{-}[\text{Re}(\text{CO})_3\text{L}]$ complexes containing the sulfonamido group as one terminal ligating group were synthesized and characterized by X-ray crystallography and NMR spectroscopy. For most sulfonamido complexes studied here, the two chelate rings have different pucker chirality, as is commonly found for a broad range of metal complexes. The complexes are stable at neutral and basic pH values and thus have potential for providing a neutral label in radiopharmaceuticals. The NMR signal averaging indicates that the rotations about the N–S and S–C bonds of the sulfonamido group are rapid on the NMR time scale.

Understanding the chemical features of the prototypical complexes by using the $fac\text{-}[\text{Re}(\text{CO})_3\text{L}]$ -analogue approach and the minimal ligand was the goal of this part of this investigation. $fac\text{-}[\text{Re}(\text{CO})_3\text{L}]^+$ complexes containing prototypical NNN or NSN tridentate

ligands, such as diethylenetriamine (dien) and simple dien derivatives, were investigated by X-ray crystallographic and NMR methods. *fac*-[Re(CO)₃L]⁺ complexes with two terminal *exo*-NH groups exhibit unusually upfield *exo*-NH NMR signals, which shift downfield on addition of Cl⁻ indicating 1:1 ion pairs forms involving one Cl⁻ to two *exo*-NH's H-bonds.

CHAPTER 1. INTRODUCTION

Inorganic compounds have found extensive usage as chemotherapeutic agents.¹ Examples include the anticancer agent cisplatin (*cis*-[Pt(NH₃)₂Cl₂]), the gold-containing antiarthritic drug Auranofin, gadolinium compounds used as magnetic resonance imaging-enhancing agents and ^{99m}Tc-technetium compounds used as radiopharmaceuticals in disease diagnosis.²

1.1 *cis*-[Pt(NH₃)₂Cl₂]

Platinum anticancer compounds are probably the most studied inorganic drugs in history and that because cisplatin is the only anticancer agent known to cure a malignancy.²⁻⁴ Cisplatin is used to treat a variety of cancers, such as head, neck, lung and bladder cancer.^{3,5} Upon entrance to the cell, the cisplatin chloro ligands are displaced by water. Water is a good leaving group, and therefore an aqua cation formed by cisplatin is thought to be the reactive form *in vivo*. Within the cell, cisplatin interacts with a number of biomolecules such as peptides (glutathione), proteins and nucleic acids. Eventually though, it is well established that the final target of cisplatin is the N7 of guanine bases of DNA.^{3,5} Binding causes the DNA strand to bend by an angle of ~40-50°. Interaction of the platinated DNA with cellular proteins, particularly high mobility group domain proteins, increase the bending of the helix and possibly prevent repair by the DNA-repair proteins, thus preventing replication and eventually causing cell death.³

Platinum is present in various classes of metal-containing medicinal agents directed at important diseases such as cancer or viral infections.^{3,4,6,7} The high affinity toward the N7 of purines, particularly guanine, in nucleic acids^{4,8} is a key feature of the Pt(II) center that may be an important property endowing Pt(II) agents with these valuable types of biological activity. Platinum drugs are clearly among the most efficacious drugs active against a broad range of cancers.³ Pt drugs would find wider use except for the well-known toxicity generally attributed

to the reaction of the Pt drugs with the sulfur atoms in biological thiols and thioethers, such as cysteine and methionine residues.⁹ Thus, it is an important goal to identify features that reduce S binding while maintaining N7 binding.

1.2 *fac*-[M(CO)₃(H₂O)₃]⁺ (M = Tc or Re)

Radiopharmaceuticals compounds, containing a radionuclide, are used widely for the diagnosis or therapy of various diseases. Metalloradiopharmaceuticals contain a metal core and an inner ligating unit (usually having chelate rings). We refer to the core and inner ligating unit as a label. The important properties of the label, which influence biological behavior, are charge and overall shape. Technetium-99m (^{99m}Tc) is the radionuclide that is most widely used in diagnostic nuclear medicine.¹⁰⁻¹³ {^{99m}Tc(V)O}³⁺ has been the metal core used most predominantly. [^{99m}TcO(MAG₃)²⁻ (MAG₃ = penta-anionic form of mercaptoacetyltriglycine in which the mercapto, amide and carboxyl groups are deprotonated) is the most widely used renal radiopharmaceuticals based on the {^{99m}Tc(V)O}³⁺ core.

Radiopharmaceuticals based on the *fac*-[^{99m}Tc(CO)₃]⁺ core are gaining extensive use because the *fac*-[^{99m}Tc(CO)₃(H₂O)₃]⁺ precursor can be conveniently generated.¹⁴⁻¹⁷ Schibli et al. showed that agents with the *fac*-^{99m}Tc(I)(CO)₃⁺ core bearing a tridentate coordinated ligand are more robust and have better pharmacokinetic profiles than agents bearing bidentate ligands.¹⁸ A recent straightforward preparation of aqueous solutions of the non-radioactive *fac*-[Re(CO)₃(H₂O)₃]⁺ precursor¹⁹ has made the synthesis of *fac*-[Re(CO)₃L] analogues convenient and allows simulation of the aqueous ^{99m}Tc synthetic chemistry.^{19,20}

Commonly employed chelating ligands (e.g., diethylenetriamine (dien),²¹ cysteine- and homocysteine-based ligands^{19,20}) contain N, O, or S donor atoms in groups such as carboxyls,²² amines,²³⁻²⁹ nitrogen heterocycles,²⁴⁻²⁶ and thioethers.^{19,20,26,27} Extensively characterized *fac*-

[Re(CO)₃L] complexes of a series of symmetric and non-symmetric NNN or NSN ligands containing combinations of amine, pyrazolyl, and thioether donors are known.²⁵⁻²⁷ During the development of radiopharmaceutical renal agents, polyamino-polycarboxylic acid ligands have been investigated.^{23,30} At high pH amine group coordination is preferred, allowing for dangling carboxyl groups, which are important in high renal clearance.^{23,30} Other studies involving nitrogen, sulfur and oxygen donors have proposed that nitrogen donor ligands are better than sulfur donor ligands for the *fac*-[Re(CO)₃L] complex formation.^{31,32} The ^{99m}Tc-tagged lanthionine agents were the first small *fac*-[^{99m}Tc(CO)₃L] agents reported to have been evaluated in humans;³³ thus, additional studies directed at gaining a more comprehensive assessment of conformation are warranted.

An important approach in the development of small (~5 kDa) metal nuclide radiopharmaceuticals is the bioconjugation of a net neutral label to hormones, small peptides, etc.³⁴ For *fac*-^{99m}Tc(I)(CO)₃⁺ agents, the ligand(s) occupying the three remaining coordination sites must have one negative group close to the metal for net neutrality. A coordinated carboxylate group provides such a unit, but it does not provide a point for ligand elaboration or for bioconjugation. Consequently, there is a need to evaluate other groups within tridentate monoanionic ligands.

1.3 Sulfonamide Ligands

Even though the sulfonamide group has been used extensively as a linking group in organic chemistry, it is in general a neglected ligand donor group for metal complexes. It has been shown that sulfonamide ligands bind well to several metals³⁵⁻⁴⁰ but compared to other nitrogen-bearing ligands, reports of metal complexes of sulfonamide ligands are few. Even though, there are some reports of Pt(II) sulfonamido complexes⁴¹⁻⁴³ none of them investigated

reactions with biomolecules. In the first part of this study, we prepared Pt(II) complexes of NNN tridentate ligands which have a sulfonamide linkage to a fluorescent group.³⁹ These compounds presented us with the opportunity to investigate the effect of the fluorophore on the fluorescence and the properties of complexes with small biomolecules and to identify the effect of the sulfonamido group on the selectivity of S vs. N7 binding.³⁹ To our knowledge, the Tc(I) and Re(I) complexes of sulfonamido ligands have never been studied. As a prelude to radiopharmaceutical studies, we analyzed a series of new neutral $\text{Re}(\text{CO})_3\text{L}$ complexes containing sulfonamide ligands which bind in a tridentate fashion involving one nitrogen of a monoanionic deprotonated sulfonamido group.⁴⁴

1.4 References

1. Orvig, C.; Abram, M. J. *Chemical Reviews* **1999**, *99*, 2201-2203.
2. Roat-Malone, R. M. In *Bioinorganic Chemistry: A Short Course.*; John Wiley & Sons, Inc., 2002.
3. Lippert, B. *Cisplatin: Chemistry and Biochemistry of a Leading Anticancer Drug*; Wiley-VCH: Weinheim, 1999.
4. Wang, D.; Lippard, S. J. *Nat. Rev. Drug Discovery* **2005**, *4*, 307-320.
5. Reedijk, J. *Chem. Rev.* **1999**, *99*, 2499-2510.
6. Vzorov, A. N.; Bhattacharyya, D.; Marzilli, L. G.; Compans, R. W. *Antiviral Res.* **2005**, *65*, 57-67.
7. Farrell, N.; Bierbach, U.; PCT Int. Appl.: USA, 1999, p 20.
8. Reedijk, J. *Inorg. Chim. Acta* **1992**, *200*, 873-881.
9. Djuran, M. I.; Lempers, E. L. M.; Reedijk, J. *Inorg. Chem.* **1991**, *30*, 2648-2652.
10. Schwochau, K. *Angew. Chem., Int. Ed. Engl.* **1994**, *33*, 2258-2267.
11. Schibli, R.; Schubiger, P. A. *Eur. J. Nucl. Med. Mol. Imaging* **2002**, *29*, 1529-1542.
12. Jurisson, S. S.; Lydon, J. D. *Chem. Rev.* **1999**, *99*, 2205-2218.

13. Bandoli, G.; Tisato, F.; Dolmella, A.; Agostini, S. *Coord. Chem. Rev.* **2006**, *250*, 561-573.
14. Alberto, R.; Schibli, R.; Egli, A.; Schubiger, P. A.; Abram, U.; Kaden, T. A. *J. Am. Chem. Soc.* **1998**, *120*, 7987-7988.
15. Alberto, R.; Schibli, R.; Waibel, R.; Abram, U.; Schubiger, A. P. *Coord. Chem. Rev.* **1999**, *192*, 901-919.
16. Alberto, R.; Schibli, R.; Schubiger, A. P.; Abram, U.; Pietzsch, H. J.; Johannsen, B. *J. Am. Chem. Soc.* **1999**, *121*, 6076-6077.
17. Schibli, R.; Alberto, R.; Abram, U.; Abram, S.; Egli, A.; Schubiger, P. A.; Kaden, T. A. *Inorg. Chem.* **1998**, *37*, 3509-3516.
18. Schibli, R.; La Bella, R.; Alberto, R.; Garcia-Garayoa, E.; Ortner, K.; Abram, U.; Schubiger, P. A. *Bioconjugate Chem.* **2000**, *11*, 345-351.
19. He, H.; Lipowska, M.; Xu, X.; Taylor, A. T.; Carlone, M.; Marzilli, L. G. *Inorg. Chem.* **2005**, *44*, 5437-5446.
20. He, H.; Lipowska, M.; Xu, X.; Taylor, A. T.; Marzilli, L. G. *Inorg. Chem.* **2007**, *46*, 3385-3394.
21. Mundwiler, S.; Candreia, L.; Hafliger, P.; Ortner, K.; Alberto, R. *Bioconjugate Chem.* **2004**, *15*, 195-202.
22. Lipowska, M.; Hansen, L.; Marzilli, L. G.; Taylor, A. *J. Nucl. Med.* **2001**, *42*, 259P-259P.
23. Lipowska, M.; Cini, R.; Tamasi, G.; Xu, X. L.; Taylor, A. T.; Marzilli, L. G. *Inorg. Chem.* **2004**, *43*, 7774-7783.
24. Wei, L.; Babich, J. W.; Ouellette, W.; Zubieta, J. *Inorg. Chem.* **2006**, *45*, 3057-3066.
25. Alves, S.; Paulo, A.; Correia, J. D. G.; Gano, L.; Smith, C. J.; Hoffman, T. J.; Santos, I. *Bioconjugate Chem.* **2005**, *16*, 438-449.
26. Alves, S.; Paulo, A.; Correia, J. D. G.; Domingos, A.; Santos, I. *J. Chem. Soc., Dalton Trans.* **2002**, 4714-4719.
27. Vitor, R. F.; Alves, S.; Correia, J. D. G.; Paulo, A.; Santos, I. *J. Organomet. Chem.* **2004**, *689*, 4764-4774.
28. Moura, C.; Fernandes, C.; Gano, L.; Paulo, A.; Santos, I. In *Technetium, Rhenium, and Other Metals in Chemistry and Nuclear Medicine*; Mazzi, U., Ed.: Padova, 2006; Vol. 7, pp 101-102.

29. Fernandes, C.; Gano, L.; Bourkoula, A.; Pirmettis, I.; Santos, I. In *Technetium, Rhenium, and Other Metals in Chemistry and Nuclear Medicine*; Mazzi, U., Ed.: Padova, 2006; Vol. 7, pp 487-490.
30. Lipowska, M.; He, H.; Xu, X.; Taylor, A. T.; Marzilli, P. A.; Marzilli, L. G. **in preparation**.
31. Lazarova, N.; Babich, J. W.; Valliant, J.; Schaffer, P.; James, S.; Zubieta, J. *Inorg. Chem.* **2005**, *44*, 6763-6770.
32. Banerjee, S. R.; Levadala, M. K.; Lazarova, N.; Wei, L.; Valliant, J. F.; Stephenson, K. A.; Babich, J. W.; Maresca, K. P.; Zubieta, J. *Inorg. Chem.* **2002**, *41*, 6417-6425.
33. Lipowska, M.; He, H. Y.; Malveaux, E.; Xu, X. L.; Marzilli, L. G.; Taylor, A. *J. Nucl. Med.* **2006**, *47*, 1032-1040.
34. Taylor, A.; Eshima, D.; Fritzberg, A. R.; Christian, P. E. *J. Nucl. Med.* **1986**, *27*, 795-803.
35. Goodwin, J. M.; Olmstead, M. M.; Patten, T. E. *J. Am. Chem. Soc.* **2004**, *126*, 14352-14353.
36. Prodi, L.; Montalti, M.; Zaccheroni, N.; Dallavalle, F.; Folesani, G.; Lanfranchi, M.; Corradini, R.; Pagliari, S.; Marchelli, R. *Helv. Chim. Acta* **2001**, *84*, 690-706.
37. Congreve, A.; Katakya, R.; Knell, M.; Parker, D.; Puschmann, H.; Senanayake, K.; Wylie, L. *New J. Chem.* **2003**, *27*, 98-106.
38. Evans, C.; Henderson, W.; Nicholson, B. K. *Inorg. Chim. Acta* **2001**, *314*, 42-48.
39. Christoforou, A. M.; Marzilli, P. A.; Marzilli, L. G. *Inorg. Chem.* **2006**, *45*, 6771-6781.
40. Carvalho, M. F. N. N.; Consiglieri, A. C.; Duarte, M. T.; Galvao, A. M.; Pombeiro, A. J. L.; Herrmann, R. *Inorg. Chem.* **1993**, *32*, 5160-5164.
41. Becker, J. J.; White, P. S.; Gagne, M. R. *Inorg. Chem.* **1999**, *38*, 798-801.
42. Evans, C.; Henderson, W.; Nicholson, B. K. *Inorg. Chim. Acta* **2001**, *314*, 42-48.
43. Tudor, M. D.; Becker, J. J.; White, P. S.; Gagne, M. R. *Organometallics* **2000**, *19*, 4376-4384.
44. Christoforou, A. M.; Fronczek, F. R.; Marzilli, P. A.; Marzilli, L. G. *Inorg. Chem.* **2007**, *in press*.

CHAPTER 2. THE NEGLECTED Pt–N(SULFONAMIDO) BOND IN PLATINUM CHEMISTRY. NEW FLUOROPHORE-CONTAINING PLATINUM COMPLEXES USEFUL FOR ASSESSING PLATINUM INTERACTIONS WITH BIOMOLECULES*

2.1 Introduction

Platinum is the metal present in various classes of inorganic medicinal agents directed at important diseases such as cancer or viral infections.¹⁻⁴ An important feature of the Pt(II) center that may be a key property endowing Pt(II) agents with these important types of activity is the high affinity toward the N7 of purines, particularly guanine, in nucleic acids.^{2,5} Platinum drugs are perhaps the best single type of anticancer drug active against a broad range of cancers.¹ Pt drugs would find wider use except for the well-known toxicity resulting from the reaction of the drugs with biological thiols and thioethers.⁶ Thus, it is highly desirable to identify features that reduce S binding while maintaining N7 binding.

Reactions of the monofunctional complex, [Pt(dien)Cl]Cl (dien = diethylenetriamine), with nucleotides have been studied extensively as an aid in assessing the nature of DNA binding of difunctional Pt(II) anticancer drugs (e.g., cisplatin).^{2,7} A study of the reaction rates of [Pt(dien)Cl]Cl with 5'-GMP (5'-GMP = 5'-guanosine monophosphate) and peptides [glutathione (GSH) and S-methylglutathione (GSMe) as models for cysteine and L-methionine (met) binding sites, respectively] showed that the Pt–sulfur bond is formed much more rapidly than the Pt–N7 bond.⁶ Several other studies, including competitive reactions of [Pt(dien)Cl]Cl with met and 5'-GMP (revealing that the kinetic product was Pt(dien)(met) and that the thermodynamic product was Pt(dien)(5'-GMP)), all indicate the same trend.⁸⁻¹⁰

* Reproduced with permission from American Chemical Society: Christoforou, A. M., Marzilli, P. A., Marzilli, L. G., "The Neglected Pt–N(sulfonamido) Bond in Pt Chemistry. New Fluorophore-Containing Pt(II) Complexes Useful for Assessing Pt(II) Interactions with Biomolecules," *Inorganic Chemistry*, **2006**, 45, 6771-6781. Copyright 2006 American Chemical Society.

Many Pt(II) complexes with ligands having the dien backbone have been synthesized and studied, e.g., *N,N',N''*-trimethyldiethylenetriamine (*N*-Me₃dien), *N,N,N',N'',N''*-pentamethyldiethylenetriamine (*N*-Me₅dien), and *N,N,N',N''*-tetramethyldiethylenetriamine (*N*-Me₄dien).¹¹⁻¹³ Preferential binding of [Pt(*N*-Me₄dien)Cl]Cl to the sulfur of glutathione and the absence of binding to an imidazole nitrogen of histidine was attributed to steric effects.¹³

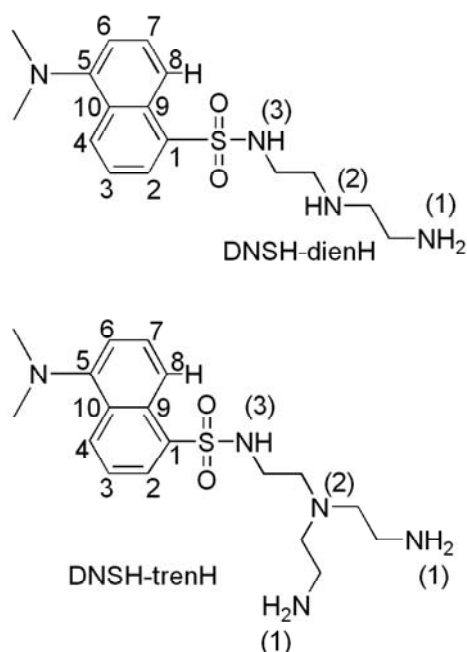


Figure 2.1. Fluorescent ligands used in this study.

In this study, we explore the chemistry of complexes with tridentate ligands bearing a sulfonamide and an aromatic fluorescent group. The ligands (Figure 2.1) used in this study are *N*-(2-((2-aminoethyl)amino)ethyl)-5-(dimethylamino)naphthalene-1-sulfonamide (DNSH-dienH, where DNSH = 5-(dimethylamino)naphthalene-1-sulfonamide) and *N*-(2-(bis(2-aminoethyl)amino)ethyl)-5-(dimethylamino)naphthalene-1-sulfonamide (DNSH-tren, where tren = tris(2-aminoethyl)amine). (The H indicates protons displaceable upon Pt binding, i.e., the

sulfonamide NH for the dienH moiety and the H8 for the DNSH moiety). The DNSH-dienH ligand afforded the $\text{Pt}(\text{DNSH-dienH})\text{Cl}_2$, $\text{Pt}(\text{DNSH-dien})\text{X}$ ($\text{X} = \text{Cl}, \text{Br}$), and $\text{Pt}(\text{DNS-dien})$ complexes, whereas DNSH-tren gave $[\text{Pt}(\text{DNSH-tren})\text{Cl}]\text{Cl}$ (Figure 2.2). These compounds presented us with the opportunity to investigate the effect of the fluorophore and the properties of complexes with small biomolecules such as 9-substituted derivatives of guanine (**G**) or of hypoxanthine (3'-inosine monophosphate, 3'-IMP).

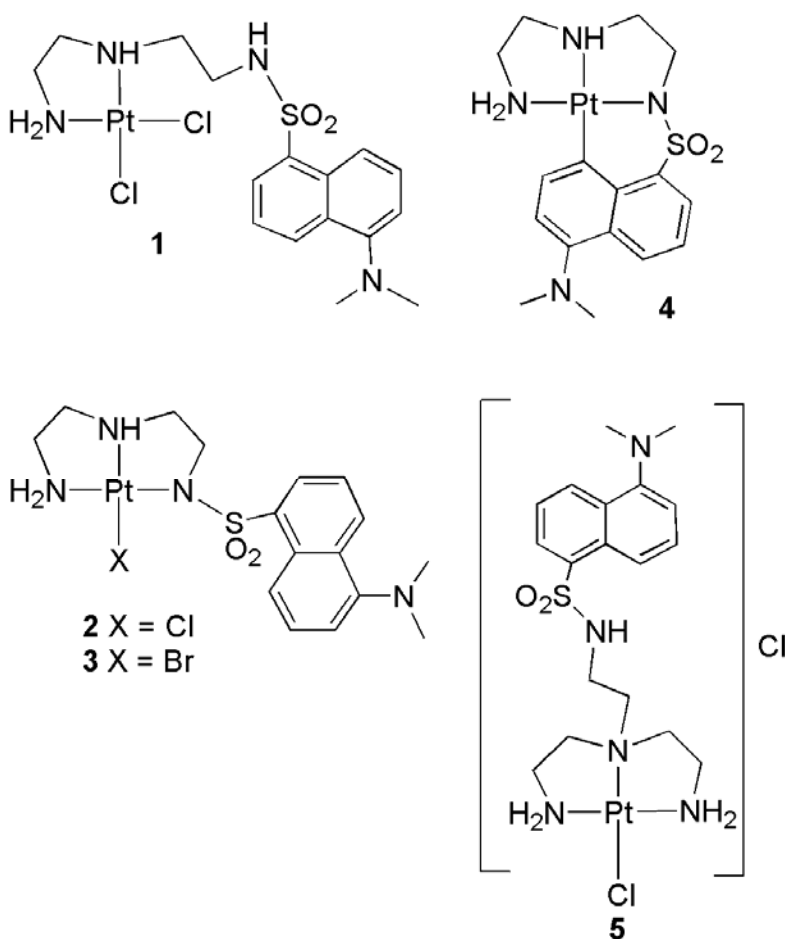


Figure 2.2. Pt(II) complexes synthesized in this study: $\text{Pt}(\text{DNSH-dienH})\text{Cl}_2$ (**1**), $\text{Pt}(\text{DNSH-dien})\text{Cl}$ (**2**), $\text{Pt}(\text{DNSH-dien})\text{Br}$ (**3**), $\text{Pt}(\text{DNS-dien})$ (**4**), and $[\text{Pt}(\text{DNSH-tren})\text{Cl}]\text{Cl}$ (**5**).

2.2 Experimental Section

2.2.1 Starting Materials

Tren from Strem, *N'*-Me-dien (*N'*-Me-dien = *N*-methyl-2,2'-diaminodiethylamine) from TCI America, Pt(en)Cl₂, *N*-Et-en = *N*-ethylethylenediamine and dien from Aldrich, and the following materials from Sigma: dansyl chloride (DNSH-Cl), 9-ethylguanine (9-EtG), and the sodium salts of 3'-guanosine monophosphate (3'-GMP), 5'-GMP, 5'-guanosine diphosphate (5'-GDP), 5'-guanosine triphosphate (5'-GTP), 3'-IMP, and met were all used as received. The DNSH-dienH and DNSH-tren ligands were prepared by known methods,^{14,15} and their ¹H NMR chemical shifts matched the reported values. *Cis*-Pt(Me₂SO)₂Cl₂,¹⁶ *cis*-Pt(Me₂SO)₂Br₂,¹⁷ [Pt(dien)Cl]Cl,¹⁸ Pt(*N*-Et-en)Cl₂,¹⁹ and [Pt(*N'*-Me-dien)Cl]Cl²⁰ were prepared as described in the literature.

2.2.2 Physical Measurements

2.2.2.1 NMR Spectroscopy. ¹H, ¹³C, and ¹⁹⁵Pt NMR spectra were recorded on either a 400 MHz or a 500 MHz Bruker NMR spectrometer using DMSO-*d*₆, except for ¹H NMR studies of adduct formation performed in D₂O/DMSO-*d*₆ solutions. Typical concentrations were 10 mM for ¹H and ¹³C NMR and 50 mM for ¹⁹⁵Pt NMR measurements. Peak positions are relative to TMS (for ¹H and ¹³C in DMSO-*d*₆) or the residual water signal (for ¹H in D₂O/DMSO-*d*₆). All NMR data were processed using XWINNMR and Mestre-C software. ¹H-¹H COSY and ROESY as well as ¹H-¹³C HSQC and HMBC NMR spectra were recorded in order to assign the signals of the products. 512 × 2048 matrices were collected for the ¹H-¹³C HSQC and HMBC experiments. Typically, 256 scans were collected per block, and an exponential apodization function with a line broadening of 0.2 Hz was used. The typical *J*_{H-C} in HMBC experiments was 8 Hz unless otherwise stated. The COSY experiments were performed at 25 °C with 16 scans per *t*₁

increment. The evolution dimension was zero-filled to 2K prior to Fourier transformation. 2D ROESY experiments were performed at 25 °C by using mixing times of 300 ms (64 scans per t_1 increment). For ^{195}Pt NMR spectra a pulse width of 20 μs , corresponding to a 30° tip angle, was used with a relaxation delay of 0.4 s. Usually, several acquisitions were recorded using a spectral window of 75,000 Hz, with 16K data points. Typically 10,000 scans were averaged for each acquisition, and the resulting FID was multiplied by an exponential function (LB = 50 Hz) prior to Fourier transformation. All ^{195}Pt NMR chemical shifts were determined in DMSO- d_6 solutions by using *cis*-Pt(Me₂SO)₂Cl₂ (-3450 ppm) as an external reference, compared to a Na₂PtCl₆ standard.²¹ Because the shift effect of the deprotonated sulfonamide of Pt(DNSH-dien)Cl was not as large as expected from the literature on the shift effect of deprotonated peptides,²² we examined a particularly wide spectral region from -1300 to -9400 ppm to ensure that the signal reported below was from this complex.

2.2.2.2 Fluorescence Spectroscopy. Spectra of Pt(II) complexes and 5'-GMP adducts (5 μM solution in H₂O/DMSO- d_6 , v/v 5/1, pH = 5.5) were recorded in a 10 mm quartz fluorescence cuvette, at room temperature, in triplicate by using a Spex Fluorolog-3 spectrofluorimeter equipped with a 450 W xenon lamp and a photomultiplier tube detector; all the spectra were blank subtracted. Emission spectra were recorded at the excitation wavelength, 360 nm.

2.2.3 Synthesis of Pt(II) Complexes

2.2.3.1 Synthesis of Pt(DNSH-dienH)Cl₂ (1). A suspension of *cis*-Pt(Me₂SO)₂Cl₂ (150 mg, 0.355 mmol) in methanol (20 mL) was treated with DNSH-dienH (119 mg, 0.355 mmol), and the reaction mixture was stirred at room temperature for 24 h. Acetonitrile (60 mL) was added slowly to the solution and the yellow solid that precipitated was collected on a filter, washed with water and diethyl ether, and dried under vacuum; yield, 87 mg (41%). ^1H NMR

spectrum (DMSO- d_6) (ppm): 8.48 (d, 1H), 8.27 (d, 1H), 8.22 (t, 1H, NH), 8.13 (d, 1H), 7.61 (m, 2H), 7.25 (d, 1H), 6.98 (s, 1H, NH), 6.15 (s, 2H, NH), 3.42 (s, 2H, CH₂), 3.38 (m, 2H, CH₂), 3.15 (m, 4H, CH₂), 2.83 (s, 6H, CH₃). Anal. Calcd for C₁₆H₂₄Cl₂N₄O₂PtS•1.5H₂O•CH₃OH: C, 30.87; H, 4.72; N, 8.47. Found: C, 31.09; H, 4.57; N, 8.02.

2.2.3.2 Synthesis of Pt(DNSH-dien)Cl (2). The Pt(DNSH-dien)Cl complex was synthesized as above for complex **1**, but with triethylamine (40 μ L, 0.293 mmol) added to the methanol suspension of *cis*-Pt(Me₂SO)₂Cl₂ immediately after addition of DNSH-dienH. The yellow solid that precipitated from the reaction mixture after 24 h of stirring was collected on a filter, washed with diethyl ether, and dried under vacuum; yield, 90 mg (45%). ¹H NMR spectrum (DMSO- d_6) (ppm): 8.60 (d, 1H), 8.39 (d, 1H), 8.27 (d, 1H), 7.47 (m, 2H), 7.15 (d, 1H), 6.61 (s, 1H, NH), 5.29 (s, 1H, NH), 5.11 (s, 1H, NH), 3.18 (m, 2H, CH₂), 2.94 (m, 4H, CH₂), 2.82 (s, 6H, CH₃), 2.65 (m, 2H, CH₂). Anal. Calcd for C₁₆H₂₃ClN₄O₂PtS•0.5CH₃OH: C, 34.08; H, 4.31; N, 9.59. Found: C, 34.47; H, 4.52; N, 9.81.

2.2.3.3 Synthesis of Pt(DNSH-dien)Br (3). A suspension of *cis*-Pt(Me₂SO)₂Br₂ (178 mg, 0.355 mmol) in methanol (20 mL) was treated with DNSH-dienH (119 mg, 0.355 mmol) and triethylamine (40 μ L, 0.293 mmol), and the reaction mixture was stirred at room temperature for 18 h. The pale yellow solid that precipitated was collected on a filter, washed with diethyl ether, and dried under vacuum; yield, 91 mg (42%). ¹H NMR spectrum (DMSO- d_6) (ppm): 8.62 (d, 1H), 8.38 (d, 1H), 8.27 (d, 1H), 7.49 (t, 1H), 7.44 (t, 1H), 7.17 (d, 1H), 6.64 (s, 1H, NH), 5.32 (s, 1H, NH), 5.14 (s, 1H, NH), 3.29 (d, 2H, CH₂), 3.05 (m, 4H, CH₂), 2.81 (s, 6H, CH₃), 2.65 (m, 2H, CH₂). Anal. Calcd for C₁₆H₂₃BrN₄O₂PtS•H₂O: C, 30.58; H, 4.01; N, 8.92. Found: C, 30.64; H, 3.81; N, 8.79.

2.2.3.4 Synthesis of Pt(DNS-dien) (4). Pt(DNS-dien) was synthesized as described for complex **2**, but with a 10-fold excess of triethylamine added (500 μL , 3.66 mmol). Yield of yellow solid, 136 mg (72%). ^1H NMR spectrum (DMSO- d_6) (ppm): 8.27 (d, 1H), 7.98 (d, 1H), 7.36 (t, 1H), 7.22 (d, 1H), 6.81 (d, 1H), 5.72 (s, 1H, NH), 5.53 (s, 1H, NH), 5.42 (s, 1H, NH), 3.64 (m, 2H, CH₂), 3.16 (m, 2H CH₂), 2.84 (m, 2H, CH₂), 2.71 (s, 6H, CH₃), 2.64 (m, 2H, CH₂). Anal. Calcd for C₁₆H₂₂N₄O₂PtS•0.5CH₃OH: C, 36.41; H, 4.43; N, 10.25. Found: C, 36.41; H, 4.07; N 10.11.

2.2.3.5 Synthesis of [Pt(DNSH-tren)Cl]Cl (5). A suspension of *cis*-Pt(Me₂SO)₂Cl₂ (200 mg, 0.474 mmol) in methanol (20 mL) was treated with DNSH-tren (180 mg, 0.474 mmol), and the reaction mixture was heated at reflux for 1 h. The pale yellow solid that precipitated after reducing the volume to 5 mL was collected on a filter, washed with water and diethyl ether, and dried in vacuo; yield, 105 mg (35%). ^1H NMR spectrum (DMSO- d_6) (ppm): 8.48 (d, 1H), 8.24 (t, 1H, NH), 8.23 (d, 1H), 8.13 (d, 1H), 7.65 (m, 1H), 7.26 (d, 1H), 5.66 (s, 1H, NH), 5.37 (s, 2H, NH), 3.46 (t, 2H, CH₂), 3.07 (m, 2H, CH₂), 2.76 (m, 4H, CH₂), 2.82 (s, 6H, CH₃). Anal. Calcd for C₁₈H₂₉Cl₂N₅O₂PtS•2H₂O: C, 31.72; H, 4.88; N, 10.28. Found: C, 31.74; H, 4.74; N, 9.99.

2.2.4 Formation of Biological Adducts

Solutions to study formation of adducts (5 mM in Pt) utilized D₂O/DMSO- d_6 (500 μL /100 μL) solutions. DMSO- d_6 was used to improve solubility; however solutions of both Pt(DNSH-dien)Cl and [Pt(DNSH-tren)Cl]Cl with a higher percentage of water were readily prepared (e.g. 5 mM in 95% H₂O and 0.1 mM in 99.9% H₂O).

2.2.4.1 G/3'-IMP Reactions. Solutions of adducts (5 mM) were prepared by treatment of Pt(DNSH-dien)Cl or [Pt(DNSH-tren)Cl]Cl in D₂O/DMSO- d_6 (500 μL /100 μL) with a stoichiometric amount of a guanine (**G**) or hypoxanthine derivative (3'-IMP) at pH ~ 5 (pH was

uncorrected). Reactions were monitored by ^1H NMR spectroscopy until the disappearance of free **G/3'**-IMP was indicated or until a constant intensity ratio between free and complexed **G/3'**-IMP was attained. When necessary, DNO_3 and NaOD solutions (0.01 M in D_2O) were used for adjusting the pH of each sample directly in the NMR tubes. 1D and 2D NMR studies were performed at 25 °C. Methanol- d_4 was added to the samples for low-temperature experiments.

2.2.4.2 Methionine Reactions. We chose conditions, such as pH, and ratios to mimic those reported previously for the parent compound, $[\text{Pt}(\text{dien})\text{Cl}]\text{Cl}$.⁸ **Challenge Reactions.** Solutions of $\text{Pt}(\text{DNSH-dien})\text{Cl}$ or $[\text{Pt}(\text{DNSH-tren})\text{Cl}]\text{Cl}$ in $\text{D}_2\text{O}/\text{DMSO-}d_6$ (500 $\mu\text{L}/100$ μL) were treated with a stoichiometric amount of methionine at pH ~ 6.4 . Reactions were monitored by ^1H NMR spectroscopy until the disappearance of free met was indicated or until a constant ratio between free and complexed met was attained. Then 1 eq. of 5'-GMP (final ratio of Pt:met:5'-GMP = 1:1:3) was added. The complementary challenge reaction, addition of 1 eq of met to a solution of the $\text{Pt}(\text{DNSH-dien})(5'\text{-GMP})$ adduct, was also investigated (final ratio of Pt:met:5'-GMP = 1:1:3). **Competition Reactions.** Solutions of $\text{Pt}(\text{DNSH-dien})\text{Cl}$ and $[\text{Pt}(\text{DNSH-tren})\text{Cl}]\text{Cl}$ in $\text{D}_2\text{O}/\text{DMSO-}d_6$ (500 $\mu\text{L}/100$ μL) were treated with met and 5'-GMP at pH ~ 6.4 (Pt:met:5'-GMP = 1:1:3) and the reactions monitored by ^1H NMR spectroscopy.

2.3 Results

2.3.1 NMR Characterization of Pt(II) Complexes

2.3.1.1 Pt(DNSH-dienH)Cl₂ (1). Reaction of *cis*- $\text{Pt}(\text{Me}_2\text{SO})_2\text{Cl}_2$ with DNSH-dienH with no added base affords $\text{Pt}(\text{DNSH-dienH})\text{Cl}_2$ (**1**) (Figure 2.2). Immediately upon dissolution of **1** in $\text{DMSO-}d_6$, one major and one minor set of NH signals were observed. The minor set, which disappeared after ~ 5 min but reappeared on addition of $[\text{Et}_4\text{N}]\text{Cl}$ (not shown), was assigned to **1**, and the major set was assigned to the solvolysis product, $[\text{Pt}(\text{DNSH-dienH})(\text{Me}_2\text{SO-}d_6)\text{Cl}]^+$ (**1-**

sol), on the basis of its ^{195}Pt NMR chemical shift (-3318 ppm), which was very similar to that of $[\text{Pt}(\text{en})(\text{Me}_2\text{SO}-d_6)\text{Cl}]^+$ (-3307 ppm).²³ NMR data are summarized in Table 2.1. The ^1H NMR aromatic signals of $[\text{Pt}(\text{DNSH-dienH})(\text{Me}_2\text{SO}-d_6)\text{Cl}]^+$ in $\text{DMSO}-d_6$ (Figure 2.3) compared to those of DNSH-dienH are not significantly affected by Pt binding to the DNSH-dienH ligand. The ^1H NMR NH signals of DNSH-dienH cannot be observed in $\text{DMSO}-d_6$ unless DNO_3 is added. We attribute this result to fast NH exchange. However, once the ligand binds to Pt(II) through N1 and N2 (for numbering, refer to Figure 2.1), the NH signals appear. We attribute this result to slower NH exchange for the coordinated ligand.

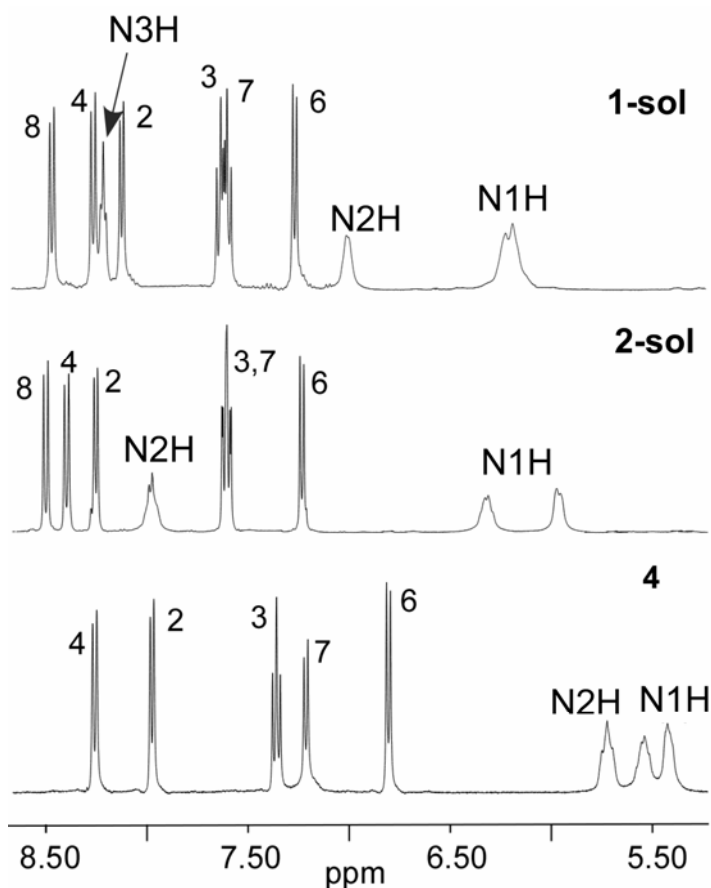


Figure 2.3. Aromatic ^1H NMR signals of the Pt(II) complexes formed by DNSH-dienH ligand; in $\text{DMSO}-d_6$, $[\text{Pt}(\text{DNSH-dienH})(\text{Me}_2\text{SO}-d_6)\text{Cl}]^+$ (**1-sol**), $[\text{Pt}(\text{DNSH-dien})(\text{Me}_2\text{SO}-d_6)]^+$ (**2-sol**), $\text{Pt}(\text{DNS-dien})$ (**4**).

Table 2.1. ^1H NMR and ^{195}Pt NMR Shifts (ppm) for Selected Ligands and Complexes^a

| ligands ^b | | | Pt(II) complex ^c | | | | | | | | | |
|-----------------------|-----------|------|-----------------------------|-------|-------|------|-------|-------|-------|-------|-------|------|
| DNSH-dienH | DNSH-tren | 1 | 1-sol | 2 | 2-sol | 3 | 4 | 5 | 5-sol | 6 | 6-sol | |
| ^{195}Pt NMR | | | | | | | | | | | | |
| | | | -3318 | -2499 | -3222 | | -3235 | -2634 | -3364 | -2721 | -3465 | |
| ^1H NMR | | | | | | | | | | | | |
| NMe ₂ | 2.83 | 2.82 | 2.83 | 2.83 | 2.82 | 2.82 | 2.81 | 2.71 | 2.82 | 2.82 | | |
| N1H | | | 5.23 | 6.15 | 5.11 | 5.97 | 5.14 | 5.42 | 5.37 | 6.31 | 5.43 | 6.55 |
| | | | 5.34 | | 5.29 | 6.34 | 5.32 | 5.53 | 5.66 | 5.95 | 5.51 | 6.66 |
| N2H | | | 6.27 | 6.98 | 6.61 | 7.89 | 6.64 | 5.72 | | | 7.34 | 8.39 |
| N3H | | | 8.05 | 8.22 | | | | | 8.24 | 8.26 | | |
| H2 | 8.11 | 8.11 | 8.13 | 8.13 | 8.27 | 8.25 | 8.27 | 7.98 | 8.13 | 8.13 | | |
| H3 | 7.59 | 7.59 | 7.61 | 7.61 | 7.47 | 7.61 | 7.44 | 7.22 | 7.65 | 7.65 | | |
| H4 | 8.29 | 8.30 | 8.27 | 8.27 | 8.39 | 8.40 | 8.38 | 8.27 | 8.23 | 8.23 | | |
| H6 | 7.25 | 7.25 | 7.25 | 7.25 | 7.15 | 7.24 | 7.17 | 6.81 | 7.26 | 7.26 | | |
| H7 | 7.61 | 7.61 | 7.61 | 7.61 | 7.47 | 7.61 | 7.49 | 7.36 | 7.65 | 7.65 | | |
| H8 | 8.46 | 8.45 | 8.48 | 8.48 | 8.60 | 8.50 | 8.62 | | 8.48 | 8.48 | | |

^a10 mM, DMSO-*d*₆, 25 °C. ^bChemical shifts of NH signals of protonated ligands, DNSH-dienH: 7.98 (N1H), 8.74 (N2H), 8.30 (N3H) and DNSH-tren: 8.01 (N1H), 8.37 (N3H). ^cPt(DNSH-dienH)Cl₂ (**1**), [Pt(DNSH-dienH)(Me₂SO-*d*₆)Cl]⁺ (**1-sol**), Pt(DNSH-dien)Cl (**2**), [Pt(DNSH-dien)(Me₂SO-*d*₆)]⁺ (**2-sol**), Pt(DNSH-dien)Br (**3**), Pt(DNS-dien) (**4**), [Pt(DNSH-tren)Cl]Cl (**5**), [Pt(DNSH-tren)(Me₂SO-*d*₆)]²⁺ (**5-sol**), [Pt(dien)Cl]Cl (**6**), and [Pt(dien)(Me₂SO-*d*₆)]²⁺ (**6-sol**).

The presence of the sulfonamide N3H signal (broad triplet, $J_{\text{H-H}} = 5.3$ Hz) is an indication that N1 and N2 participate in the binding to Pt(II) but N3 does not. For N3 to bind Pt(II), it must be deprotonated. Thus, the NH signals of the DNSH-dienH ligand provide very useful information for assessing the formation of the Pt(DNSH-dienH)Cl₂ complex.

The combined use of ¹H-¹H COSY and ROESY NMR experiments allowed assignment of all the aromatic signals. In particular, two sets of coupled signals have been identified from the COSY spectrum, corresponding to the DNSH H2, H3, and H4 protons and H6, H7, and H8 protons (for numbering, refer to Figure 2.1). The ROESY cross-peaks between the dimethylamino signal and two aromatic signals allowed identification of the H4 and H6 signals and, from these, of the other signals. ¹H-¹³C HMBC and HSQC NMR experiments were used for ¹³C NMR signal assignment (Table 2.2). From the ¹H-¹³C HSQC NMR experiment, the signals of the carbons bearing a proton were identified easily because the proton spectrum was already assigned. The HMBC cross-peak between the proton signal of the DNSH dimethylamino group with the C5 signal was the key in assigning the rest of the peaks.

2.3.1.2 [Pt(DNSH-dien)(Me₂SO-*d*₆)]⁺ (2-sol). Soon after Pt(DNSH-dien)Cl (**2**) (Figure 2.2) was dissolved in DMSO-*d*₆, two sets of ¹H NMR signals were observed. After ~2 h one set of signals disappeared. This set reappeared when [Et₄N]Cl was added (not shown). The two sets are thus clearly from the Pt(DNSH-dien)Cl complex (**2**) and the solvolysis product, [Pt(DNSH-dien)(Me₂SO-*d*₆)]⁺ (**2-sol**). The latter predominates and is almost the exclusive species present in the absence of added chloride salt. The data presented here are for [Pt(DNSH-dien)(Me₂SO-*d*₆)]⁺ (Figure 2.3). ¹H and ¹³C NMR spectral assignments, summarized in Tables 2.1 and 2.2, were made in the same way as for [Pt(DNSH-dienH)(Me₂SO-*d*₆)Cl]⁺ (**1-sol**). The most significant difference in the spectra of **2-sol** (with a tridentate ligand) and **1-sol** (with a bidentate ligand) is

the absence of the sulfonamide N3H signal for **2-sol**. For the $[\text{Pt}(\text{DNSH-dien})(\text{Me}_2\text{SO-}d_6)]^+$ cation, the most upfield aromatic ^{13}C NMR signal is C6 (114.9 ppm). An H8-C6 cross-peak is present in the HMBC spectra of $[\text{Pt}(\text{DNSH-dien})(\text{Me}_2\text{SO-}d_6)]^+$ and $[\text{Pt}(\text{DNSH-dienH})(\text{Me}_2\text{SO-}d_6)\text{Cl}]^+$ (not shown). In aqueous/DMSO- d_6 (500 $\mu\text{L}/100 \mu\text{L}$), **2** immediately gave evidence for a solvolysis product; careful studies varying solvent composition indicate this species, which is involved in the **G**/3'-IMP reactions and the 5'-GMP/met competition reactions, is $[\text{Pt}(\text{DNSH-dien})(\text{Me}_2\text{SO-}d_6)]^+$ (**2-sol**). When **2-sol** was heated at 70 °C for 14 h in $\text{D}_2\text{O}/\text{DMSO-}d_6$ (500 $\mu\text{L}/100 \mu\text{L}$) the H8 DNSH signal disappeared and H7 became a doublet; an incipient AB pattern between H7 and H6 signals was observed. The fluorescence emission spectrum of **2-sol** is less intense than that of **1-sol**, Figure 2.4.

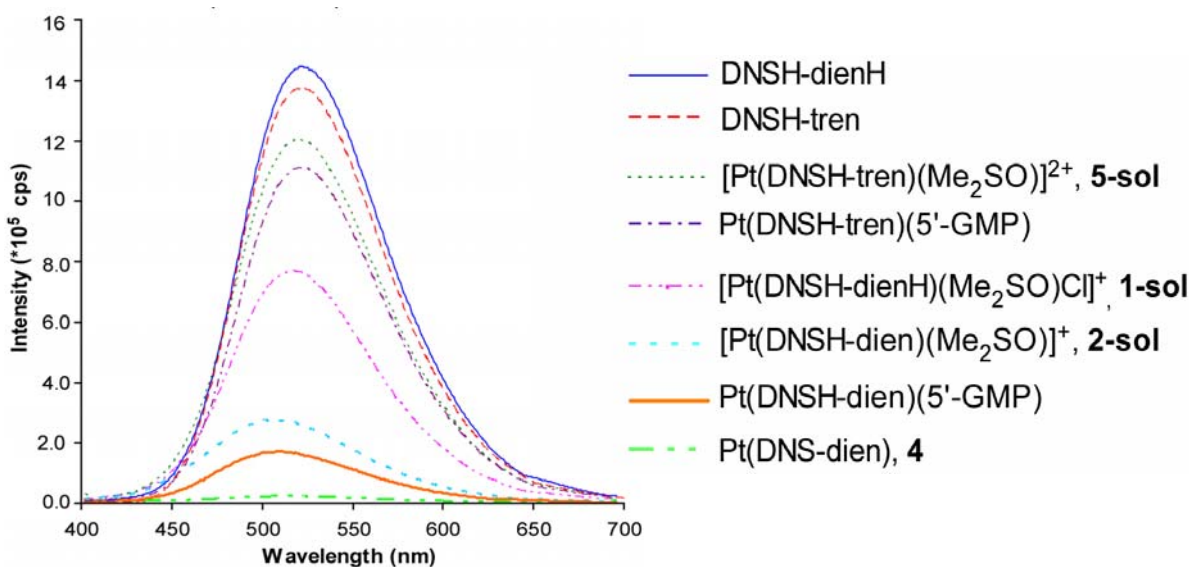


Figure 2.4. Fluorescence emission spectra of the DNSH-dienH and DNSH-tren ligands and their Pt(II) complexes.

Table 2.2. ^{13}C NMR Chemical Shifts (ppm) for $[\text{Pt}(\text{DNSH-dienH})(\text{Me}_2\text{SO-}d_6)\text{Cl}]^+$ (**1-sol**), $[\text{Pt}(\text{DNSH-dien})(\text{Me}_2\text{SO-}d_6)]^+$ (**2-sol**), and $\text{Pt}(\text{DNS-dien})$ (**4**) Complexes in $\text{DMSO-}d_6$ (10 mM, 25 °C)

| | Pt(II) complex | | |
|------------------|----------------|--------------|----------|
| | 1-sol | 2-sol | 4 |
| NMe ₂ | 45.1 | 45.1 | 45.3 |
| C1 | 135.4 | 137.2 | 141.7 |
| C2 | 127.9 | 127.0 | 121.6 |
| C3 | 123.5 | 123.6 | 121.8 |
| C4 | 129.0 | 129.1 | 126.3 |
| C5 | 151.2 | 151.1 | 145.8 |
| C6 | 115.2 | 114.9 | 114.0 |
| C7 | 128.5 | 127.3 | 128.4 |
| C8 | 119.0 | 119.9 | 126.8 |
| C9 | 129.1 | 129.6 | 137.0 |
| C10 | 129.8 | 128.3 | 128.9 |

2.3.1.3 Pt(DNS-dien) (4). This product (**4**), formed under the most basic conditions used, has 5 of the 6 aromatic ^1H NMR signals expected (Figure 2.3), providing evidence that **4** is $\text{Pt}(\text{DNS-dien})$ (Figure 2.2). Two sets of coupled signals were identified by the COSY spectrum (Figure 2.5A), corresponding to the DNS protons, H2, H3, and H4 of one ring, and H6 and H7 of the ring containing the dimethylamino group. In the ROESY experiment (Figure 2.5B), cross-peaks were observed between the H7 signal and the two N1H signals of the dien moiety. Also, the expected H6-H7, H2-H3, and H3-H4 cross-peaks were observed. All aromatic signals were upfield (Table 2.1) compared to the corresponding signals of $[\text{Pt}(\text{DNSH-dien})(\text{Me}_2\text{SO-}d_6)]^+$ (**2-sol**). Of note, the H7 signal is coupled to ^{195}Pt ($J_{\text{Pt-H}} = 22$ Hz).

^1H - ^{13}C HSQC and HMBC NMR experiments were used to assign the ^{13}C NMR spectrum (Table 2.2) and to confirm the structure of **4**. For Pt(DNS-dien) three ^1H - ^{13}C HMBC experiments were carried out with different $J_{\text{H-C}}$ values (6.25, 8, and 10 Hz), but none of the spectra exhibited an H8-C6 cross-peak as found in ^1H - ^{13}C HMBC experiments ($J_{\text{H-C}} = 8$ Hz) with [Pt(DNSH-dien)(Me₂SO-*d*₆)]⁺ and [Pt(DNSH-dienH)(Me₂SO-*d*₆)Cl]⁺.

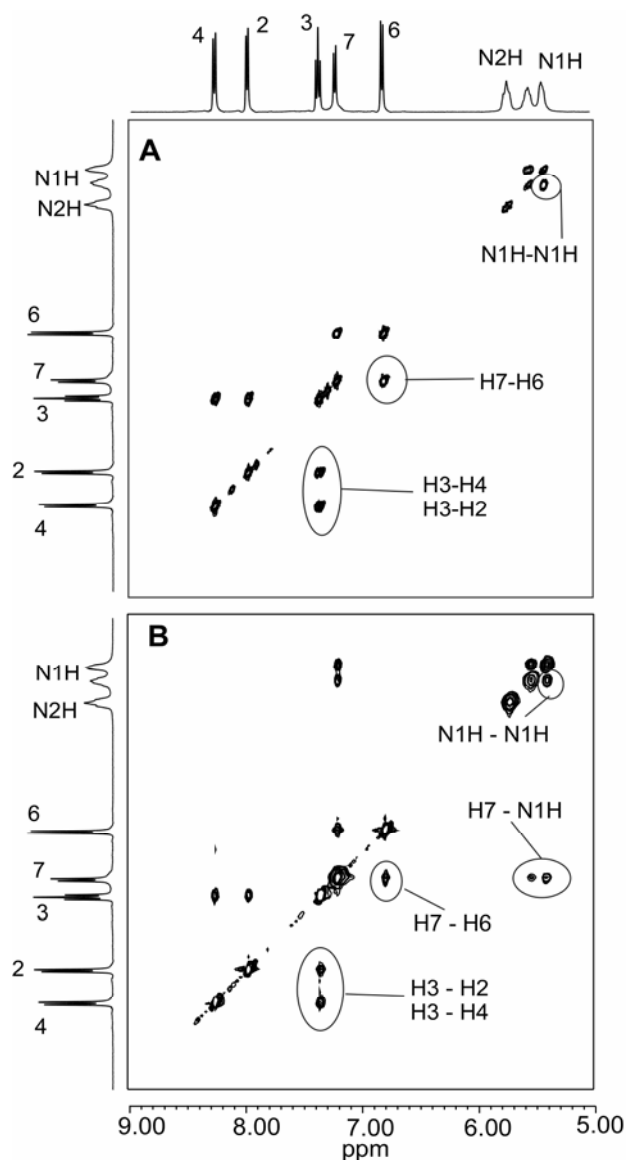


Figure 2.5. **A** ^1H - ^1H COSY spectrum of Pt(DNS-dien) in DMSO-*d*₆ at 298 K. **B.** ^1H - ^1H ROESY spectrum of Pt(DNS-dien) in DMSO-*d*₆ at 298 K.

2.3.1.4 [Pt(DNSH-tren)Cl]Cl (5). [Pt(DNSH-tren)Cl]Cl (**5**) (Figure 2.2) was prepared by treating *cis*-Pt(Me₂SO)₂Cl₂ with DNSH-tren. In DMSO-*d*₆ the ¹H NMR aromatic signals of the DNSH group are not significantly affected by Pt binding (Table 2.1). Upon dissolution in DMSO-*d*₆ the signals of **5** decreased slightly and a downfield set of NH ¹H NMR signals for [Pt(DNSH-tren)(Me₂SO-*d*₆)]²⁺ (**5-sol**) increased. However, only ~10% of [Pt(DNSH-tren)(Me₂SO-*d*₆)]²⁺ (**5-sol**) formed. In contrast, when **5** was dissolved in a mixture of aqueous/DMSO-*d*₆ (500 μL/100 μL, pH = 6.3), **5-sol** formed to a much greater extent (~85% after 2 hours). **5-sol** was the reactive species present in the **G/3'**-IMP reactions and the 5'-GMP/met competition reaction.

2.3.2 Pt(DNSH-dien)(G/3'-IMP) and Pt(DNSH-tren)(G/3'-IMP) Adducts

The solvent used for all adducts was D₂O/DMSO-*d*₆, 500 μL/100 μL, unless otherwise specified. For low temperature experiments, the solvent mixture was D₂O/DMSO-*d*₆/methanol-*d*₄ (500 μL/100 μL/100 μL).

2.3.2.1 Pt(DNSH-tren)(G/3'-IMP) (G = 3'-GMP, 5'-GMP). The Pt(DNSH-tren)(3'-GMP) adduct (pH = 6.32) exhibited one H8 and one H1' NMR signal downfield of the respective signals of free 3'-GMP (Table 2.3). The aromatic signals of the DNSH group were not shifted by 3'-GMP binding (Table 2.4).

Results similar to those for Pt(DNSH-tren)(3'-GMP) were observed for the Pt(DNSH-tren)(5'-GMP) adduct. For Pt(DNSH-tren)(3'-IMP), the resonances of both H8 and H2 shifted downfield of the corresponding resonances of free 3'-IMP. Selected ¹H NMR shifts for both free and bound **G/3'**-IMP in Pt(DNSH-tren)(**G/3'**-IMP) adducts are listed in Table 2.3.

Table 2.3. ^1H NMR Chemical Shifts (ppm) for $\text{Pt}(\text{DNSH-dien})(\text{G}/3'\text{-IMP})$ and $\text{Pt}(\text{DNSH-tren})(\text{G}/3'\text{-IMP})$ Adducts in $\text{D}_2\text{O}/\text{DMSO-}d_6$ 500 $\mu\text{L}/100 \mu\text{L}$, 25 $^\circ\text{C}$

| G/3'- IMP | pH | free H8 (H2) | H8 (H2) | free H1' | H1' |
|--------------------------------|-----------|-------------------------|--------------------|---------------------|------------|
| Pt(DNSH-tren)(G/3'-IMP) | | | | | |
| 5'-GMP | 6.32 | 8.09 | 8.61 | 5.89 | 5.96 |
| 3'-GMP | 6.32 | 8.00 | 8.40 | 5.90 | 5.94 |
| 3'-IMP | 6.26 | 8.38 | 8.83 | 6.12 | 6.17 |
| | | (8.23) | (8.30) | | |
| Pt(DNSH-dien)(G/3'-IMP) | | | | | |
| 9-EtG | 5.23 | 8.01 | 8.11 | | |
| 5'-GMP | 5.21 | 8.11 | 8.27 | 5.87 | 5.69 |
| | | | 8.25 | | |
| 3'-GMP | 5.20 | 8.04 | 8.30 | 5.91 | 5.81 |
| | | | 8.28 | | |
| 5'-GDP | 5.25 | 8.14 | 8.30 | 5.90 | 5.69 |
| | | | 8.28 | | |
| 5'-GTP | 5.17 | 8.15 | 8.30 | 5.89 | 5.68 |
| | | | 8.27 | | |
| 3'-IMP | 5.23 | 8.39 | 8.72 | 6.13 | 6.01 |
| | | (8.22) | (8.10) | | |
| | | | 8.69 | | |
| | | | (8.09) | | |

2.3.2.2 Pt(DNSH-tren)(met-S)]²⁺. We studied the spectrum of the $[\text{Pt}(\text{DNSH-tren})(\text{met-S})]^{2+}$ adduct (pH = 6.4, at which met has a neutral overall charge), which exhibited a sharp (FWHM = 3 Hz) S-methyl NMR signal (2.51 ppm) downfield of the S-methyl signal of free met

(2.13 ppm). The α CH signal of $[\text{Pt}(\text{DNSH-tren})(\text{met-S})]^{2+}$ was downfield (3.90 ppm) of that of free met (3.82 ppm). The aromatic and the dimethylamino DNSH signals were not shifted.

Challenge Reaction. A few hours after addition of three equivalents of 5'-GMP to the solution of the $[\text{Pt}(\text{DNSH-tren})(\text{met-S})]^{2+}$ cation, the NMR signals of the bound met decreased, and signals of the $\text{Pt}(\text{DNSH-tren})(5'\text{-GMP})$ adduct appeared. After 20 and 40 days, respectively, the $\text{Pt}(\text{DNSH-tren})(5'\text{-GMP})$ to $[\text{Pt}(\text{DNSH-tren})(\text{met-S})]^{2+}$ product distribution was 70:30 and 100:0 (no signals for the met adduct remained). **Competition Reaction.** Figure 2.6 describes the time course of the competition reaction of **5-sol** with met and 5'-GMP (1:1:3). In the initial stages of the competition reaction the peaks of free met decreased in size and the peaks of the $[\text{Pt}(\text{DNSH-tren})(\text{met-S})]^{2+}$ adduct appeared, while only a small amount of the $\text{Pt}(\text{DNSH-tren})(5'\text{-GMP})$ adduct was observed (Figure 2.6). In later stages the signals of $[\text{Pt}(\text{DNSH-tren})(\text{met-S})]^{2+}$ began decreasing and those of $\text{Pt}(\text{DNSH-tren})(5'\text{-GMP})$ increased. Finally, after about two months, only $\text{Pt}(\text{DNSH-tren})(5'\text{-GMP})$ signals could be detected.

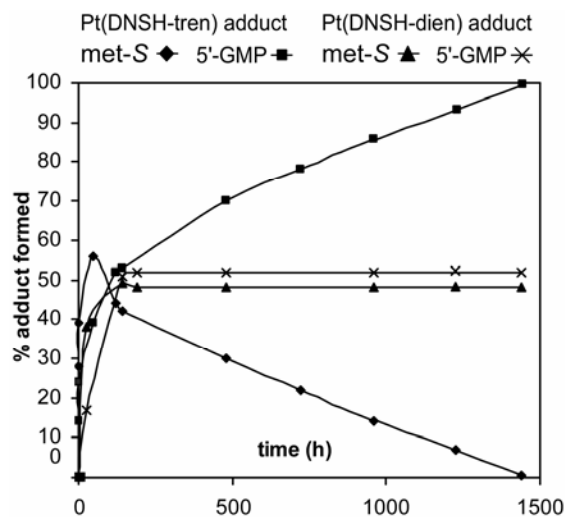


Figure 2.6. Time courses of competition reactions of $[\text{Pt}(\text{DNSH-tren})(\text{Me}_2\text{SO-}d_6)]^{2+}$ (**5-sol**) and $[\text{Pt}(\text{DNSH-dien})(\text{Me}_2\text{SO-}d_6)]^+$ (**2-sol**) with met and 5'-GMP.

2.3.2.3 [Pt(DNSH-dien)(9-EtG)]⁺. The [Pt(DNSH-dien)(9-EtG)]⁺ adduct (pH = 5.23), prepared as described above, showed one set of ¹H NMR signals. Compared to free 9-EtG, the H8 signal was downfield (Table 2.3), but the CH₃ and CH₂ signals of the ethyl group were shifted upfield to 1.17 from 1.48 ppm and to 3.92 from 4.11 ppm, respectively. The DNSH signals of the adduct were upfield of the signals of [Pt(DNSH-dien)(Me₂SO-*d*₆)]⁺ (Table 2.4). A spectrum recorded at -5 °C showed no broadening of the H8 signal.

2.3.2.4 Pt(DNSH-dien)(3'-GMP). For Pt(DNSH-dien)(3'-GMP) (pH = 5.20), two aromatic singlets of similar intensity (Figure 2.7) integrate to a total of one proton. These singlets appear downfield of the H8 signal of free 3'-GMP and are assigned to H8 of bound 3'-GMP by two NOE cross-peaks to the H1' signal.²⁴ There was one H1' signal for the adduct, upfield of the H1' signal of free 3'-GMP (Table 2.3). Also, only one set of DNSH aromatic signals was observed, upfield of the corresponding signals of the starting complex (Table 2.4). Spectra were also recorded from -5 °C to 65 °C in 5 °C intervals. The spectra recorded below 25 °C exhibited two well-resolved 3'-GMP H8 signals, downfield from the H8 doublet for the DNSH group. In spectra measured above 25 °C, these signals began to overlap because the DNSH H8 doublet shifted downfield. Also, the H2 doublet and H3 triplet of the DNSH group each shifted downfield and in some cases the spectra indicated that these were in fact two very closely spaced overlapping signals (of roughly equal size).

2.3.2.5 Pt(DNSH-dien)(G/3'-IMP) (G = 5'-GMP, 5'-GDP, 5'-GTP). The ¹H NMR spectra of the other Pt(DNSH-dien)(G) adducts were similar to that of Pt(DNSH-dien)(3'-GMP) (Tables 2.3 and 2.4). The Pt(DNSH-dien)(3'-IMP) adduct gave two upfield-shifted H2 signals in addition to the two downfield-shifted H8 signals and one upfield H1' signal, as observed for the G adducts (Table 2.3).

Table 2.4. ^1H NMR Chemical Shifts (ppm) of the DNSH Moiety of $([\text{Pt}(\text{DNSH-tren})(\text{Me}_2\text{SO}-d_6)]^{2+}$ (**5-sol**), $[\text{Pt}(\text{DNSH-dien})(\text{Me}_2\text{SO}-d_6)]^+$ (**2-sol**), and $\text{Pt}(\text{DNSH-dien})(\text{G}/3'-\text{IMP})$ in $\text{D}_2\text{O}/\text{DMSO}-d_6$ (500 $\mu\text{L}/100 \mu\text{L}$)

| DNSH signals | 5-sol | 2-sol | Pt(DNSH-dien)(G/3'-IMP) | | | |
|------------------|--------------|--------------|-------------------------|--------|--------|--------|
| | | | 9-EtG | 3'-GMP | 5'-GMP | 3'-IMP |
| pH | 6.37 | 5.21 | 5.23 | 5.20 | 5.21 | 5.23 |
| NMe ₂ | 2.92 | 2.94 | 2.94 | 2.93 | 2.94 | 2.93 |
| H2 | 8.28 | 8.40 | 8.10 | 8.01 | 8.03 | 8.00 |
| H3 | 7.74 | 7.78 | 7.48 | 7.48 | 7.48 | 7.45 |
| H4 | 8.57 | 8.52 | 8.22 | 8.19 | 8.20 | 8.19 |
| H6 | 7.49 | 7.49 | 7.43 | 7.43 | 7.45 | 7.54 |
| H7 | 7.78 | 7.78 | 7.63 | 7.66 | 7.65 | 7.70 |
| H8 | 8.32 | 8.67 | 8.30 | 8.27 | 8.26 | 8.27 |

2.3.2.6 Pt(DNSH-dien)(met-S). The $[\text{Pt}(\text{DNSH-dien})(\text{met-S})]^+$ adduct in $\text{D}_2\text{O}/\text{DMSO}-d_6$ has a broad S-methyl signal (FWHM = 16 Hz, 2.49 ppm), which was downfield of this signal in the spectrum of free met (2.18 ppm). **Challenge Reaction.** No replacement of the bound met or bound 5'-GMP was observed even 60 days after addition of three equivalents of 5'-GMP to the met adduct or one equivalent of met to the 5'-GMP adduct, respectively. **Competition Reaction.** $[\text{Pt}(\text{DNSH-dien})(\text{Me}_2\text{SO}-d_6)]^+$ was treated with met and 5'-GMP (1:1:3). Roughly equal amounts of $[\text{Pt}(\text{DNSH-dien})(\text{met-S})]^+$ and $\text{Pt}(\text{DNSH-dien})(5'-\text{GMP})$ were formed throughout the course of the reaction (Figure 2.6).

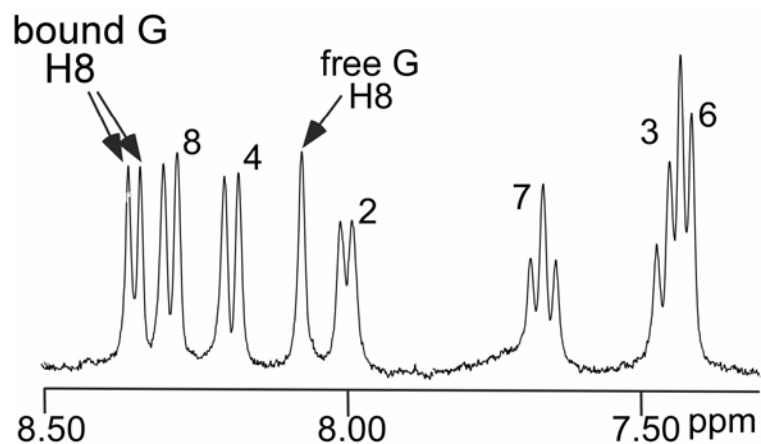


Figure 2.7. Aromatic region of the ^1H NMR spectrum of the $\text{Pt}(\text{DNSH-dien})(3'\text{-GMP})$ adduct.

2.4 Discussion

2.4.1 $\text{Pt}(\text{DNSH-dienH})\text{Cl}_2$ (1)

Under the least basic synthetic conditions used, *cis*- $\text{Pt}(\text{Me}_2\text{SO})_2\text{Cl}_2$ and DNSH-dienH formed $\text{Pt}(\text{DNSH-dienH})\text{Cl}_2$, with DNSH-dienH acting as a bidentate ligand (central N2 and terminal N1) (Figure 2.2). One key piece of evidence for this conclusion is the presence of the sulfonamide N3H ^1H NMR signal at a shift similar to that of the free DNSH-dienH ligand, as expected for an unbound sulfonamide group because N3H must deprotonate prior to Pt binding. $\text{Pt}(\text{en})\text{Cl}_2$ and $\text{Pt}(N\text{-Et-en})\text{Cl}_2$ (*N*-Et-en = *N*-ethylethylenediamine), when dissolved in $\text{DMSO-}d_6$, give the monosolvated species, in which only one Cl ligand is replaced by DMSO.^{23,25} ^1H NMR data indicate that DMSO replaces one of the two chlorides of $\text{Pt}(N\text{-Et-en})\text{Cl}_2$ more readily than the other one. The ^{195}Pt NMR shifts for $\text{Pt}(\text{en})\text{Cl}_2$ and $\text{Pt}(N\text{-Et-en})\text{Cl}_2$ are -2345 and -2364 ppm, respectively, whereas these are -3307 and -3325 ppm for $[\text{Pt}(\text{en})(\text{Me}_2\text{SO-}d_6)\text{Cl}]^+$ ²³ and $[\text{Pt}(N\text{-Et-en})(\text{Me}_2\text{SO-}d_6)\text{Cl}]^+$, respectively. $[\text{Pt}(\text{en})(\text{Me}_2\text{SO-}d_6)_2]^{2+}$ has a ^{195}Pt NMR chemical shift of -3650 ppm.²³ The ^{195}Pt NMR shifts of these monosolvated complexes are very close to the value (-3318 ppm) obtained for $[\text{Pt}(\text{DNSH-dienH})(\text{Me}_2\text{SO-}d_6)\text{Cl}]^+$, thus indicating that in $\text{DMSO-}d_6$ only one

Cl has been replaced to form $[\text{Pt}(\text{DNSH-dienH})(\text{Me}_2\text{SO-}d_6)\text{Cl}]^+$ (**1-sol**, Table 2.1). The insignificant changes in the shifts of the DNSH ^1H NMR signals and in fluorescence intensity (see below and Figure 2.4) indicate that the DNSH moiety occupies a remote position relative to the Pt.

2.4.2 Pt(DNSH-dien)X (X = Cl (2) or Br (3))

The key spectroscopic evidence that the DNSH-dienH ligand acts as a tridentate ligand in Pt(DNSH-dien)X is the absence of the N3H signal indicative of a deprotonated sulfonamide N3, a requirement for a sulfonamide to bind to metals. The Cl and Br ligands are readily displaced in DMSO- d_6 to give $[\text{Pt}(\text{DNSH-dien})(\text{Me}_2\text{SO-}d_6)]^+$ (**2-sol**). The behavior of Pt(DNSH-dien)X in DMSO- d_6 is similar to that of $[\text{Pt}(\text{dien})\text{Cl}]\text{Cl}$. Immediately after dissolution in DMSO- d_6 , $[\text{Pt}(\text{dien})\text{Cl}]\text{Cl}$ showed two sets of NH NMR signals. The upfield set, assigned to $[\text{Pt}(\text{dien})\text{Cl}]^+$, decreased with time, whereas the downfield set, assigned to $[\text{Pt}(\text{dien})(\text{Me}_2\text{SO-}d_6)]^{2+}$, increased with time, and a ratio of $\sim 1:1$ was observed at equilibrium. The shifts of the central secondary NH signals were more downfield than those of the terminal primary amines in both $[\text{Pt}(\text{dien})\text{Cl}]^+$ and $[\text{Pt}(\text{dien})(\text{Me}_2\text{SO-}d_6)]^{2+}$.²⁶ The same trends were observed in the spectrum of Pt(DNSH-dien)Cl in DMSO- d_6 , in which the NH signals of $[\text{Pt}(\text{DNSH-dien})(\text{Me}_2\text{SO-}d_6)]^+$ were downfield of those of Pt(DNSH-dien)Cl, and the central N2H signal was downfield from the terminal N1H signals. Comparing the chemical shifts of the NH signals, we observed that all NH signals were shifted upfield for Pt(DNSH-dien)Cl relative to $[\text{Pt}(\text{dien})\text{Cl}]\text{Cl}$ (Table 2.1). The reason for the upfield position of the shifts is undoubtedly the stronger electron donation to Pt(II) by a sulfonamido group than by a terminal amine group.

2.4.3 Pt(DNS-dien) (4)

The DNSH-dienH ligand can act as a quadridentate N₃C ligand (terminal N1, central N2, and sulfonamido N3 of the dien moiety and C8 of the DNS moiety), giving the chelate complex, Pt(DNS-dien) (**4**) (Figure 2.2). The key evidence for C8 coordination was the missing H8 ¹H NMR signal. The upfield-shifted positions of the aromatic and dimethylamino signals of the DNS moiety of **4**, vs. the corresponding signals of [Pt(DNSH-dien)(Me₂SO-*d*₆)]⁺ (**2-sol**), are also consistent with the formation of a Pt–C8 bond. For example, the H7 signal moved upfield by 0.25 ppm. Furthermore, the coupling to ¹⁹⁵Pt of the proton (H7) on the carbon adjacent to the metallated carbon (C8) was ³J_{Pt-H} = 22 Hz. These results are comparable to those observed in related Pt(II) complexes.²⁷⁻²⁹ For example, Carlone et al.²⁹ found that in a Pt(II) complex with 3-nitro-9-[(2-dialkylaminoethyl)amino]acridine attached by a Pt–C bond the resonance for the proton adjacent to the Pt–C bond shifted upfield by 0.26 ppm and was coupled to ¹⁹⁵Pt (³J_{Pt-H} = 35 Hz).²⁹ The C8 ¹³C NMR signal of **4** had shifted downfield from the free ligand signal after formation of the Pt–C bond, as reported for other Pt(II) complexes with a Pt–C bond. (X-ray structural analysis was also used to confirm the formation of the Pt–C bond in several cases).^{27,30} The N2H signal of the N₃C complex is relatively upfield (by ~1.5 ppm) compared to complexes having N,N,N coordination. We believe that this upfield shift is a result of the greater trans influence (compared to a Cl or Me₂SO-*d*₆ ligand) of the negatively charged C8 atom trans to the N2H.

2.4.4 [Pt(DNSH-tren)Cl]Cl (5)

This complex was designed to be a control, with the DNSH group remote from Pt. The similarity of the DNSH signals to that of the free ligand and the presence of the sulfonamide NH signal confirm that the desired structure formed. An unusual feature of this compound is that it

did not readily undergo solvolysis in DMSO- d_6 ($\sim 10\%$ $[\text{Pt}(\text{DNSH-tren})(\text{Me}_2\text{SO-}d_6)]^{2+}$ (**5-sol**) formed). The primary amine NH signals of **5** and **5-sol** have shifts very similar to those of $[\text{Pt}(\text{dien})\text{Cl}]\text{Cl}$ (**6**) and $[\text{Pt}(\text{dien})(\text{Me}_2\text{SO-}d_6)]^{2+}$ (**6-sol**), respectively. Upon dissolution in DMSO- d_6 , **6** converted to an $\sim 1:1$ **6:6-sol** mixture. $[\text{Pt}(N'\text{-Me-dien})\text{Cl}]\text{Cl}$ was used as model for **5** and it was found to undergo solvolysis by only $\sim 15\%$. Thus, the presence of an alkyl group on the central N decreases DMSO solvolysis. The shielding effect of $\text{Me}_2\text{SO-}d_6$ compared to Cl causes ~ 700 ppm upfield ^{195}Pt NMR shifts of the $\text{Me}_2\text{SO-}d_6$ solvolysis product relative to the starting $[\text{Pt}(\text{dien})\text{Cl}]^+$, $[\text{Pt}(\text{DNSH-tren})\text{Cl}]^+$, and $\text{Pt}(\text{DNSH-dien})\text{Cl}$ complexes in DMSO- d_6 .

2.4.5 Fluorescence Spectroscopy

The fluorescence intensity of *N*-dansyl-*N'*-ethylthiourea was quenched by 87% after addition of Pt(II).³¹ This significant decrease was attributed to the “heavy atom effect.”³¹ The presence of Pt(II) enhances the rate of the spin-forbidden process ($S_1 \rightarrow T_1$).³²⁻³⁴ The fluorescence intensity of the DNSH-tren ligand is decreased by only 20% on formation of $[\text{Pt}(\text{DNSH-tren})(\text{Me}_2\text{SO})]^{2+}$ (Figure 2.4). We attribute the small degree of the decrease to the remote position of the fluorophore from the Pt. Fluorescence spectra of $[\text{Pt}(\text{DNSH-dienH})(\text{Me}_2\text{SO})\text{Cl}]^+$, $[\text{Pt}(\text{DNSH-dien})(\text{Me}_2\text{SO})]^{2+}$, and $\text{Pt}(\text{DNS-dien})$ showed progressively more significant quenching of the fluorescence intensity compared to that of the DNSH-dienH ligand (Figure 2.4), probably due to the heavy atom effect³³ of Pt(II). The greater quenching of the fluorescence intensity as the hapticity of the DNSH-dienH ligand is associated with the increased proximity of the dansyl group to the Pt. The high level of quenching of $\text{Pt}(\text{DNS-dien})$ relative to $[\text{Pt}(\text{DNSH-dienH})(\text{Me}_2\text{SO})\text{Cl}]^+$ and $[\text{Pt}(\text{DNSH-dien})(\text{Me}_2\text{SO})]^{2+}$ may also be attributed to the Pt–C8 bond, which has changed the electronic properties of the fluorophore, in addition to the heavy-atom effect.^{33,34} In the $\text{Pt}(\text{DNSH-dien})(5'\text{-GMP})$ adduct, the observed additional

quenching is attributed to efficient energy transfer from the naphthalene ring to the guanine base.³⁵ The insignificant additional quenching of the fluorescence intensity of Pt(DNSH-tren)(5'-GMP) relative to that of [Pt(DNSH-tren)(Me₂SO)]²⁺ (**5-sol**) is explained by the remote position of the nucleotide relative to the fluorophore.

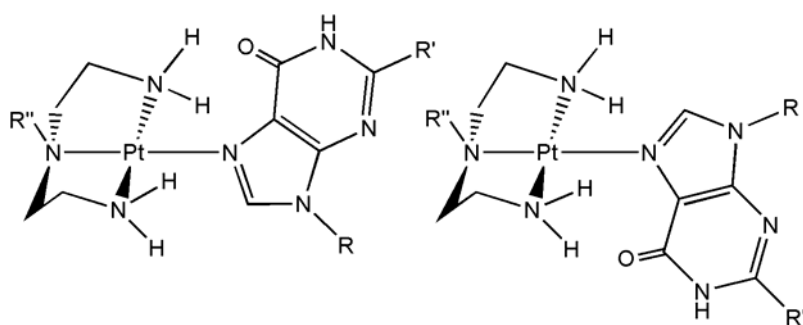


Figure 2.8. The two 6-oxopurine orientations for Pt complexes with dien-type ligands symmetric about a plane perpendicular to the coordination plane and bisecting the ligand. For the two possible rotamers of Pt(DNSH-tren)(G/3'-IMP) adducts: R is a sugar-phosphate; R' = H (IMP) or NH₂ (GMP); R'' = CH₂CH₂NHDNSH. For dien analogs, R'' = H.

2.4.6 Pt(DNSH-tren)(G/3'-IMP) (G = 3'-GMP, 5'-GMP) adducts

The 6-oxopurine nucleobase of G/3'-IMP lies with its plane roughly perpendicular to the Pt coordination plane. In a Pt(II) complex possessing a carrier ligand unsymmetrical with respect to the coordination plane but symmetrical about a plane perpendicular to the coordination plane, two 6-oxopurine orientations are possible (Figure 2.8), and hence two magnetically inequivalent sets of signals are expected for slow rotation of the 6-oxopurine about the Pt–N7 bond. For Pt(DNSH-tren)(G/3'-IMP) adducts, O6 can be on either the same or the opposite side of the coordination plane as the CH₂CH₂NHDNSH substituent. In related cases with tridentate dien-type ligands with both terminal nitrogens substituted, two downfield-shifted H8 signals

indicating slow rotation of the two rotamers have been observed.^{11,12} The observation of only one downfield-shifted H8 (and one H2 for 3'-IMP) signal and only one H1' signal for each Pt(DNSH-tren)(G/3'-IMP) adduct is attributed to nucleobase binding to Pt via N7 and to rapid rotation around the Pt–N7 bond preventing the observation of separate signals for the two rotamers. For Pt(dien)(G) adducts, fast rotation around the Pt–N7 bond is expected because both terminal nitrogens are primary amino groups. Only one H8 signal was observed,³⁶ as expected. The aromatic signals of the DNSH group were unaffected by G/3'-IMP binding to [Pt(DNSH-tren)(Me₂SO-*d*₆)]²⁺ (**5-sol**), most likely because the DNSH group is not close to the bound 6-oxopurine base.

2.4.7 [Pt(DNSH-tren)(met-S)]²⁺ Adduct

The downfield shifts of the S-methyl and CH signals of met on binding to [Pt(DNSH-tren)(Me₂SO-*d*₆)]²⁺ (**5-sol**) reported above are attributed to S binding to Pt. Similar shifts were reported for [Pt(dien)(met-S)]²⁺.^{8,37} Thus, the adduct is [Pt(DNSH-tren)(met-S)]²⁺. **Challenge reaction.** After addition of 5'-GMP to a [Pt(DNSH-tren)(met-S)]²⁺ solution, the met-S adduct converted completely to the 5'-GMP adduct. This result was expected because the 5'-GMP adduct is expected to be the thermodynamic product on the basis of challenge studies reported for the [Pt(dien)(met-S)]²⁺ adduct.³⁷ **Competition reaction.** Initially the [Pt(DNSH-tren)(met-S)]²⁺ adduct formed to a much greater extent than the Pt(DNSH-tren)(5'-GMP) adduct in a competition reaction of met and 5'-GMP for [Pt(DNSH-tren)(Me₂SO-*d*₆)]²⁺ (**5-sol**), indicating that [Pt(DNSH-tren)(met-S)]²⁺ was the preferred kinetic product. With time, the N7-bound 5'-GMP (thermodynamic) product formed (Figure 2.6), as found previously for the [Pt(dien)(met-S)]²⁺ and [Pt(dien)(GSMe-S)]²⁺ adducts.^{6,8,37} At 40 h at the same pH (6.3) and same Pt(II):met:5'-GMP ratio (1:1:3), **5-sol** formed 55% of the met adduct, while [Pt(dien)(H₂O)]²⁺ formed 42% of

the met adduct.⁸ These results of intermolecular displacement support the previous findings that the Pt–S (thioether) bond is the kinetically favored bond type, whereas the Pt–N7 bond is the thermodynamically favored bond type.⁸ Because the dansyl fluorophore of **5-sol** is positioned away from the Pt(II) binding site, its presence did not affect the reactivity or selectivity toward N-bearing (GMP) or S-bearing (met) biological targets of Pt(II).

2.4.8 Possible Rotamers for the Pt(DNSH-dien)(G/3'-IMP) Adducts

Although the central N2 is not substituted as in **5**, the central N2H atom breaks the symmetry of the Pt coordination plane in Pt(DNSH-dien)(G/3'-IMP) adducts. Therefore the nucleobase, which is perpendicular to the plane, has two orientations (Figure 2.9). Also, the DNSH group has two possible orientations, with the dimethylamino group on the same or the opposite side of the coordination plane as the central N2H. Four rotamers are conceivable for the Pt(DNSH-dien)(G/3'-IMP) adduct illustrated. However, the DNSH group normally exhibits fast rotation around the C-sulfonamide bond,³⁸ leading to averaging of the signals of the different rotamers involving the DNSH group. Thus, for slow Pt–N7 rotation, two rotamers at most can be detected on the NMR time scale for each of the two Pt(DNSH-dien) chiralities.

2.4.9 [Pt(DNSH-dien)(9-EtG)]⁺

[Pt(DNSH-dien)(9-EtG)]⁺ has only one 9-EtG H8 signal, which showed no broadening even in a spectrum recorded at -5 °C, indicating that rotation around the Pt–N7 bond is too fast to allow observation of separate signals for the two rotamers.³⁹ Usually, when 9-EtG binds to Pt(II), the Et group signals move downfield;⁴⁰ the upfield-shifted Et signals of [Pt(DNSH-dien)(9-EtG)]⁺ are undoubtedly due to the proximity of the 9-EtG to the anisotropic DNSH moiety.

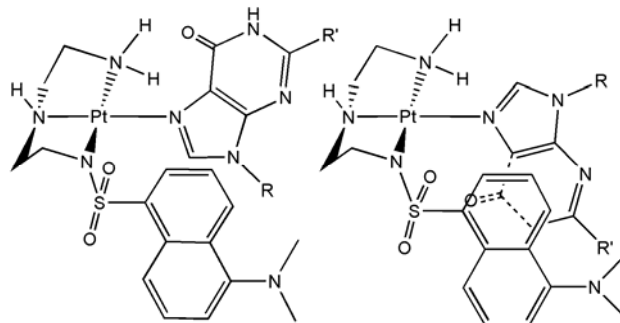


Figure 2.9. Two of the conceivable rotamers of Pt(DNSH-dien)(G/3'-IMP) complexes. Rotamers illustrated have one of the conceivable DNSH orientations and two base orientations with O6 on the same and the opposite side of the proton on the central N2. For 9-EtG (R = ethyl; R' = NH₂), the mirror image of the adduct is an enantiomer. For nucleotides (R is a sugar-phosphate and R' = H (IMP) or NH₂ (GMP)) the adducts with the mirror image of the Pt(DNSH-dien) moiety are diastereoisomers of the rotamers shown.

Only one H8 signal was observed for the [Pt(DNSH-dien)(9-EtG)]⁺ adduct. For G adducts, the presence of the sugar-phosphate group is known to slow rotation.^{12,39} Because the rotation around the Pt–N7 bond in [Pt(DNSH-dien)(9-EtG)]⁺ could be faster than in nucleotide adducts, we investigated Pt(DNSH-dien)(nucleotide) adducts to determine if the presence of the bulky DNSH moiety on one side of Pt(II) binding site could slow the rotation enough to allow the observation of H8 signals of more than one rotamer.

2.4.10 Pt(DNSH-dien)(G/3'-IMP) (G = 5'-GMP, 5'-GDP, 5'-GTP)

The results for these Pt(DNSH-dien) 6-oxopurine nucleotide adducts were similar, and we shall refer mainly to the results obtained for the 3'-GMP adduct. Two H8 signals of approximately equal intensity were observed at 25 °C, as expected if the adducts for each Pt(DNSH-dien) chirality are formed to a comparable extent and if for each Pt(DNSH-dien) chirality the two 6-oxopurine rotamers rotate rapidly on the NMR time scale about the Pt–N7 bond. A previous study of the Pt(*N*-Me₃dien)(G) (G = 3'-GMP, 5'-GMP) adducts showed broad peaks at room temperature, and low temperature was necessary for the rotation to be slow

enough to give sharp NMR signals for the two rotamers.¹² Apparently the presence of the bulkier DNSH moiety on one side of Pt(II) binding site cannot slow the rotation enough to allow the observation of more than one rotamer (for a 6-oxopurine nucleotide) at room temperature.

The aromatic DNSH and H1' signals of the Pt(DNSH-dien)(3'-GMP) adduct shifted upfield when compared to those of the starting [Pt(DNSH-dien)(Me₂SO-*d*₆)]⁺ complex and free 3'-GMP, respectively (Tables 2.3 and 2.4). These upfield shifts of the aromatic signals of the DNSH group and of the H1' signal upon adduct formation are consistent with the proximity of the 3'-GMP to the DNSH group. On binding of the 6-oxopurine derivatives to Pt, the 3'-IMP H2 signals are shifted upfield (in contrast to the typical slight downfield shift), and the purine H8 signals are shifted downfield by about 0.3 ppm (an amount that is less than that for Pt(DNSH-tren)(G/3'-IMP) (Table 2.3) and less than the typical 0.5 to 0.7 ppm).^{36,37}

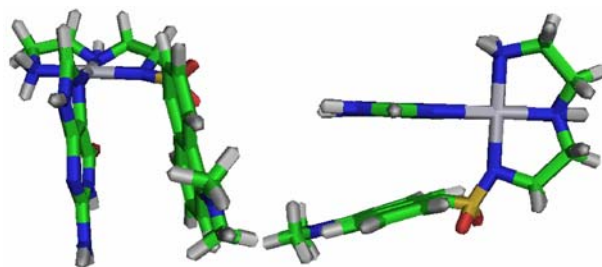


Figure 2.10. Proposed stacking interaction between the G/3'-IMP base and the DNSH moiety viewed along (left) and from the top (right) of the coordination plane. The average separation of the dansyl and the guanine planes is 3.6 Å.

The DNSH aromatic group is attached to the Pt(II) through a sulfonamido group, which keeps the naphthalene ring in proximity to the nucleobase. The observation of the relatively upfield shifts does not necessarily establish a stacking interaction (Figure 2.10). However, there is evidence for purine-aromatic group stacking in Pt(DNSH-dien)(G) adducts. As the

temperature was increased from below room temperature to 65 °C, the DNSH moiety signals shifted downfield. This result is expected if the upfield shifting at low temperature is in part due to stacking, because the average proximity of the two groups, which is fixed by the Pt–N bonds, would not change with temperature in the absence of stacking at low temperature. When Heetebrij et al.⁴¹ treated [Pt(en)(NH₂(CH₂)₆NH-dinitrophenyl)Cl]Cl (a monofunctional complex) with 5'-GMP, they observed that the dinitrophenyl group signals shifted upfield, which they attributed to a stacking interaction between the guanine base of 5'-GMP and the dinitrophenyl group. Stacking is possible because of the long, flexible (CH₂)₆ chain. Also, the 5'-GMP adduct exhibited only one downfield 5'-GMP H8 signal, indicating rapid rotation about the Pt–N7 bond. In this regard, this adduct is similar to the **G** adducts formed by [Pt(dien)Cl]Cl^{6,36,37} and by Pt(DNSH-dien)Cl. The 5'-GMP H8 signal of the Pt(en)(NH₂(CH₂)₆NH-dinitrophenyl)(5'-GMP) adduct had a typical downfield shift. The aromatic group is attached by a flexible (CH₂)₆ chain and apparently may not approach the purine base as closely as the dansyl group does in the adducts reported here.

2.4.11 [Pt(DNSH-dien)(met-S)]⁺

The downfield shifts of the S-methyl signal of the [Pt(DNSH-dien)(met-S)]⁺ adduct are attributed to binding of Pt(II) to the S of met.³⁷ When met binds both through S and N, the rate of inversion at S decreased enough that broadening can be observed in NMR spectra.⁴² A slightly later report concluded that, in the [Pt(dien)(met-S)]²⁺ adduct, where met is bound only through S, the inversion is fast on the NMR scale and therefore broadening of the S-methyl signal was not observed.³⁷ Our finding that the S-methyl signal for the [Pt(DNSH-tren)(met-S)]²⁺ adduct is sharp appears to support this suggestion. However, if the S of the monodentate met of the [Pt(DNSH-dien)(met-S)]⁺ adduct inverted rapidly, we should observe two sharp S-methyl

signals, one for each Pt(DNSH-dien) chirality. If these signals overlapped, the overlapped signal should be sharp. The broad S-methyl signal of the $[\text{Pt}(\text{DNSH-dien})(\text{met-S})]^+$ adduct suggests a possible alternative explanation for the sharp S-methyl signal of $[\text{Pt}(\text{dien})(\text{met-S})]^{2+}$: the difference in shifts for the two $[\text{Pt}(\text{dien})(\text{met-S})]^{2+}$ diastereoisomers is too small to cause broadening of the S-methyl signal. If this explanation holds, then the rate of inversion at S cannot be assessed by ^1H NMR methods when the two cis coordination environments are too similar. **Challenge Reactions.** No replacement of the bound monodentate ligand was observed after addition of 5'-GMP or met to a solution of the $[\text{Pt}(\text{DNSH-dien})(\text{met-S})]^+$ or the $\text{Pt}(\text{DNSH-dien})(5'\text{-GMP})$ adduct, respectively. The presence of the Pt-sulfonamido bulky group close to the binding site affected its selectivity toward N7 over sulfur binding. **Competition Reaction.** No kinetic selectivity of $[\text{Pt}(\text{DNSH-dien})(\text{Me}_2\text{SO-}d_6)]^+$ (**2-sol**) toward met over 5'-GMP was observed, and the ratio of the two adducts throughout the formation reaction was approximately 1:1 (Figure 2.6). In contrast, the competition reactions of $[\text{Pt}(\text{DNSH-tren})(\text{Me}_2\text{SO-}d_6)]^{2+}$ (**5-sol**) (Figure 2.6) and $[\text{Pt}(\text{dien})\text{Cl}]\text{Cl}^{6,9,10}$ show preferential kinetic binding by met followed by thermodynamic binding by 5'-GMP. The presence of a bulky group very close to the Pt(II) binding site in **2-sol** significantly affected the selectivity of Pt(II) toward met and 5'-GMP.

2.5 Conclusions

The DNSH-dienH ligand can act as a bidentate, tridentate, or quadridentate ligand. The observation of only two H8 ^1H NMR signals for the $\text{Pt}(\text{DNSH-dien})(6\text{-oxopurine nucleotide})$ adducts indicates rapid rotation around the Pt-N7 bond. Thus, the addition of a bulky substituent on just one terminal N of a dien-type ligand has been shown to be insufficient to slow the rotation around the Pt-N7 bond. The upfield shifts of the signals of the DNSH group of all **G/3'-IMP** adducts, the ethyl group of the 9-EtG adduct, and the H2 and H1' of nucleotide adducts all

indicate that the dansyl naphthalene group and the 6-oxopurine base are close and parallel. The additional quenching found for the Pt(DNSH-dien)(5'-GMP) adduct can be attributed to energy transfer, which is effective because of the close proximity of the dansyl group to the guanine base.³⁵ This quenching is avoided when the aromatic fluorophore is positioned remotely from Pt(II), as exemplified by [Pt(DNSH-tren)Cl]Cl. This latter compound and [Pt(dien)Cl]Cl, which have no substituents on the terminal amino groups to influence the approach of the incoming monodentate ligand, have similar reactivity patterns toward 5'-GMP and met. The resulting adducts and those derived from Pt(DNSH-dien)Cl exhibit similar dynamic properties. However, the bulky dansyl group near the reaction site of Pt(DNSH-dien)Cl increases the reactivity toward 5'-GMP relative to that toward met. This effect could be explained by stacking between the dansyl group and the guanine base of 5'-GMP.

2.6 References

1. Lippert, B. *Cisplatin: Chemistry and Biochemistry of a Leading Anticancer Drug*; Wiley-VCH: Weinheim, 1999.
2. Wang, D.; Lippard, S. J. *Nat. Rev. Drug Discovery* **2005**, *4*, 307-320.
3. Vzorov, A. N.; Bhattacharyya, D.; Marzilli, L. G.; Compans, R. W. *Antiviral Res.* **2005**, *65*, 57-67.
4. Farrell, N.; Bierbach, U.; PCT Int. Appl.: USA, 1999, p 20.
5. Reedijk, J. *Inorg. Chim. Acta* **1992**, *200*, 873-881.
6. Djuran, M. I.; Lempers, E. L. M.; Reedijk, J. *Inorg. Chem.* **1991**, *30*, 2648-2652.
7. Lippert, B. *Coord. Chem. Rev.* **2000**, *200*, 487-516.
8. Soldatovic, T.; Bugarcic, Z. D. *J. Inorg. Biochem.* **2005**, *99*, 1472-1479.
9. Teuben, J. M.; van Boom, S. S. G. E.; Reedijk, J. *J. Chem. Soc., Dalton Trans.* **1997**, 3979-3380.

10. van Boom, S. S. G. E.; Chen, B. W.; Teuben, J. M.; Reedijk, J. *Inorg. Chem.* **1999**, *38*, 1450-1455.
11. Carlone, M.; Fanizzi, F. P.; Intini, F. P.; Margiotta, N.; Marzilli, L. G.; Natile, G. *Inorg. Chem.* **2000**, *39*, 634-641.
12. Carlone, M.; Marzilli, L. G.; Natile, G. *Inorg. Chem.* **2004**, *43*, 584-592.
13. Djuran, M. I.; Dimitrijevic, D. P.; Milinkovic, S. U.; Bugarcic, Z. D. *Transition Met. Chem. (London)* **2002**, *27*, 155-158.
14. Corradini, R.; Dossena, A.; Galaverna, G.; Marchelli, R.; Panagia, A.; Sartor, G. *J. Org. Chem.* **1997**, *62*, 6283-6289.
15. Prodi, L.; Montalti, M.; Zaccheroni, N.; Dallavalle, F.; Folesani, G.; Lanfranchi, M.; Corradini, R.; Pagliari, S.; Marchelli, R. *Helv. Chim. Acta* **2001**, *84*, 690-706.
16. Price, J. H.; Schramm, R. F.; Wayland, B. B.; Williams, A. *Inorg. Chem.* **1972**, *11*, 1280-1284.
17. Kukushkin, Y. N.; Vyaz'menskii, Y. E.; Zorina, L. I.; Pazukhina, Y. L. *Zh. Neorg. Khim.* **1968**, *13*, 1595-1599.
18. Annibale, G.; Brandolisio, M.; Pitteri, B. *Polyhedron* **1995**, *14*, 451-453.
19. Melius, P.; McAuliffe, C. A. *J. Med. Chem.* **1975**, *18*, 1150-1151.
20. Natile, G.; Albertin, G.; Bordignon, E.; Orio, A. A. *J. Chem. Soc., Dalton Trans.* **1976**, 626-631.
21. Marzilli, L. G.; Hayden, Y.; Reily, M. D. *Inorg. Chem.* **1986**, *25*, 974-978.
22. Kirvan, G. E.; Margerum, D. W. *Inorg. Chem.* **1985**, *24*, 3017-3021.
23. Kerrison, J. S.; Sadler, P. J. *Inorg. Chim. Acta* **1985**, *104*, 197-201.
24. Tate, S.-i.; Ono, A.; Kainosho, M. *J. Am. Chem. Soc.* **1994**, *116*, 5977-5978.
25. Fanizzi, F. P.; Intini, F. P.; Maresca, L.; Natile, G. *Inorg. Chem.* **1990**, *29*, 29-33.
26. Guo, Z. J.; Sadler, P. J.; Zang, E. *Chem. Commun. (Cambridge, U. K.)* **1997**, 27-28.
27. Brooks, J.; Babayan, Y.; Lamansky, S.; Djurovich, P. I.; Tsyba, I.; Bau, R.; Thompson, M. E. *Inorg. Chem.* **2002**, *41*, 3055-3066.

28. Jolliet, P.; Gianini, M.; von Zelewsky, A.; Bernardinelli, G.; Stoeckli-Evans, H. *Inorg. Chem.* **1996**, *35*, 4883-4888.
29. Carlone, M.; Di Masi, N. G.; Maresca, L.; Margiotta, N.; Natile, G. *Bioinorg. Chem. Appl.* **2004**, *2*, 93-104.
30. Slagt, M. Q.; Rodriguez, G.; Grutters, M. M. P.; Gebbink, R. J. M. K.; Klopper, W.; Jenneskens, L. W.; Lutz, M.; Spek, A. L.; Van Koten, G. *Chem.--Eur. J.* **2004**, *10*, 1331-1344.
31. Schuster, M.; Sandor, M. *Fresenius. J. Anal. Chem.* **1996**, *356*, 326-330.
32. Basu, G.; Kubasik, M.; Anglos, D.; Secor, B.; Kuki, A. *J. Am. Chem. Soc.* **1990**, *112*, 9410-9411.
33. Kavarnos, G.; Cole, T.; Scribe, P.; Dalton, J. C.; Turro, N. J. *J. Am. Chem. Soc.* **1971**, *93*, 1032-1034.
34. deSilva, A. P.; Gunaratne, H. Q. N.; Gunnlaugsson, T.; Huxley, A. J. M.; McCoy, C. P.; Rademacher, J. T.; Rice, T. E. *Chem. Rev.* **1997**, *97*, 1515-1566.
35. Heinlein, T.; Knemeyer, J.-P.; Piestert, O.; Sauer, M. *J. Phys. Chem. B* **2003**, *107*, 7957-7964.
36. Kong, P.-C.; Theophanides, T. *Bioinorganic Chemistry* **1975**, *5*, 51-58.
37. Barnham, K. J.; Djuran, M. I.; Murdoch, P. d. S.; Sadler, P. J. *J. Chem. Soc., Chem. Commun.* **1994**, 721-722.
38. Lyapkalo, I. M.; Reissig, H. U.; Schafer, A.; Wagner, A. *Helv. Chim. Acta* **2002**, *85*, 4206-4215.
39. Ano, S. O.; Intini, F. P.; Natile, G.; Marzilli, L. G. *Inorg. Chem.* **1999**, *38*, 2989-2999.
40. Raudaschl-Sieber, G.; Schollhorn, H.; Thewalt, U.; Lippert, B. *J. Am. Chem. Soc.* **1985**, *107*, 3591-3595.
41. Heetebrij, R. J.; Talman, E. G.; Von Velzen, M. A.; Von Gijlswijk, R. P. M.; Snoeijers, S. S.; Schalk, M.; Wiegant, J.; Von der Rijke, F.; Kerkhoven, R. M.; Raap, A. K.; Tanke, H. J.; Reedijk, J.; Houthoff, H. J. *ChemBiochem* **2003**, *4*, 573-583.
42. Murdoch, P. d. S.; Ranford, J. D.; Sadler, P. J.; Berners-Price, S. J. *Inorg. Chem.* **1993**, *32*, 2249-2255.

CHAPTER 3. *fac*-Re(CO)₃L COMPLEXES CONTAINING TRIDENTATE MONOANIONIC LIGANDS (L⁻) WITH A SELDOM-STUDIED SULFONAMIDO GROUP AS ONE TERMINAL LIGATING GROUP*

3.1 Introduction

Metal nuclide radiopharmaceuticals contain a metal core and an inner ligating unit, usually having chelate rings. We refer to this part of the agent as a label, and important properties of the label, which influence biological behavior, are charge and overall shape. Technetium-99m (^{99m}Tc) is the most widely used diagnostic radionuclide in nuclear medicine.¹⁻⁴ {^{99m}Tc(V)O}³⁺ has been the metal core used most predominantly, but recently the development of the advantageous [^{99m}Tc(CO)₃(H₂O)₃]⁺ precursor has opened new directions for radiolabeling.⁵⁻⁷ Schibli et al. showed that agents with the *fac*-^{99m}Tc(I)(CO)₃⁺ core bearing a tridentate coordinated ligand are more robust and have better pharmacokinetic profiles than agents bearing bidentate ligands.⁸ Commonly employed chelating ligands (e.g., diethylenetriamine (dien),⁹ cysteine- and homocysteine-based ligands^{10,11}) contain N, O, or S donor atoms in groups such as carboxyls,¹² amines,¹³⁻¹⁹ nitrogen heterocycles,¹⁴⁻¹⁶ and thioethers.^{10,11,16,17}

An important approach in the development of small (~5 kDa) metal nuclide radiopharmaceuticals is the bioconjugation of a net neutral label to hormones, small peptides, etc.²⁰ For *fac*-^{99m}Tc(I)(CO)₃⁺ agents, the ligand(s) occupying the three remaining coordination sites must have one negative group close to the metal for net neutrality. A coordinated

* Reproduced with permission from American Chemical Society: Christoforou, A. M., Fronczek, F. R., Marzilli, P. A., Marzilli, L. G., "*fac*-Re(CO)₃L Complexes Containing Tridentate Monoanionic Ligands (L⁻) with a Seldom-Studied Sulfonamido Group As One Terminal Ligating Group" *Inorganic Chemistry*, **2007**, in press. Unpublished work copyright 2007 American Chemical Society.

carboxylate group provides such a unit, but it does not provide a point for ligand elaboration or for bioconjugation. Consequently, there is a need to evaluate other groups within tridentate monoanionic ligands. In this study, we explore ligands which provide one metal-bound negative group and which offer a diverse chemistry, allowing bioconjugation via internal ligand atoms or via a seldom-used negative terminal ligating group.²¹ We use ligands containing the sulfonamide group, which has been shown to bind well to several metals²²⁻²⁹ but Tc complexes with this group have not been studied.

The non-radioactive $fac\text{-}[\text{Re}(\text{CO})_3(\text{H}_2\text{O})_3]^+$ analogue is useful in understanding the chemistry of agents derived from the $[\text{}^{99\text{m}}\text{Tc}(\text{CO})_3(\text{H}_2\text{O})_3]^+$ species.¹⁰ As a prelude to radiopharmaceutical studies, we analyzed a series of new $\text{Re}(\text{CO})_3\text{L}$ complexes formed by treating $[\text{fac}\text{-}\text{Re}(\text{CO})_3(\text{H}_2\text{O})_3]^+$ with four new ligands, **LH**, bearing a sulfonamide group (Figure 3.1). These ligands, $\text{tmbSO}_2\text{-}N,N\text{-Me}_2\text{dienH}$, $\text{tmbSO}_2\text{-}N'\text{-MedienH}$, $\text{tmbSO}_2\text{-dienH}$, and $\text{tmbSO}_2\text{-dipnH}$, bind in a tridentate fashion involving one nitrogen of a monoanionic deprotonated sulfonamido group. The H's in the ligand names (*cf.* caption of Figure 3.1) designate the sulfonamide NH proton that is absent in the deprotonated bound ligand. We provide the first detailed analysis of X-ray structures with a sulfonamido group bound to Re.

Given the promise of the ${}^{99\text{m}}\text{Tc}(\text{CO})_3\text{L}$ agents (L^- = a facially coordinated tridentate ligand), it is clearly important to understand how the ligand pucker depends on the various components that can influence it (donor atoms, chains linking these atoms, exocyclic substituents, etc.). Because the chelate ring atoms act as a fulcrum, the configuration of asymmetric centers, the shape, and the conformation of the rings can have a large effect on the overall shape of the agent, and hence on its biological activity.

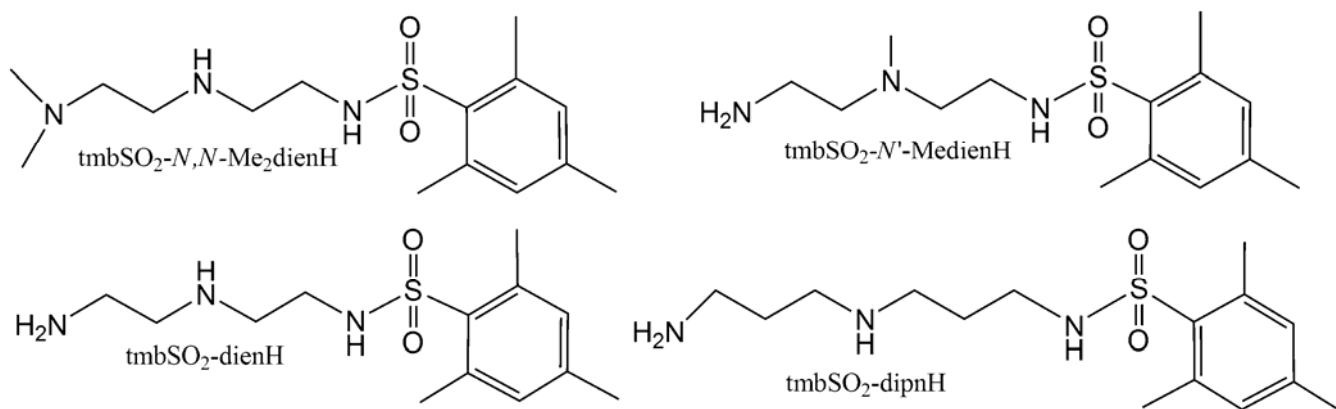
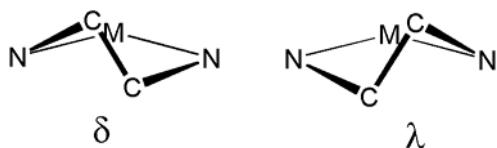


Figure 3.1. Ligands used in this study: *N*-[2-(2-dimethylaminoethylamino)-ethyl]-2,4,6-trimethylbenzenesulfonamide (tmbSO₂-*N,N*-Me₂dienH); *N*-{2-[(2-aminoethyl)-methylamino]-ethyl}-2,4,6-trimethylbenzenesulfonamide (tmbSO₂-*N'*-MedienH); *N*-[2-(2-aminoethylamino)-ethyl]-2,4,6-trimethylbenzenesulfonamide (tmbSO₂-dienH); and *N*-[3-(3-aminopropylamino)-propyl]-2,4,6-trimethylbenzenesulfonamide (tmbSO₂-dipnH).

Although chelate ring pucker and factors affecting pucker have not been thoroughly examined for radiopharmaceuticals, extensive structural information exists for a large number of complexes with other metals containing chelate rings with an ethylene group bridge between ligating atoms. Many of these structures have been analyzed by using principal component analysis (pca) and other methods.³⁰⁻³⁷ When diethylenetriamine-type ligands bind to a metal center in a tridentate fashion, the pucker of the two five-membered chelate rings can have either δ or λ chirality (Chart 1), leading to four possible combinations of chelate ring chirality: $\delta\lambda$, $\lambda\delta$, $\lambda\lambda$, and $\delta\delta$.

Chart 3.1



In pca studies on X-ray structures from the Cambridge Structural Database (CSD) of $[M(\text{dien})_2]^{n+}$ ($M = \text{Ni}, \text{Co}, \text{Zn}, \text{Cu}, \text{Cr}, \text{Rh}, \text{and Ir}$)³¹ and of $[M(\text{dien})L_n]$ ³² complexes and $M(\text{dien})$

fragments³⁰, the $\delta\lambda$ and $\lambda\delta$ conformation combinations were found much more frequently than combinations with the same pucker chirality ($\delta\delta$ and $\lambda\lambda$). On the other hand, Schmidtke and Garthoff³³ suggested that, because of steric effects of the hydrogen atoms of the ethylene chains, *fac* coordination would favor a $\delta\delta$ or $\lambda\lambda$ combination. Thus, factors influencing pucker (which in turn affect shape) are not well understood, and in a recent study, we found that the rings have the same pucker in complexes of lanthionine (LANH₂).¹¹ The new Re(CO)₃L complexes studied here offer the opportunity to determine how widespread the occurrence of $\delta\lambda$ and $\lambda\lambda$ combinations is.

3.2 Experimental Section

3.2.1 Starting Materials

N,N-dimethyldiethylenetriamine (*N,N*-Me₂dien) from Ames Laboratories, *N*-methyl-2,2'-diaminodiethylamine (*N'*-Medien) from TCI America, and bis(3-aminopropyl)amine (dipn), dien, 2-mesitylenesulfonyl chloride (tmsSO₂Cl), dansyl chloride (DNS-Cl), and Re₂(CO)₁₀ from Aldrich were all used as received. The DNS-dienH ligand (*N*-(2-((2-aminoethyl)amino)ethyl)-5-(dimethylamino)naphthalene-1-sulfonamide)³⁸ and the [Re(CO)₃(H₂O)₃]OTf^{d0} (OTf = trifluoromethanesulfonate) precursor were prepared by known methods.

3.2.2 Physical Measurements

¹H NMR spectra were recorded on either a 300 MHz or 400 MHz spectrometer. Peak positions are relative to TMS or solvent residual peak, with TMS as reference. All NMR data were processed with XWINNMR and Mestre-C software. IR spectra were recorded on a Bruker TENSOR 37 spectrometer, and the values for the CO stretching frequencies are given in Appendix B.³⁹

3.2.2.1 X-ray Data Collection and Structure Determination. All single crystals suitable for X-ray crystallography were obtained by slow evaporation from acetone or methanol. Single crystals were placed in a cooled nitrogen gas stream at ~100 K on a Nonius Kappa CCD diffractometer fitted with an Oxford Cryostream cooler with graphite-monochromated Mo K α (0.71073 Å) radiation. Data reduction included absorption corrections by the multi-scan method, with HKL SCALEPACK.⁴⁰ All X-ray structures were determined by direct methods and difference Fourier techniques and refined by full-matrix least squares techniques, by using SHELXL97.⁴¹ All non-hydrogen atoms were refined anisotropically. All hydrogen atoms were visible in difference maps, but were placed in idealized positions. One methyl group (C17) of **5** has its hydrogen atoms disordered into a "doughnut" of electron density, which was modeled as six half-populated positions. A torsional parameter was refined for each methyl group. Mercury Software was used as aid for measuring structural parameters.

3.2.3 Synthesis of Re(CO)₃L

The crude ligands, **LH**, were synthesized by a slight modification of Krapcho's method.⁴² A solution of the sulfonyl (tmbSO₂Cl) or acetyl chloride (tmbCOCl) (~5 mmol, 100 mL of dioxane) was added dropwise over the course of about 2 h to a solution of the amine (~50 mmol, 100 mL of dioxane). The reaction mixture was stirred at RT for 10 h. The dioxane was completely removed under vacuum, and water (50 mL) was added. The product was extracted into CH₂Cl₂ (2 × 100 mL), and the solvent was removed under rotary evaporation. The oil thus obtained was used to synthesize the Re(CO)₃L complexes as follows: an aqueous solution of [Re(CO)₃(H₂O)₃]⁺ (10 mL, 0.1 mmol) was treated with a methanol (1 mL) solution of the ligand (0.1 mmol). The pH was adjusted to ~5 and the reaction mixture was heated at reflux for 10 h,

then allowed to cool at RT, and the pH was increased to ~ 7. The resulting white solid that precipitated was collected on a filter, washed with water, and dried under vacuum.

3.2.3.1 Re(CO)₃(tmbSO₂-*N,N*-Me₂dien) (1). This general method just described, with tmbSO₂Cl (1 g) and *N,N*-Me₂dien (6.5 mL), yielded the crude tmbSO₂-*N,N*-Me₂dienH ligand (750 mg, 51% yield). ¹H NMR (ppm) in CDCl₃: 6.94 (s, 2H), 2.90 (t, 2H, CH₂), 2.66 (t, 2H, CH₂), 2.64 (s, 6H, CH₃), 2.55 (t, 2H, CH₂), 2.33 (t, 2H, CH₂), 2.29 (s, 3H, CH₃), 2.20 (s, 6H, NCH₃). Treatment of [Re(CO)₃(H₂O)₃]⁺ (0.1 mmol) with tmbSO₂-*N,N*-Me₂dienH (32 mg) as described above afforded Re(CO)₃(tmbSO₂-*N,N*-Me₂dien) as a white powder (26 mg, 44% yield). Crystals obtained by slow evaporation from methanol were characterized by single-crystal X-ray crystallography. ¹H NMR (ppm) spectrum in acetone-*d*₆: 6.91 (s, 2H), 6.17 (b, 1H, N₂H), 3.54-3.10 (m, 6H, CH₂), 3.10 (s, 6H, N-CH₃), 2.70 (s, 6H, CH₃), 2.59 (m, 2H, CH₂), 2.24 (s, 3H, CH₃).

3.2.3.2 Re(CO)₃(tmbSO₂-*N'*-Medien) (2). The general method, with 1 g of tmbSO₂Cl and 6 mL of *N'*-Medien, afforded the crude tmbSO₂-*N'*-MedienH ligand (650 mg, 48% yield). ¹H NMR (ppm) in CDCl₃: 6.95 (s, 2H), 2.93 (t, 2H, CH₂), 2.75 (t, 2H, CH₂), 2.64 (s, 6H, CH₃), 2.44 (t, 2H, CH₂), 2.38 (t, 2H, CH₂), 2.29 (s, 3H, CH₃), 2.08 (s, 3H, *N'*-CH₃). Treatment of [Re(CO)₃(H₂O)₃]⁺ (0.1 mmol) with tmbSO₂-*N'*-MedienH (30 mg) as described above afforded Re(CO)₃(tmbSO₂-*N'*-Medien) as a white powder (24 mg, 42% yield). Crystals obtained by slow evaporation from acetone were characterized by single-crystal X-ray crystallography. ¹H NMR (ppm) spectrum in acetone-*d*₆: 6.91 (s, 2H), 4.94 (b, 1H, N₁H), 3.87 (b, 1H, N₁H), 3.42-3.53 (m, 3H, CH₂), 3.24 (s, 3H, *N'*-CH₃), 3.01-3.18 (m, 5H, CH₂), 2.64 (s, 6H, CH₃), 2.24 (s, 3H, CH₃).

3.2.3.3 Re(CO)₃(tmbSO₂-dien) (3). The general method, with tmbSO₂Cl (1 g) and dien (5.2 mL), yielded the crude tmbSO₂-dienH ligand (600 mg, 54% yield). ¹H NMR (ppm) in

CDCl₃: 6.93 (s, 2H), 2.92 (t, 2H, CH₂), 2.73 (t, 2H, CH₂), 2.67 (t, 2H, CH₂), 2.63 (s, 6H, CH₃), 2.59 (t, 2H, CH₂), 2.28 (s, 3H, CH₃). Treatment of [Re(CO)₃(H₂O)₃]⁺ (0.1 mmol) with tmbSO₂-dienH (31.2 mg) as described above afforded Re(CO)₃(tmbSO₂-dien) as a white powder (21 mg, 38% yield). Crystals obtained by slow evaporation from methanol were characterized by single-crystal X-ray crystallography. ¹H NMR (ppm) spectrum in acetone-*d*₆: 6.90 (s, 2H), 6.17 (b, 1H, N2H), 4.75 (b, 1H, N1H), 3.98 (b, 1H, N1H), 3.36-3.00 (m, 8H, CH₂), 2.65 (s, 6H, CH₃), 2.24 (s, 3H, CH₃).

3.2.3.4 Re(CO)₃(tmbSO₂-dipn) (5). The general method, with tmbSO₂Cl (1 g) and dipn (6 mL), produced the crude tmbSO₂-dipnH ligand (600 mg, 42% yield). ¹H NMR (ppm) in CDCl₃: 6.94 (s, 2H), 2.98 (t, 2H, CH₂), 2.76 (t, 2H, CH₂), 2.71 (t, 2H, CH₂), 2.63 (t, 2H, CH₂), 2.63 (s, 6H, CH₃), 2.29 (s, 3H, CH₃), 1.62 (m, 4H, CH₂). Treatment of [Re(CO)₃(H₂O)₃]⁺ (0.1 mmol) with tmbSO₂-dipnH (32 mg) as described above afforded Re(CO)₃(tmbSO₂-dipn) as a white powder (24 mg, 41% yield). Crystals obtained by slow evaporation from acetone were characterized by single-crystal X-ray crystallography. ¹H NMR (ppm) spectrum in acetone-*d*₆: 6.93 (s, 2H), 5.20 (b, 1H, N2H), 4.64 (b, 1H, N1H), 3.98 (b, 1H, N1H), 3.46 (m, 2H, CH₂), 3.28 (s, 2H, CH₂), 3.10-3.19 (m, 3H, CH₂), 3.94 (s, 2H, CH₂), 2.66 (s, 6H, CH₃), 2.25 (s, 3H, CH₃), 1.90 (s, 2H, CH₂), 1.66-1.75 (s, 2H, CH₂).

3.3 Results and Discussion

In a modification of the method of Krapcho,⁴² monoaddition of the relatively large hydrophobic aromatic tmbSO₂ group to triamines produced hydrophobic ligands that were readily extracted into CH₂Cl₂ from water (with the excess of unchanged triamine remaining in the water layer). This method afforded a series of triamine ligand derivatives (**LH**) in sufficient yield and purity for use in preparing Re complexes. These ligand derivatives bind to the *fac*-

Re(I)(CO)₃ center as tridentate deprotonated monoanionic ligands L⁻, thereby forming complexes with a neutral core.

3.3.1 X-Ray Characterization

Crystal data and structural refinement details are summarized in Table 3.1 for new complexes and in Appendix B³⁹ for the previously briefly described compound Re(CO)₃(DNS-dien), **4**.⁴³ All the complexes reported here have a distorted octahedral structure, with the three carbonyl ligands coordinated facially (Figure 3.2). The remaining coordination sites are occupied by two sp³ N amines and one sp² N from a sulfonamido group.

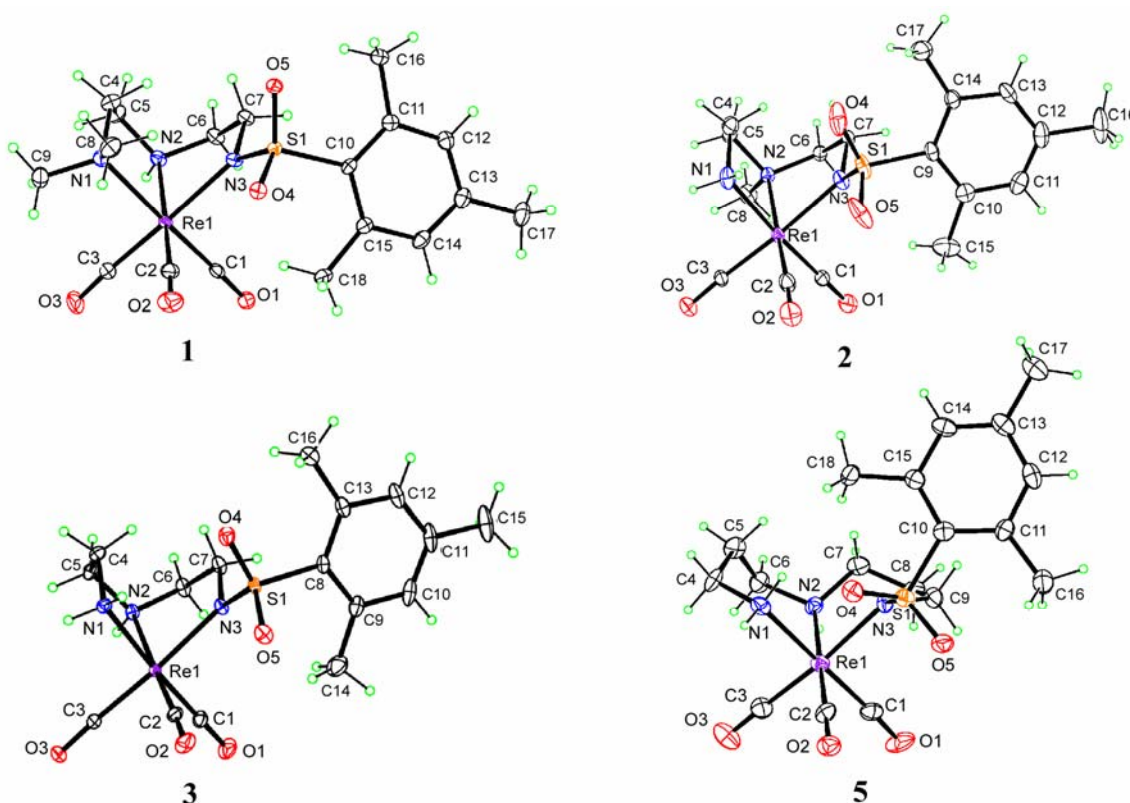


Figure 3.2. Perspective drawings of the S configuration of Re(CO)₃(tmbSO₂-N,N-Me₂dien) (**1**), Re(CO)₃(tmbSO₂-N'-Medien) (**2**), Re(CO)₃(tmbSO₂-dien) (**3**), and Re(CO)₃(tmbSO₂-dipn) (**5**). Thermal ellipsoids are drawn with 50% probability.

Table 3.1. Crystal Data and Structural Refinement for $\text{Re}(\text{CO})_3\text{L}$ Complexes in Which L^- Contains a Sulfonamido Group

| Re(CO) ₃ L complex | | | | |
|---|---|---|---|---|
| | 1 | 2 | 3 | 5 |
| empirical formula | C ₁₈ H ₂₆ N ₃ O ₅ ReS | C ₁₇ H ₂₄ N ₃ O ₅ ReS •0.5H ₂ O | C ₁₆ H ₂₂ N ₃ O ₅ ReS •0.5CH ₃ OH | C ₁₈ H ₂₆ N ₃ O ₅ ReS |
| fw | 582.68 | 577.66 | 570.65 | 582.68 |
| crystal system | monoclinic | monoclinic | triclinic | triclinic |
| space group | <i>C2/c</i> | <i>P2/c</i> | <i>P</i> $\bar{1}$ | <i>P</i> $\bar{1}$ |
| unit cell dimensions | | | | |
| <i>a</i> (Å) | 38.994 (2) | 15.945 (2) | 7.6603 (5) | 7.956 (3) |
| <i>b</i> (Å) | 14.7085 (10) | 10.9504 (15) | 7.8808 (5) | 11.833 (4) |
| <i>c</i> (Å) | 14.6254 (10) | 12.2394 (16) | 16.6154 (12) | 12.129 (4) |
| α (°) | 90.0 | 90.0 | 98.181 (4) | 115.71(2) |
| β (°) | 94.642 (4) | 100.451 (7) | 95.974 (4) | 94.66 (2) |
| γ (°) | 90.0 | 90.0 | 98.736 (4) | 98.50 (2) |
| <i>V</i> (Å ³) | 8360.8 (9) | 2101.6 (5) | 973.20 (11) | 1003.9 (6) |
| <i>T</i> (K) | 90 | 115 | 90 | 115 |
| <i>Z</i> | 16 | 4 | 2 | 2 |
| ρ_{calc} (g/cm ³) | 1.852 | 1.826 | 1.947 | 1.928 |
| abs coeff (mm ⁻¹) | 5.947 | 5.916 | 6.386 | 6.191 |
| $2\theta_{\text{max}}$ (°) | 71.2 | 68.4 | 82.2 | 52 |
| <i>R</i> indices ^a | 0.028 | 0.039 | 0.025 | 0.045 |
| wR2 = [<i>I</i> > 2 σ (<i>I</i>)] ^b | 0.063 | 0.095 | 0.069 | 0.091 |
| data/param | 19029/516 | 7997/253 | 12822/257 | 3910/255 |

$$^a R = (\sum ||F_o| - |F_c||) / \sum |F_o|; ^b wR2 = [\sum [w(F_o^2 - F_c^2)^2] / \sum [w(F_o^2)^2]]^{1/2}$$

Table 3.2. Selected Bonded and Non-bonded Distances (Å) and Bond Angles (deg) for Re(CO)₃(tmbSO₂-*N,N*-Me₂dien) (**1**), Re(CO)₃(tmbSO₂-*N'*-Medien) (**2**), Re(CO)₃(tmbSO₂-dien) (**3**), Re(CO)₃(DNS-dien) (**4**), and Re(CO)₃(tmbSO₂-dipn) (**5**)

| Re(CO) ₃ L complex | | | | | |
|-------------------------------|-------------------------|-------------|-------------|-------------|-----------|
| | 1 | 2 | 3 | 4 | 5 |
| bond distances | | | | | |
| Re–N1 | 2.2873 (19)/2.2880 (19) | 2.222 (4) | 2.2247 (15) | 2.204 (3) | 2.209 (7) |
| Re–N2 | 2.2065 (19)/2.2156 (18) | 2.232 (3) | 2.2172 (15) | 2.222 (3) | 2.249 (7) |
| Re–N3 | 2.2022 (18)/2.2007 (17) | 2.195 (3) | 2.1898 (15) | 2.166 (3) | 2.197 (6) |
| bond angles | | | | | |
| N1–Re–N2 | 78.87 (7)/78.15 (7) | 78.79 (13) | 78.24 (6) | 77.48 (11) | 86.4 (2) |
| N2–Re–N3 | 75.89 (7)/75.45 (7) | 76.62 (12) | 75.96 (5) | 74.42 (12) | 81.5 (2) |
| N1–Re–N3 | 86.79 (7)/86.75 (7) | 84.06 (14) | 84.06 (6) | 82.77 (12) | 84.7 (2) |
| N2–Re–C2 | 171.57 (9)/172.02 (8) | 173.97 (18) | 171.58 (7) | 171.86 (13) | 178.8 (3) |
| non-bonded distances | | | | | |
| N1 to N2 | 2.855/2.839 | 2.826 | 2.803 | 2.769 | 3.051 |
| N2 to N3 | 2.711/2.702 | 2.702 | 2.745 | 2.653 | 2.903 |
| C4 to C7 | 3.258/3.234 | 3.169 | 3.206 | 3.907 | |
| C4H to C7H | 2.156/2.112 | 1.991 | 2.027 | 3.927 | |
| C5 to C6 | 2.496/2.497 | 2.494 | 2.509 | 2.494 | |
| C5H to C6H | 2.256/2.269 | 2.289 | 2.291 | 2.361 | |

Typically, the Re–C(3) bond distances, involving the CO group trans to the sulfonamido group, are not significantly different from those of the other Re–CO bonds. Although we found that the aromatic rings facilitated our efforts to obtain crystals, these rings generally were not stacked. The closest distance between carbons of two benzene rings (3.69 Å) was found for Re(CO)₃(tmbSO₂-*N,N*-Me₂dien) (**1**), in which the two carbons were in the two slightly different

molecules of the asymmetric unit. This distance of 3.69 Å is too long to indicate stacking interactions between the aromatic rings.

3.3.1.1 Bond Lengths and Hybridization. The average Re–N bond length of ~2.2 Å (see Table 3.2 for selected bond lengths and angles of the sulfonamido complexes) found in the sulfonamido complexes is consistent with distances found in relevant Re(CO)₃ complexes containing dien, such as [Re(CO)₃(dien)]Br.⁹ The ~0.2 Å longer Re–N bonds in Re(CO)₃L compared to relevant Pt–N bonds (e.g., including terminal amines (2.063(9) and 2.063(10) Å, and the secondary amine, 2.002(8) Å, of [Pt(dien)Cl]Cl⁴⁴) are explained by the greater radius for Re(I). The Re–N1 bond (to the terminal amine) in Re(CO)₃(tmbSO₂-*N,N*-Me₂dien) (**1**) is significantly longer than the other Re–N bonds in **1** and the other sulfonamido compounds **2-5**. This lengthening is attributed to the bulkiness of the two methyl groups on N1 (for **1**) compared to the smaller H group in all other sulfonamido compounds.

The sp² N donors can form shorter Re–N bonds than can the sp³ N donors.^{14,45} Typical Re–sp² N bond lengths range from 2.14 to 2.18 Å, as measured in a number of Re structures containing Re–N bonds (aromatic sp² N, e.g., in pyridyl ligands), whereas a typical Re–sp³ N bond length is ~2.2 Å.^{10,11,14} The sp²-hybridized N3 should affect the S–N3–C7, S–N3–Re, and C7–N3–Re angles. However, although we have several structures to compare, the differences between molecules were generally consistent with expectations for Re–sp² N vs. Re–sp³ N centers, but are small and thus are masked by steric and solid-state effects.

The N–SO₂ bond lengths for the deprotonated sulfonamido group, between 1.561(3)-1.5902(18) Å for complexes **1** to **5**, are within the relatively broad range for N–SO₂ bonds (1.5-1.7 Å) found in deprotonated sulfonamides bound to a metal (e.g., Cu, Zn, and Ni).^{22,24}

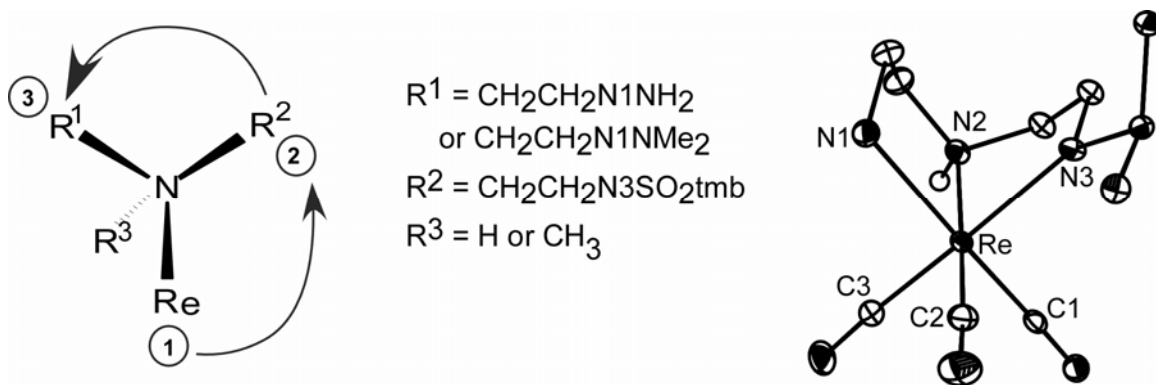


Figure 3.3. Absolute configuration. When the structure is viewed with the non-chelate ring substituent on N2 projecting away from the viewer (left), the absolute configuration at N2 (left) and Re (right) is designated to be S for a counterclockwise trace for the other N substituents (Re, R^1 , and R^2) according to higher priority as shown. When the trace is clockwise the absolute configuration is R.

3.3.1.2 Bite Angles. The N1 to N2 and N2 to N3 distances within five-membered chelate rings in the $\text{Re}(\text{CO})_3\text{L}$ complexes have a narrow range of values (Table 3.2). The distances of about 2.7 Å are similar to relevant distances in complexes with higher valent metal centers (e.g., Re(V) and Pt(II)) with shorter M–N bonds (~2 Å) (e.g., in $[\text{Pt}(\text{dien})\text{Cl}]\text{Cl}$ the N to N distances average about 2.72 Å).⁴⁴ The combination of the long Re–N bonds (compared to other M–N bonds) and typical N to N distances results in more acute values for N–Re–N chelate ring bite angles (less than 90°) and for trans N–Re–C angles (less than 180°) (see Table 3.2). For complexes with five-membered rings (**1-4**), the N2–Re–N3 bite angle (N3 is part of the sulfonamido group) is smaller (74.42°–76.62°) than the N1–Re–N2 bite angle (77.5°–78.9°). These values are significantly smaller than the respective bite angles, 81.5° and 86.4°, in $\text{Re}(\text{CO})_3(\text{tmbSO}_2\text{-dipn})$ (**5**), as expected from the large six-membered rings in this complex. Nevertheless, these angles for **5** are less than that (~89.5°) for $\text{Re}(\text{CO})_3(\text{N,N,N',N'-tetramethyl-1,3-propylenediamine})\text{Br}$.⁴⁶ Although the methyl groups cause the Re–N bonds to be very long

(2.3 Å), the complex also has a very long N to N distance (3.25 Å), explaining the large bite angle.

3.3.1.3 Chirality and Conformation of Chelate Rings. For **1**, **2**, and **3**, the pucker of the two chelate rings has different chirality. As mentioned, a different chirality for the pucker of each dien chelate ring is found most often.³⁰⁻³² Because the ligands in this study are unsymmetrical, we report chirality combinations by giving the pucker chirality of the ring with the terminal amine followed by that of the ring with the sulfonamido group. Also, we specify the absolute configuration because the unsymmetrical nature of the ligand creates asymmetric central nitrogen (N2) and Re centers. Specifically, this combination for **1-3** is $\lambda\delta$ for the enantiomer with the S absolute configuration (determined by the absolute configuration at N2, Figure 3.3). In contrast, both chelate rings of $\text{Re}(\text{CO})_3(\text{DNS-dien})$ (**4**) have pucker with the same chirality (both λ for the S configuration). This less-common situation with the same pucker chirality for both rings also occurs in the $\text{Re}(\text{CO})_3(\text{LANH})$ complexes.¹¹ The meridionally coordinated ligand in the pseudo square planar $\text{Pt}(\text{tmbSO}_2\text{-}N,N\text{-Me}_2\text{dien})\text{Cl}$ complex (work in progress), has the $\delta\lambda$ chirality combination (S absolute configuration at central N).

In an early study based on IR data, Schmidtke and Garthoff³³ determined that the $\delta\delta$ or $\lambda\lambda$ combination was the most favorable for facial coordination of diethylenetriamine in complexes of several metals (Cr, Co, Rh) and proposed that steric effects of the hydrogens of the ethylene chain would also favor the $\delta\delta$ or $\lambda\lambda$ combination. We compared selected non-bonded distances for **1-4** (Table 3.2) involving chelate ring carbons and hydrogens on these carbons projecting toward the center of the triangular face occupied by L^- . Whether the pucker chirality of the two chelate rings in a given complex is the same or different, the C5 to C6 (Figure 3.4) and C5H to C6H distances are not very different. In contrast, when the chirality of the two

chelate rings is the same, the C4 to C7 (Figure 3.4) and C4H to C7H distances are larger than when the chirality is different. For example, the C4 to C7 distance for **4** (same chirality) is 3.9 Å, whereas the respective distance for complexes **1-3** (different chirality) is ~ 2 Å.

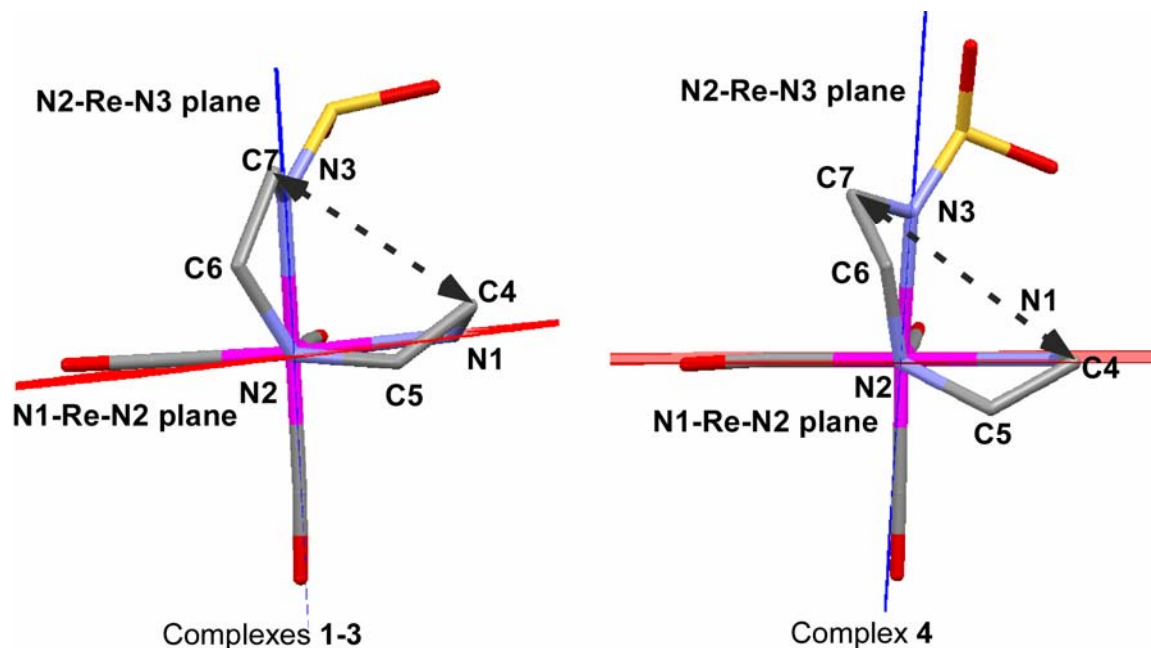


Figure 3.4. Illustration of the shorter C4 to C7 non-bonded distances for complexes **1-3** (different pucker chirality) compared to complex **4** (same pucker chirality). Note the similarity of the C5 to C6 non-bonded distances. Also shown are the position of C4 and C5 atoms relative to N1–Re–N2 plane (red line), and C6 and C7 atoms relative to N2–Re–N3 (blue line) plane.

It is obvious from Figure 3.4 that the distance from C4 to C7 is much larger when the pucker chirality is the same in both rings, as it is in complex **4**, compared to when the chirality is different. Our observations appear to support the early suggestion of Schmidtke and Garthoff,³³ and the $\delta\delta$ and $\lambda\lambda$ combinations should be favored. However, later literature surveys^{31,32} find that X-ray structures of complexes more frequently have different chirality in the two rings. In particular, one pca study on X-ray structures from the Cambridge Structural Database (CSD) showed that 74 fragments had the $\delta\lambda$ chirality combination, 16 fragments had the $\lambda\delta$ chirality combination, 18 fragments had $\delta\delta$ and 18 enantiomeric fragments had the $\lambda\lambda$ chirality

combination.³⁰ This study agreed with earlier pca studies.^{31,32} This overwhelming evidence for a predominance of structures with different pucker chirality is surprising, given that the distances between hydrogens or carbons on the two rings (Table 3.2, Figure 3.4) are clearly shorter than the sum of the van der Waals radii both for carbon (3.4 Å) and hydrogen (2.4 Å).⁴⁷ This proximity leads to steric repulsion between rings, as suggested by Schmidtke and Garthoff.³³ Additional studies are needed to clarify factors influencing pucker, but at this time it seems reasonable to assume in designing radiopharmaceuticals with the ^{99m}Tc(CO)₃ label that the pucker chirality of the rings will be different.

3.3.2 Solution Behavior

3.3.2.1 Trimethylbenzyl Group Rotation. In the X-ray structures of the tmb-sulfonamido complexes (**1**, **2**, **3**, and **5**) the 3 and 5 protons and the 2 and 6 methyl groups of the tmbSO₂ group are not equivalent. When modeling software is used to rotate the tmb group around the S–C bond, beginning with the solid-state structure of **3**, clashes are observed between the methyl groups and a CH₂ group of the chelate ring. For **3** the distance from C7 to C16 (of the CH₃ group in position 2) becomes as short as ~1.9 Å, much less than the sum of the van der Waals radii for two carbons (3.4 Å).⁴⁷ The resulting impediment to rotation about the S–C(tmb) bond should lead to well separated ¹H NMR signals. Indeed, in Re(CO)₃(tmbCO-dien), (tmbCO-dienH = *N*-[2-(2-aminoethylamino)-ethyl]-2,4,6-trimethylbenzamide, unpublished work), where the tmb is linked through a deprotonated amido instead of a sulfonamido group, the ¹H NMR signals of the 3 and 5 protons and the 2 and 6 methyl groups of the tmbCO group are separate, consistent with the expected slow rotation from a similar comparison using modeling software. However, even at low temperature, these tmb ¹H NMR signals are not resolved for the tmb-sulfonamido complexes. (The ¹H NMR spectrum of **1** (acetone-*d*₆) recorded at -90 °C has no

significant difference from the one recorded at 25 °C.) Further examination of the possible rotations around the S–C and N3–S bonds in the tmb-sulfonamido complexes reveals that concerted rotations about both these bonds can allow the tmb group to rotate more freely. In particular, if the N3–S bond is rotated by $\sim 56^\circ$, the tmb group can rotate freely around the S–C(tmb) bond, and the closest distance between C7 and C16 (of the CH₃ group in position 2) is ~ 3.2 Å; slight changes in bond angles should increase this distance.

The structures of **1-5** indicate considerable conformational freedom around the N–S bond. In contrast, the N–C bond in the relatively planar amido group has more double bond character than the N–S bond of the sulfonamido group. These features limit the CO group to only two favorable orientations, and in both orientations serious clashes are observed when the tmb group is rotated around the C–C(tmb) bond. In addition, the sulfonamido group has longer bonds (N–S and S–C) compared to the respective bonds (N–C and C–C) of the amido group in Re(CO)₃(tmbCO-dien). Therefore, we believe that synchronous rotations about the longer N–S and S–C bonds can explain the relatively free rotation of the tmb group, especially because the sulfonamide group is known to be in relatively faster rotation than the amide group.⁴⁸

3.3.2.2 NMR Characterization of Re(CO)₃L (L[−] = tmbSO₂-N,N-Me₂dien[−], tmbSO₂-N'-Medien[−], tmbSO₂-dien[−], DNS-dien[−] and tmbSO₂-dipn[−]). The Re(CO)₃L complexes were characterized by NMR spectroscopy (Table 3.3) in different solvents (DMSO-*d*₆, and acetone-*d*₆). For a given solvent, the shifts of the respective N1H₂ and N2H signals were similar in all complexes reported here. For complexes **2-5** with a terminal amino group, the NH signals of this group have a separation (Δ ppm) of between 1 to 2 ppm in DMSO-*d*₆. In general, terminal amino groups in Pt complexes have two separate signals with Δ ppm between 0.1 to 0.3.²⁶ Specifically, in DMSO-*d*₆ the amino groups of **2-5** all have one downfield-shifted NH signal with a normal

shift between 5.21 and 5.46 ppm, which is comparable to the shifts (5.11-5.66 ppm) of the respective NH signals of the NH₂ group in Pt(DNSH-dien)Cl and [Pt(dien)Cl]Cl.²⁶ The upfield-shifted NH signal of **2-5** is between 3.30-3.59 ppm, which is ~1.5 ppm abnormally upfield compared to the NH signals of Pt(II) complexes.

Table 3.3. Selected ¹H NMR Chemical Shifts (ppm) of Re(CO)₃(tmbSO₂-*N,N*-Me₂dien) (**1**), Re(CO)₃(tmbSO₂-*N'*Medien) (**2**), Re(CO)₃(tmbSO₂-dien) (**3**), Re(CO)₃(DNS-dien) (**4**), and Re(CO)₃(tmbSO₂-dipn) (**5**)^a

| Re(CO) ₃ L complex | | | | | |
|--------------------------------|----------|----------------------|----------|----------------------|----------------------|
| | 1 | 2^a | 3 | 4^a | 5^a |
| DMSO- <i>d</i> ₆ | | | | | |
| N1HB/Me | 2.96 | 3.30 | 3.48 | 3.59 | 3.30 |
| N1HA/Me | 2.96 | 5.46 | 5.22 | 5.21 | 5.25 |
| N2H | 6.77 | | 6.76 | 6.79 | 5.81 |
| acetone- <i>d</i> ₆ | | | | | |
| N1HB/Me | 3.10 | 3.87 | 3.98 | 4.09 | 4.00 |
| N1HA/Me | 3.11 | 4.94 | 4.75 | 4.77 | 4.66 |
| N2H | 6.17 | | 6.17 | 6.23 | 5.20 |

^a Assignments of the NH signals of **2**, **4** and **5** were made by analogy with signals for **3** assigned by COSY spectra.

An ¹H-¹H COSY experiment for **3** in combination with torsion angles allowed assignment of the NH signals. According to the Karplus equation,⁴⁹ when the torsion angle between two protons is 90°, no coupling is observed between the two protons (³*J* ≈ 0 Hz); a maximum ³*J* is observed (³*J* ≈ 9.5 Hz) when the torsion angle is 180°. For Re(CO)₃(tmbSO₂dien) (**3**), the NH₂ signals are correlated by a COSY cross-peak. Also, the downfield N1H signal is coupled to both C4H signals, whereas the upfield N1H signal is coupled to only one C4H signal.

The H1B–N1–C4–H4B torsion angle is $\sim 80^\circ$ for **3**, predicting a weak N1H1B–C4HB COSY cross-peak, whereas the H1A–N1–C4–H4A torsion angle is $\sim 157^\circ$ (close to 180°) for **3**, predicting a strong N1HA–C4HA COSY cross-peak. The H1B–N1–C4–H4A and H1A–N1–C4–H4B torsion angles are both similar for both compounds and the N1HB–C4HA and N1HA–C4HB cross-peaks were of similar size. Therefore, the downfield NH₂ signal can be identified as H1A (anti to the sulfonamido group) and the upfield NH₂ signal as H1B. The reasons that the NH1A signal for **2-5** has a normal shift and the N1HB signal has an unusually upfield shift are unclear, and further investigation is required.

3.3.2.3 Reactions of Sulfonamido Complexes. Under neutral conditions (DMSO-*d*₆/D₂O 250 μ L/550 μ L, pH = 7.70) no change was observed in the ¹H NMR signals of **3** even after 2 days. When a DMSO-*d*₆ solution of **3** (3 mM) was made basic (dien, 10 equiv) no change was observed in the ¹H NMR signals of **3**, even after the solution was heated at $\sim 60^\circ\text{C}$ for 16 h. Thus, **3** is stable under neutral and basic conditions, and a good ligand such as dien did not replace the tmbSO₂-dien ligand. Within minutes after the sulfonamido complex **3** (4 mM) was dissolved under acidic conditions (DMSO-*d*₆/1 M HNO₃, 600 μ L/20 μ L, final [H⁺] = 0.3 M), the ¹H NMR spectrum was recorded. The sulfonamide NH signal appeared, (7.53 ppm), the N2H signal shifted upfield (5.65 ppm), and the N1H signals moved downfield (5.41 and 4.08 ppm). Similar results were observed when complex **5** was dissolved in the same acidic conditions; a downfield sulfonamide signal appeared (7.76 ppm), the N2H signal (5.29 ppm) as well as the N1H signal (5.03 ppm) shifted upfield, the second N1H signal was under the water signal. These NMR data indicate that the sulfonamido nitrogen dissociates on protonation and the ligand is now bound to the *fac*-Re(CO)₃ moiety in a bidentate fashion through N1 and N2. Bidentate binding for the DNS-dienH ligand has been reported in the Pt(DNS-dienH)Cl₂ complex.²⁶

Comparisons of the ^1H NMR spectrum for the latter complex to those obtained for **3** and **5** under acidic conditions leave little doubt about the bidentate nature of the products. In these cases, the signal of the central NH is substantially upfield in the bidentate ligand compared to the tridentate ligand. A similar relationship of the NH shifts has been reported for $\text{Re}(\text{CO})_3$ complexes of an N_3 ligand.

3.4 Conclusions

The tridentate monoanionic sulfonamido ligands studied here bind to the *fac*- $\text{Re}(\text{CO})_3$ core, giving an inner coordination sphere with a neutral charge. In strongly acidic conditions the sulfonamido group dissociates with protonation, giving a monocationic inner coordination sphere. The sulfonamido group in these complexes can act as a potential anchor for bioconjugation, indicating that this class of tridentate ligands should be useful in the development of radiopharmaceuticals with a $^{99\text{m}}\text{Tc}(\text{CO})_3$ label. The dangling group connected through the sulfonamido bond undergoes free rotation on the NMR time scale, even at low temperature. Most complexes reported here have different chirality in each chelate ring, even though less severe steric clashes are expected when both chelate rings have the same chirality. We find in published and in our ongoing studies that the related amido complexes are much more difficult to synthesize, consistent with the paucity of related amido complexes in the literature. In contrast, the sulfonamido group has somewhat similar chemistry and more use of this group should be made in coordination chemistry.

3.5 References

1. Schwochau, K. *Angew. Chem., Int. Ed. Engl.* **1994**, 33, 2258-2267.
2. Schibli, R.; Schubiger, P. A. *Eur. J. Nucl. Med. Mol. Imaging* **2002**, 29, 1529-1542.
3. Jurisson, S. S.; Lydon, J. D. *Chem. Rev.* **1999**, 99, 2205-2218.

4. Bandoli, G.; Tisato, F.; Dolmella, A.; Agostini, S. *Coord. Chem. Rev.* **2006**, *250*, 561-573.
5. Alberto, R.; Schibli, R.; Schubiger, A. P.; Abram, U.; Pietzsch, H. J.; Johannsen, B. *J. Am. Chem. Soc.* **1999**, *121*, 6076-6077.
6. Alberto, R.; Schibli, R.; Egli, A.; Schubiger, P. A.; Abram, U.; Kaden, T. A. *J. Am. Chem. Soc.* **1998**, *120*, 7987-7988.
7. Schibli, R.; Alberto, R.; Abram, U.; Abram, S.; Egli, A.; Schubiger, P. A.; Kaden, T. A. *Inorg. Chem.* **1998**, *37*, 3509-3516.
8. Schibli, R.; La Bella, R.; Alberto, R.; Garcia-Garayoa, E.; Ortner, K.; Abram, U.; Schubiger, P. A. *Bioconjugate Chem.* **2000**, *11*, 345-351.
9. Mundwiler, S.; Candreia, L.; Hafliger, P.; Ortner, K.; Alberto, R. *Bioconjugate Chem.* **2004**, *15*, 195-202.
10. He, H.; Lipowska, M.; Xu, X.; Taylor, A. T.; Carlone, M.; Marzilli, L. G. *Inorg. Chem.* **2005**, *44*, 5437-5446.
11. He, H.; Lipowska, M.; Xu, X.; Taylor, A. T.; Marzilli, L. G. *Inorg. Chem.* **2007**, *46*, 3385-3394.
12. Lipowska, M.; Hansen, L.; Marzilli, L. G.; Taylor, A. *J. Nucl. Med.* **2001**, *42*, 259P-259P.
13. Lipowska, M.; Cini, R.; Tamasi, G.; Xu, X. L.; Taylor, A. T.; Marzilli, L. G. *Inorg. Chem.* **2004**, *43*, 7774-7783.
14. Wei, L.; Babich, J. W.; Ouellette, W.; Zubieta, J. *Inorg. Chem.* **2006**, *45*, 3057-3066.
15. Alves, S.; Paulo, A.; Correia, J. D. G.; Gano, L.; Smith, C. J.; Hoffman, T. J.; Santos, I. *Bioconjugate Chem.* **2005**, *16*, 438-449.
16. Alves, S.; Paulo, A.; Correia, J. D. G.; Domingos, A.; Santos, I. *J. Chem. Soc., Dalton Trans.* **2002**, 4714-4719.
17. Vitor, R. F.; Alves, S.; Correia, J. D. G.; Paulo, A.; Santos, I. *J. Organomet. Chem.* **2004**, *689*, 4764-4774.
18. Moura, C.; Fernandes, C.; Gano, L.; Paulo, A.; Santos, I. In *Technetium, Rhenium, and Other Metals in Chemistry and Nuclear Medicine*; Mazzi, U., Ed.; Padova, 2006; Vol. 7, pp 101-102.

19. Fernandes, C.; Gano, L.; Bourkoula, A.; Pirmettis, I.; Santos, I. In *Technetium, Rhenium, and Other Metals in Chemistry and Nuclear Medicine*; Mazzi, U., Ed.: Padova, 2006; Vol. 7, pp 487-490.
20. Taylor, A.; Eshima, D.; Fritzberg, A. R.; Christian, P. E. *J. Nucl. Med.* **1986**, *27*, 795-803.
21. Mundwiler, S.; Waibel, R.; Spingler, B.; Kunze, S.; Alberto, R. *Nucl. Med. Biol.* **2005**, *32*, 473-484.
22. Goodwin, J. M.; Olmstead, M. M.; Patten, T. E. *J. Am. Chem. Soc.* **2004**, *126*, 14352-14353.
23. Prodi, L.; Montalti, M.; Zaccheroni, N.; Dallavalle, F.; Folesani, G.; Lanfranchi, M.; Corradini, R.; Pagliari, S.; Marchelli, R. *Helv. Chim. Acta* **2001**, *84*, 690-706.
24. Congreve, A.; Katakya, R.; Knell, M.; Parker, D.; Puschmann, H.; Senanayake, K.; Wylie, L. *New J. Chem.* **2003**, *27*, 98-106.
25. Evans, C.; Henderson, W.; Nicholson, B. K. *Inorg. Chim. Acta* **2001**, *314*, 42-48.
26. Christoforou, A. M.; Marzilli, P. A.; Marzilli, L. G. *Inorg. Chem.* **2006**, *45*, 6771-6781.
27. Carvalho, M. F. N. N.; Consiglieri, A. C.; Duarte, M. T.; Galvao, A. M.; Pombeiro, A. J. L.; Herrmann, R. *Inorg. Chem.* **1993**, *32*, 5160-5164.
28. Heiden, Z. M.; Rauchfuss, T. B. *J. Am. Chem. Soc.* **2006**, *128*, 13048-13049.
29. Murata, K.; Ikariya, T.; Noyori, R. *J. Org. Chem.* **1999**, *64*, 2186-2187.
30. Harris, S. E.; Pascual, I.; Orpen, A. G. *J. Chem. Soc., Dalton Trans.* **2001**, 2996-3009.
31. Rodríguez, V.; Gutiérrez-Zorrilla, J. M.; Vitoria, P.; Luque, A.; Román, P.; Martínez-Ripoll, M. *Inorg. Chim. Acta* **1999**, *290*, 57-63.
32. Orpen, A. G. *Chem. Soc. Rev.* **1993**, *22*, 191-197.
33. Schmidtke, H. H.; Garthoff, D. *Inorg. Chim. Acta* **1968**, *2*, 351-356.
34. Konno, M.; Marumo, F.; Saito, Y. *Acta Crystallogr., Sect. B: Struct. Sci.* **1973**, *B 29*, 739-744.
35. Kobayashi, A.; Marumo, F.; Saito, Y. *Acta Crystallogr., Sect. B: Struct. Sci.* **1972**, *28*, 3591-3595.
36. Bond, A. M.; Hambley, T. W.; Snow, M. R. *Inorg. Chem.* **1985**, *24*, 1920.

37. Okiyama, K.; Sato, S.; Saito, Y. *Acta Crystallogr., Sect. B: Struct. Sci.* **1979**, *35*, 2389-2392.
38. Corradini, R.; Dossena, A.; Galaverna, G.; Marchelli, R.; Panagia, A.; Sartor, G. *J. Org. Chem.* **1997**, *62*, 6283-6289.
39. Christoforou, A. M.; Fronczek, F. R.; Marzilli, P. A.; Marzilli, L. G. *Inorg. Chem.* **2007**, *in press*.
40. Otwinowski, Z.; Minor, W. *Macromolecular crystallography, part A*; New York Academic Press: New York, 1997; Vol. 276.
41. Sheldrick, G. M. In *Program for Crystal Structure Solution and Refinement*; University of Gottingen: Gottingen, Germany, 1997.
42. Krapcho, A. P.; Kuell, C. S. *Synth. Commun.* **1990**, *20*, 2559-2564.
43. Marzilli, L. G.; Christoforou, A. M.; Maheshwari, V.; Adams, K. M.; Fronczek, F. R.; Marzilli, P. A. In *Technetium, Rhenium, and Other Metals in Chemistry and Nuclear Medicine*; Mazzi, U., Ed.; SGEEditoriali: Padova, 2006; Vol. 7, pp 3-8.
44. Britten, J. F.; Lock, C. J. L.; Pratt, W. M. C. *Acta Crystallogr., Sect. B: Struct. Sci.* **1982**, *B38*, 2148-2155.
45. Correia, J. D. G.; Domingos, A.; Santos, I.; Alberto, R.; Ortner, K. *Inorg. Chem.* **2001**, *40*, 5147-5151.
46. Horn, E.; Onai, S. Z. *Kristallogr. - New Cryst. Struct.* **2001**, *216*, 75-76.
47. Bondi, A. *J. Phys. Chem.* **1964**, *68*, 441-451.
48. Lyapkalo, I. M.; Reissig, H. U.; Schafer, A.; Wagner, A. *Helv. Chim. Acta* **2002**, *85*, 4206-4215.
49. Karplus, M. *J. Am. Chem. Soc.* **1963**, *85*, 2870-2871.

CHAPTER 4. *fac*-[Re(CO)₃L]⁺ COMPLEXES WITH N-CH₂-CH₂-X-CH₂-CH₂-N TRIDENTATE LIGANDS. SYNTHETIC, X-RAY CRYSTALLOGRAPHIC AND NMR SPECTROSCOPIC INVESTIGATIONS

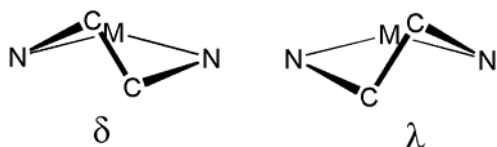
4.1 Introduction

Radiopharmaceuticals based on the *fac*-[^{99m}Tc(CO)₃]⁺ core are gaining extensive use because the *fac*-[^{99m}Tc(CO)₃(H₂O)₃]⁺ precursor can be conveniently generated.¹⁻⁴ Agents with a tridentately coordinated ligand (**L**) of the type, *fac*-[^{99m}Tc(CO)₃L], are more robust and have better pharmacokinetic profiles than agents bearing mono- or bidentate ligands.⁵ A recent straightforward preparation of aqueous solutions of the non-radioactive *fac*-[Re(CO)₃(H₂O)₃]⁺ precursor⁶ has made the synthesis of *fac*-[Re(CO)₃L] analogues convenient and allows simulation of the aqueous ^{99m}Tc synthetic chemistry.^{6,7} (Note: All specific complexes mentioned in this work have a facial geometry; therefore the *fac*- designation is used henceforth only for referring to a general class of compounds.) The most commonly employed **L** contain N, O, and S as donor atoms from amine,⁸⁻¹⁰ pyridyl,¹¹ carboxyl⁸ or thioether^{6,7} groups. Extensively characterized *fac*-[Re(CO)₃L] complexes of a series of symmetric and non-symmetric NNN or NSN ligands containing combinations of amine, pyrazolyl, and thioether donors are known.¹²⁻¹⁴ During the development of radiopharmaceutical renal agents, polyamino-polycarboxylic acid ligands have been investigated.^{8,15,16} At high pH amine group coordination is preferred, allowing for dangling carboxyl groups, which are important in high renal clearance. Other studies involving nitrogen, sulfur and oxygen donors have proposed that nitrogen donor ligands are better than sulfur donor ligands for *fac*-[Re(CO)₃L] complex formation.^{11,17}

The location in space of the chelate ring atoms is a key factor in designing *fac*-[^{99m}Tc(CO)₃L] agents because these atoms act as a fulcrum for the pendant groups. In turn, the position of the pendant group has a significant effect on the overall shape of the agent and hence

on its biological activity. For diethylenetriamine-type ligands bound to a metal center in a tridentate fashion, the pucker of the two five-membered chelate rings can have either δ or λ chirality (Chart 1), leading to four possible combinations of chelate ring chirality: $\delta\lambda$, $\lambda\delta$, $\lambda\lambda$, and $\delta\delta$. X-ray structures from the Cambridge Structural Database (CSD) of $[M(\text{dien})_2]^{n+}$ ($M = \text{Ni, Co, Zn, Cu, Cr, Rh, and Ir}$)¹⁸ and of $[M(\text{dien})\text{L}_n]^{19}$ complexes and $M(\text{dien})$ fragments²⁰ were analyzed by principal component analysis (pca) studies, and the $\delta\lambda$ and $\lambda\delta$ conformation combinations were found more frequently than $\delta\delta$ and $\lambda\lambda$ combinations. These results contradicted the Schmidtke and Garthoff²¹ suggestion that a *fac*-coordinated dien favors a $\delta\delta$ or $\lambda\lambda$ combination because of steric effects of the hydrogen atoms on the ethylene chains.

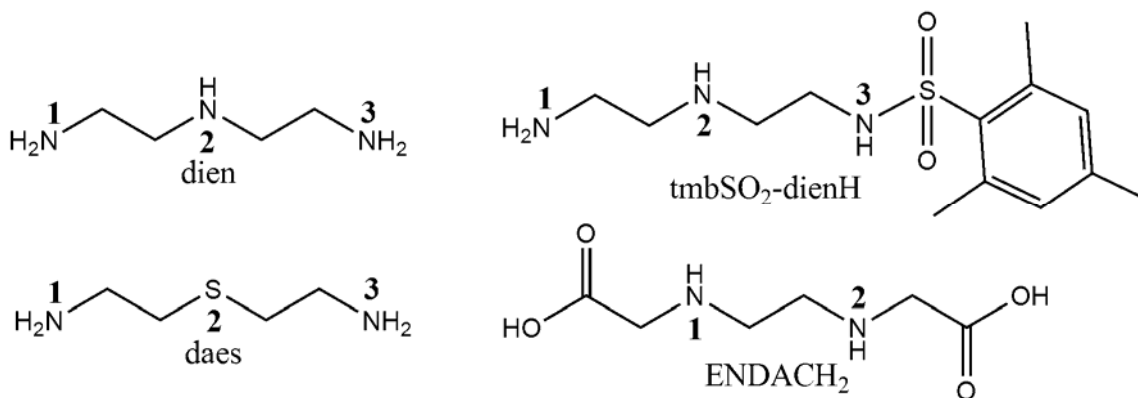
Chart 4.1



In a previous study¹⁰ we explored the chirality of the ligand pucker in a series of *fac*- $[\text{Re}(\text{CO})_3\text{L}]$ complexes with tridentate monoanionic ligands containing the diethylenetriamine moiety and an aromatic group connected through a sulfonamide group, such as *N*-[2-(2-aminoethylamino)ethyl]-2,4,6-trimethylbenzenesulfonamide (tmbSO₂-dienH) (Chart 2). (The H in the ligand names indicates the number of dissociable protons in the ligand and the complex.) Our results showed that *fac*-coordinated sulfonamido ligands have different chirality in each chelate ring more frequently than they have the same chirality, in agreement with the pca reports.^{19,20} In contrast, the two chelate rings in the Re analogue of $[\text{}^{99\text{m}}\text{Tc}(\text{CO})_3(\text{LANH})]$ agents (LANH₂ = lanthionine, a natural dicysteine-derived dipeptide linked through a common sulfur and exhibiting tridentate NSN binding) were found to have the same chirality.⁷ The ^{99m}Tc-tagged lanthionine agents were the first small *fac*- $[\text{}^{99\text{m}}\text{Tc}(\text{CO})_3\text{L}]$ agents reported to have been evaluated

in humans;²² thus, additional studies directed at gaining a more comprehensive assessment of conformation are warranted.

Chart 4.2



Normally the two protons of a primary amino group bound to a metal are magnetically inequivalent and are expected to have two separate ¹H NMR signals with similar shifts. The similarity in shifts is understandable because the inductive effects of the surrounding atoms on the amine nitrogen should be transmitted nearly equally to the protons. However, in several past studies we found unusually upfield- and (in fewer cases) downfield-shifted NH signals for *fac*-[Re(CO)₃L] complexes with terminal amino groups, (e.g., *fac*-[Re(CO)₃L] complexes of *S*-methyl-L-cysteine,⁶ methionine,⁶ *chiral*-LANH₂,⁷ and sulfonamide ligands such as tmbSO₂-dienH),¹⁰ whereas in some other cases (e.g., *fac*-[Re(CO)₃L] complexes of *meso*-LANH₂ and ethylenediamine-*N*-acetic acid, ENACH) the NH signals had similar shifts. The tridentate ligand in [Re(CO)₃(ENDAC)]⁻ (ENDACH₂ = ethylenediamine-*N,N'*-diacetic acid, Chart 2) binds through a terminal amine group (NHCH₂CO₂⁻) and a secondary NH group anchoring two chelate rings. Two isomers were crystallized, one with an *endo*-NH proton (pointing toward the carbonyl groups) and the other with an *exo*-NH proton (pointing away from the carbonyl groups).⁸ In this study, we have examined *fac*-[Re(CO)₃L] complexes with less elaborate prototypical ligands,

ones lacking large pendant substituents, in order to establish base-line behavior and thereby define parameters useful for assessing the effects of the pendant groups. These unusual shifts have led us to investigate the interaction of the complex with solvent as well as with the chloride anion. Such an investigation can be viewed as creating a very preliminary set of empirical observations relevant to the very difficult problem of predicting biodistribution, which is influenced by interactions of the agent with the solvent and the anions present in the media.

4.2 Experimental Section

4.2.1 Starting Materials

Diethylenetriamine (dien), *N,N,N'*-trimethyldiethylenetriamine (*N,N,N'*-Me₃dien), *N,N,N',N'',N''*-pentamethyldiethylenetriamine (*N,N,N',N'',N''*-Me₅dien), and Re₂(CO)₁₀ from Aldrich, *N,N*-dimethyldiethylenetriamine (*N,N*-Me₂dien) from Ames Laboratories, and *N*-methyl-2,2'-diaminodiethylamine (*N'*-Medien) and 2,2'-diaminodiethyl sulfide (daes) from TCI America were all used as received. [Re(CO)₃(H₂O)₃]OTf (OTf = trifluoromethanesulfonate)⁶ and [Pt(dien)Cl]Cl²³ were prepared by known methods.

4.2.2 Physical Measurements

4.2.2.1 NMR Spectroscopy. ¹H NMR spectra were recorded on either a 300 MHz or 400 MHz spectrometer. Peak positions are relative to TMS or solvent residual peak, with TMS as reference. All NMR data were processed with XWINNMR and Mestre-C software.

4.2.2.2 X-ray Data Collection and Structure Determination. Single crystals were placed in a cooled nitrogen gas stream at ~100 K on a Nonius Kappa CCD diffractometer fitted with an Oxford Cryostream cooler with graphite-monochromated Mo K α (0.71073 Å) radiation. Data reduction included absorption corrections by the multi-scan method, with HKL SCALEPACK.²⁴ All X-ray structures were determined by direct methods and difference Fourier

techniques and refined by full-matrix least squares, using SHELXL97.²⁵ All non-hydrogen atoms were refined anisotropically. All hydrogen atoms were visible in difference maps, but were placed in idealized positions. A torsional parameter was refined for each methyl group.

4.2.3 Synthesis of *fac*-[Re(CO)₃L]⁺

4.2.3.1 *fac*-[Re(CO)₃L]PF₆ and *fac*-[Re(CO)₃L]BF₄. An aqueous solution of [Re(CO)₃(H₂O)₃]OTf (10 mL, 0.1 mmol) was treated with **LH** (0.1 mmol). The pH was adjusted to ~6, and the reaction mixture was heated at reflux for 10 h. The reaction mixture was allowed to cool to room temperature and the volume was reduced to 5 mL by rotary evaporation. Solid NaPF₆ or NaBF₄ was added, and the white precipitate that formed was collected on a filter, washed with ether, and dried under vacuum. X-ray quality crystals were obtained from the filtrate or by slow evaporation from an acetone solution.

4.2.3.2 [Re(CO)₃(dien)]PF₆ (1a**).** Treatment of the [Re(CO)₃(H₂O)₃]⁺ (0.1 mmol) solution with dien (10 μL) as described above afforded [Re(CO)₃(dien)]PF₆ as a white powder (10 mg, 27% yield) after the addition of NaPF₆ (10 mg). The product was characterized by single crystal X-ray crystallography. ¹H NMR spectrum (ppm) in DMSO-*d*₆: 6.98 (b, 1H, NH), 5.43 (b, 2H, NH), 4.13 (b, 2H, NH), 2.83 (m, 4H, CH₂), 2.70 (m, 4H, CH₂).

4.2.3.3 [Re(CO)₃(dien)]BF₄ (1b**).** Treatment of the [Re(CO)₃(H₂O)₃]⁺ (0.1 mmol) solution with dien (10 μL) as described above afforded [Re(CO)₃(dien)]BF₄ as a white powder (9 mg, 19% yield) after the addition of NaBF₄ (10 mg). The product was characterized by single crystal X-ray crystallography. ¹H NMR spectrum (ppm) in DMSO-*d*₆: identical to that of **1a**.

4.2.3.4 [Re(CO)₃(*N'*-Medien)]₄(PF₆)₃(SO₃CF₃) (2**).** Treatment of the [Re(CO)₃(H₂O)₃]⁺ (0.1 mmol) solution with *N'*-Medien (12 μL) as described above afforded [Re(CO)₃(*N'*-Medien)]PF₆ as a white powder (17 mg, 44% yield) after the addition of NaPF₆ (10 mg). The

product was characterized by single crystal X-ray crystallography. ^1H NMR (ppm) spectrum in $\text{DMSO-}d_6$: 5.59 (b, 2H, NH), 4.17 (b, 2H, NH), 3.13 (s, 3H, CH_3), 3.08 (m, 2H, CH_2), 2.92-2.66 (m, 6H, CH_2).

4.2.3.5 $[\text{Re}(\text{CO})_3(N,N\text{-Me}_2\text{dien})]\text{PF}_6$ (3). Treatment of the $[\text{Re}(\text{CO})_3(\text{H}_2\text{O})_3]^+$ (0.1 mmol) solution with $N,N\text{-Me}_2\text{dien}$ (13 μL) as described above afforded $[\text{Re}(\text{CO})_3(N,N\text{-Me}_2\text{dien})]\text{PF}_6$ as a white powder (15 mg, 38% yield) after the addition of NaPF_6 (10 mg). The product was characterized by single crystal X-ray crystallography. ^1H NMR (ppm) spectrum in $\text{DMSO-}d_6$: 7.02 (b, 1H, NH), 5.68 (b, 1H, NH), 4.28 (b, 1H, NH), 3.06 (s, 3H, CH_3), 2.95 (m, 4H, CH_2), 2.76 (s, 3H, CH_3), 2.75 (m, 4H, CH_2).

4.2.3.5 *meso-exo*- $[\text{Re}(\text{CO})_3(N,N',N''\text{-Me}_3\text{dien})]\text{PF}_6$ (*meso-exo-4*). Treatment of the $[\text{Re}(\text{CO})_3(\text{H}_2\text{O})_3]^+$ (0.1 mmol) solution with $N,N',N''\text{-Me}_3\text{dien}$ (15 μL) as described above afforded the *meso-exo* isomer of $[\text{Re}(\text{CO})_3(N,N',N''\text{-Me}_3\text{dien})]\text{PF}_6$ as colorless crystals (9 mg, 22% yield) after the addition of NaPF_6 (10 mg). The product was characterized by single crystal X-ray crystallography. ^1H NMR (ppm) spectrum in $\text{DMSO-}d_6$: 5.22 (b, 2H, NH), 3.18 (s, 3H, CH_3), 2.97 (m, 4H, CH_2), 2.95 (d, 6H, CH_3), 2.77 (m, 2H, CH_2).

4.2.3.6 Solids with the $[\text{Re}(\text{CO})_3(N,N,N',N'',N'''\text{-Me}_5\text{dien})]^+$ cation. Treatment of the $[\text{Re}(\text{CO})_3(\text{H}_2\text{O})_3]^+$ (0.1 mmol) solution with $N,N,N',N'',N'''\text{-Me}_5\text{dien}$ (18 μL) as described above followed by addition of NaBF_4 (10 mg) or of NaPF_6 (10 mg) afforded, respectively, colorless crystals of $[\text{Re}(\text{CO})_3(N,N,N',N'',N'''\text{-Me}_5\text{dien})]\text{OTf}\cdot[\text{Re}(\text{CO})_3(\mu_3\text{-OH})_4]\cdot 3.35\text{H}_2\text{O}$ (**5**) from x-ray (10 mg, 36% yield) and a white powder of $[\text{Re}(\text{CO})_3(N,N,N',N'',N'''\text{-Me}_5\text{dien})]\text{PF}_6$ (**5a**) (15 mg, 23% yield). **5a** was recrystallized from acetone, and both crystal types were characterized by single crystal X-ray crystallography. ^1H NMR (ppm) spectrum of **5a** in $\text{DMSO-}d_6$: 3.23 (s, 6H,

CH₃), 3.21 (m, 4H, CH₂), 3.19 (s, 3H, CH₃), 3.06 (m, 2H, CH₂), 2.93 (m, 2H, CH₂), 2.81 (s, 6H, CH₃).

4.2.3.7 [Re(CO)₃(daes)]PF₆ (6). Treatment of the [Re(CO)₃(H₂O)₃]⁺ (0.1 mmol) solution with daes (10 μL) as described above afforded [Re(CO)₃(daes)]PF₆ as crystals (10 mg, 20% yield) after the addition of NaPF₆ (10 mg). The product was characterized by single crystal X-ray crystallography. ¹H NMR (ppm) spectrum in DMSO-*d*₆: 5.55 (b, 2H, NH), 4.22 (b, 2H, NH), 2.94 (m, 2H, CH₂), 2.75 (m, 6H, CH₂).

4.3 Results and Discussion

4.3.1 X-Ray Characterization

All complexes exhibit a distorted octahedral structure, with the three carbonyl ligands occupying one face. The remaining coordination sites are occupied by three amines for complexes **1** to **5** (Figure 4.1) and two amine nitrogens and a thioether sulfur for **6** (Figure 4.2). Crystal data and details of the structure refinement for complexes **1** to **6** are summarized in Table 4.1. The Re–N and Re–S bond lengths and the N–Re–N and S–Re–N angles (see Table 4.2 for selected bond lengths and angles) are comparable to values of relevant complexes containing amine and thioether groups.^{6,7,9,10} Because of the longer Re–S (~2.2 Å) and C–S (~1.8 Å) bonds compared to the Re–N (~2 Å) and C–N (~1.4 Å) bonds, the S–Re–N chelate ring bite angles and the N to S and C5 to C6 non-bonded distances are larger in **6** compared to the respective parameters in **1** to **5**, Table 4.3. However, near the terminal amines, the structure becomes more similar for the NSN vs. the NNN compounds as illustrated in Appendix C. The implication of this result is that pendant groups on terminal amines should project outward in a similar manner for both types of chelates, whereas pendant groups on the carbons adjacent to the donor atom anchoring the two chelate rings will project in a very different manner.

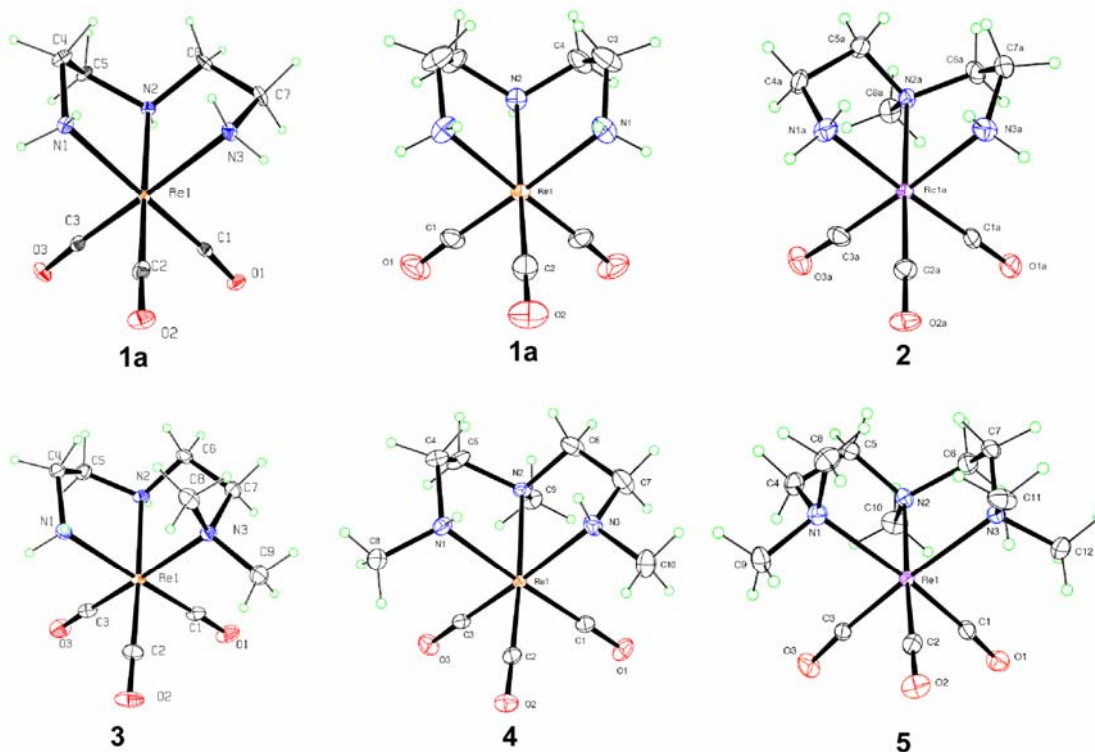


Figure 4.1. Perspective drawings of $[\text{Re}(\text{CO})_3(\text{dien})]\text{PF}_6$ (**1a**), $[\text{Re}(\text{CO})_3(\text{dien})]\text{BF}_4$ (**1b**), $[\text{Re}(\text{CO})_3(N'\text{-Medien})]_4(\text{PF}_6)_3(\text{SO}_3\text{CF}_3)$ (**2**), $[\text{Re}(\text{CO})_3(N,N\text{-Me}_2\text{dien})]\text{PF}_6$ (**3**), meso-exo- $[\text{Re}(\text{CO})_3(N,N',N''\text{-Me}_3\text{dien})]\text{PF}_6$ (**meso-exo-4**), $[\text{Re}(\text{CO})_3(N,N,N',N'',N'''\text{-Me}_5\text{dien})]\text{OTf} \cdot [\text{Re}(\text{CO})_3(\mu_3\text{-OH})]_4 \cdot 3.35\text{H}_2\text{O}$ (**5**) and $[\text{Re}(\text{CO})_3(N,N,N',N'',N'''\text{-Me}_5\text{dien})]\text{OTf}$ (**5a**). Counter ions are omitted for clarity. Thermal ellipsoids are drawn with 50% probability.

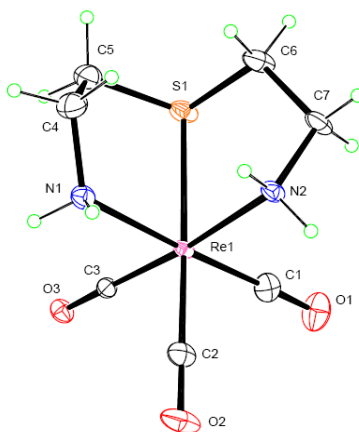


Figure 4.2. Perspective drawing of $[\text{Re}(\text{CO})_3(\text{daes})]\text{PF}_6$ (**6**). The counter ion is omitted for clarity. Thermal ellipsoids are drawn with 50% probability.

Table 4.1. Crystal Data and Structure Refinement for [Re(CO)₃(dien)]PF₆ (**1a**), [Re(CO)₃(dien)]BF₄ (**1b**), [Re(CO)₃(*N'*-Medien)]₄(PF₆)₃(SO₃CF₃) (**2**), [Re(CO)₃(*N,N*-Me₂dien)]PF₆ (**3**), *meso-exo*-[Re(CO)₃(*N,N',N''*-Me₃dien)]PF₆ (*meso-exo-4*), [Re(CO)₃(*N,N,N',N'',N''*-Me₅dien)]OTf·[Re(CO)₃(μ_3 -OH)]₄·3.35H₂O (**5**) and [Re(CO)₃(daes)]PF₆ (**6**)

| | 1a | 1b | 2 | 3 | <i>meso-exo-4</i> | 5 | 6 |
|--|---|--|--|--|---|---|--|
| formula | C ₇ H ₁₃ N ₃ O ₃ RePF ₆ | C ₇ H ₁₃ N ₃ O ₃ Re BF ₄ | 4(C ₈ H ₁₅ N ₃ O ₃ Re (CF ₃ O ₃ S)(PF ₆) ₃) | C ₉ H ₁₇ N ₃ O ₃ Re PF ₆ | C ₁₀ H ₁₉ N ₃ O ₃ ReP F ₆ | C ₁₂ H ₂₃ N ₃ ReS(CF ₃ O ₃ S)(C ₁₂ H ₄ O ₁₆ Re ₄)3.35(H ₂ O) | C ₇ H ₁₂ N ₂ O ₃ ReSPF ₆ |
| fw | 518.37 | 460.21 | 2133.70 | 436.43 | 560.45 | 588.50 | 535.42 |
| crystal system | orthorhombic | monoclinic | monoclinic | orthorhombic | monoclinic | triclinic | orthorhombic |
| space group | <i>Pna</i> 2 ₁ | <i>Cm</i> | <i>Pc</i> | <i>P</i> 2 ₁ 2 ₁ 2 ₁ | <i>P</i> 2 ₁ / <i>c</i> | <i>P</i> $\bar{1}$ | <i>Pna</i> 2 ₁ |
| <i>a</i> (Å) | 16.396 (2) | 9.566 (2) | 11.4999 (6) | 8.6289 (10) | 14.6964 (15) | 9.6358 (10) | 12.3209 (12) |
| <i>b</i> (Å) | 8.5554 (10) | 10.267 (3) | 11.6824 (9) | 12.0976 (13) | 13.2755 (12) | 15.0396 (15) | 8.3770 (10) |
| <i>c</i> (Å) | 9.7512 (12) | 8.010 (2) | 22.8706 (15) | 15.363 (2) | 17.146 (2) | 15.4932 (15) | 14.1136.7 (3) |
| β (°) | 90 | 125.730 (11) | 90.145 (4) | 90 | 91.165 (4) | 98.815 (5) | 90 |
| <i>V</i> (Å ³) | 1367.8 (3) | 638.6 (3) | 3072.6 (3) | 1603.7 (3) | 3344.5 (6) | 2208.2 (4) | 1456.7 (3) |
| <i>T</i> (K) | 90 | 173 | 90 | 90 | 90 | 90 | 90 |
| <i>Z</i> | 4 | 2 | 2 | 4 | 8 | 2 | 4 |
| ρ_{calc} (mg/m ³) | 2.517 | 2.393 | 2.306 | 2.263 | 2.226 | 2.710 | 2.441 |
| abs coeff (mm ⁻¹) | 9.084 | 9.570 | 8.096 | 7.754 | 7.440 | 13.80 | 8.670 |
| 2 θ_{max} (°) | 72.8 | 73.6 | 71.2 | 80.4 | 74.0 | 37.4 | 73.6 |
| <i>R</i> indices ^a | 0.027 | 0.047 | 0.036 | 0.048 | 0.042 | 0.036 | 0.054 |
| wR2 = [<i>I</i> > 2 σ (<i>I</i>)] ^b | 0.063 | 0.063 | 0.083 | 0.057 | 0.092 | 0.087 | 0.072 |
| data/param | 6131/192 | 2578/99 | 26464/804 | 9946/221 | 15639/452 | 16677/570 | 6569/192 |

$$^a R = (\sum ||F_o| - |F_c||) / \sum |F_o|; ^b wR2 = [\sum [w(F_o^2 - F_c^2)^2] / \sum [w(F_o^2)^2]]^{1/2}$$

Table 4.2. Selected Bond Distances (Å) and Angles (deg) for [Re(CO)₃(dien)]PF₆ (**1a**), [Re(CO)₃(dien)]BF₄ (**1b**), [Re(CO)₃(N'-Medien)]₄(PF₆)₃(SO₃CF₃) (**2**), [Re(CO)₃(N,N-Me₂dien)]PF₆ (**3**), *meso-exo*-[Re(CO)₃(N,N',N''-Me₃dien)]PF₆ (*meso-exo-4*), [Re(CO)₃(N,N,N',N'',N''-Me₅dien)]OTf·[Re(CO)₃(μ₃-OH)]₄·3.35H₂O (**5**) and [Re(CO)₃(daes)]PF₆ (**6**)^a

| | 1a | 1b | 2 | 3 | <i>meso-exo-4</i> | 5 | 6 ^a |
|----------------|------------|-----------|------------|-----------|-------------------|------------|--------------------------|
| bond distances | | | | | | | |
| Re–N1 | 2.238 (3) | 2.213 (8) | 2.197 (5) | 2.240 (2) | 2.233 (3) | 2.233 (5) | 2.243 (5) |
| Re–N2 | 2.201 (3) | 2.222 (8) | 2.250 (4) | 2.205 (2) | 2.238 (3) | 2.230 (4) | 2.4737 (10) ^a |
| Re–N3 | 2.244 (3) | | 2.215 (5) | 2.265 (2) | 2.220 (3) | 2.295 (4) | 2.226 (3) ^a |
| bond angles | | | | | | | |
| N1–Re–N2 | 77.50 (12) | 77.9 (3) | 78.84 (18) | 77.28 (9) | 79.62 (13) | 78.93 (16) | 80.15 (9) ^a |
| N2–Re–N3 | 76.56 (12) | 77.9 (3) | 77.20 (17) | 78.65 (9) | 77.91 (13) | 79.38 (15) | 81.06 (12) ^a |
| N1–Re–N3 | 87.14 (12) | 87.6 (6) | 87.8 (2) | 91.21 (9) | 86.70 (14) | 99.15 (16) | 85.7 (2) ^a |

^a For **6**, parameters involving S and N2 are placed in the rows containing N2 and N3 values, respectively.

The length of the Re–N bonds depends on the number and size of the substituents replacing the ligand NH groups. The Re–N bonds in complexes in which N1 and N3 have two methyl substituents (**3** and **5**) are significantly longer than any of the other Re–N bonds in **1** to **4**, in which N1, N2 and N3 have at most one methyl substituent replacing an H atom. This lengthening is attributed to the bulkiness of the methyl groups compared to the smaller H group. When the amine group has only one methyl group as a substituent, the Re–NHCH₃ bonds are numerically but not significantly longer than the Re–NH₂ bonds. For both the *endo* and *exo* Re(CO)₃(ENDACH) complexes (which crystallize as neutral complexes),⁸ the Re–NHCH₂COOH bonds are significantly longer than the Re–NH₂ bond of Re(CO)₃(ENAC)⁸ and the Re–NH₂ bonds of the complexes presented here. It is evident that a single methyl group substituent on an amine group probably does not have enough bulk to cause significant lengthening of Re–N bonds, whereas larger substituents (e.g., CH₂COOH in Re(CO)₃(ENDACH) in the solid state) or two substituents (e.g., two methyl groups in **3** and **5**) have sufficient bulk to make the Re–N bonds significantly longer.

In the solid state of **1b** and **6**, intermolecular hydrogen bonding is observed between the N2H or N1H₂ (*cf.* Figures 4.1 and 4.2 for numbering) and a carbonyl group of another molecule in the unit cell (N to O distance = 3.03 Å for **1b** and 2.96 Å for **6**). In complex **2**, hydrogen bonding is observed between the N1H₂ group and the OTf counter ion (N to O distance = 2.87 Å). No hydrogen bonding was observed in the solid-state structures of **1a**, **3**, **4** and **5**. In the [Re(CO)₃(dien)]Br crystal, intermolecular hydrogen bonding was observed between one Br[−] counter anion and a terminal NH₂ group and a central NH of two separate cations.⁹

4.3.1.1 [Re(CO)₃(dien)]X. The [Re(CO)₃(dien)]Br salt just mentioned was prepared from (NEt₄)₂[ReBr₃(CO)₃];⁹ however, because [Re(CO)₃(dien)]⁺ serves as an important prototypical

model complex for elaborated tridentate amine ligands, we synthesized the $[\text{Re}(\text{CO})_3(\text{dien})]^+$ complex by using $[\text{Re}(\text{CO})_3(\text{H}_2\text{O})_3]\text{OTf}$ as a precursor and crystallized both the PF_6^- (**1a**) and the BF_4^- (**1b**) salts. The dien ligand has different chirality in each chelate ring of $[\text{Re}(\text{CO})_3(\text{dien})]\text{Br}$ and $[\text{Re}(\text{CO})_3(\text{dien})]\text{BF}_4$, but the same chirality in $[\text{Re}(\text{CO})_3(\text{dien})]\text{PF}_6$. The crystal structure of $[\text{Re}(\text{CO})_3(\text{dien})]\text{Br}$ contains two similar but independent cations in the asymmetric unit. Overlaying of these two cations with $[\text{Re}(\text{CO})_3(\text{dien})]\text{BF}_4$ (**1b**) gave RMS = 0.0101 and 0.0125 (from overlaying the Re, N1, N2, and N3 atoms). In contrast, overlaying of these two cations with $[\text{Re}(\text{CO})_3(\text{dien})]\text{PF}_6$ (**1a**) gave RMS = 0.0384 and 0.0378. The fit between **1a** and $[\text{Re}(\text{CO})_3(\text{dien})]\text{Br}$ seems to be less good than that of **1b** and $[\text{Re}(\text{CO})_3(\text{dien})]\text{Br}$; such a finding can be explained because the chirality of the pucker of the two chelate rings is different in $[\text{Re}(\text{CO})_3(\text{dien})]\text{Br}$ and **1b**, whereas the chirality of the pucker of the two chelate rings is the same in $[\text{Re}(\text{CO})_3(\text{dien})]\text{PF}_6$ (**1a**).

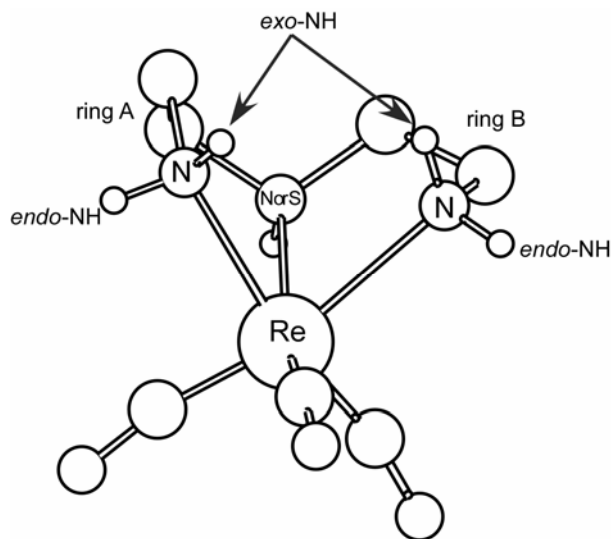


Figure 4.4. Designation of rings A and B when the structure shown in the ORTEP is viewed with the non-chelate ring substituent on N2 projecting away from the viewer. Also depicted are the *endo*-NH protons (pointing toward the carbonyl groups) and the *exo*-NH protons (pointing away from the carbonyl groups).

4.3.1.2 Solids with the $[\text{Re}(\text{CO})_3(\text{N},\text{N},\text{N}',\text{N}'',\text{N}''\text{-Me}_5\text{dien})]^+$ Cation. The structure of the $[\text{Re}(\text{CO})_3(\text{N},\text{N},\text{N}',\text{N}'',\text{N}''\text{-Me}_5\text{dien})]\text{PF}_6$ (**5a**) salt was disordered and did not allow analysis of the chirality of the chelate rings. Therefore, we chose to report the crystallographic data and to seek another salt for obtaining information on chelate ring pucker. We isolated and characterized $[\text{Re}(\text{CO})_3(\text{N},\text{N},\text{N}',\text{N}'',\text{N}''\text{-Me}_5\text{dien})]\text{OTf}\cdot[\text{Re}(\text{CO})_3(\mu_3\text{-OH})_4]\cdot 3.35\text{H}_2\text{O}$ (**5**). The $[\text{Re}(\text{CO})_3(\mu_3\text{-OH})_4]$ cubane-type cluster is well known to form in solutions of $[\text{Re}(\text{CO})_3(\text{H}_2\text{O})_3]^+$ at high pH.²⁶ In the unit cell, the carbonyl groups of the $[\text{Re}(\text{CO})_3(\text{N},\text{N},\text{N}',\text{N}'',\text{N}''\text{-Me}_5\text{dien})]^+$ cation are oriented toward the carbonyl groups of one of the Re atoms of the cluster with O to O non-bonding distances as close as 3.101 Å (Figure 4.3). The CSD contains many examples of this cluster but none have a co-crystallized Re(I) complex.

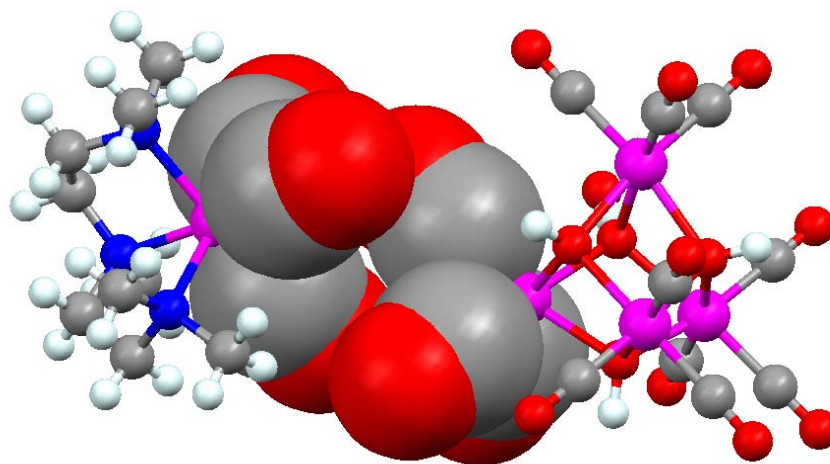


Figure 4.3. View of the relative orientations of the $[\text{Re}(\text{CO})_3(\text{N},\text{N},\text{N}',\text{N}'',\text{N}''\text{-Me}_5\text{dien})]^+$ cation and the neutral $[\text{Re}(\text{CO})_3(\mu_3\text{-OH})_4]$ molecule in the crystal of **5**, showing the interactions of the CO ligands depicted in the space filling-mode.

4.3.1.3 Chirality and Conformation of Chelate Rings. The two rings formed upon dien binding are designated as A (left ring) and B (right ring) in Figure 4.4. Throughout the text and in Table 4.3 we report chirality combinations by giving the pucker chirality of ring A followed

by that of ring B for the ORTEP structures shown in Figure 4.1. The two chelate ring puckers of **2** to **6** have the same chirality, as found for **1a**. Thus, only the **1b** structure has different pucker chirality in each of the two chelate rings, which is the combination most commonly observed. The case of both rings having the same pucker chirality was observed in the $[\text{Re}(\text{CO})_3(\textit{meso}\text{-LANH})]$ and $[\text{Re}(\text{CO})_3(\textit{chiral}\text{-LANH})]$ complexes⁷ and in the sulfonamido $[\text{Re}(\text{CO})_3(\text{DNSH-dien})]$ complex (DNSH-dienH = *N*-(2-((2-aminoethyl)amino)ethyl)-5-(dimethylamino)naphthalene-1-sulfonamide).¹⁰ The meridionally coordinated ligand in the pseudo square planar complex, $[\text{Pt}(\text{dien})\text{Cl}]\text{Cl}$,²⁷ has the $\lambda\delta$ chirality combination. It is obvious from Table 4.3 that the distance from C4 to C7 is much larger when the pucker chirality is the same in both rings, as it is in complexes **1a** and **2** to **6**, compared to when the ring chirality is different, as it is in **1b** and $[\text{Re}(\text{CO})_3(\text{dien})]\text{Br}$. The distances between hydrogens or carbons on the two rings when the rings have the same chirality are shorter than the sum of the van der Waals radii for both carbon (3.4 Å) and hydrogen (2.4 Å).²⁸ This proximity should cause steric repulsion between rings, as suggested by Schmidtke and Garthoff,²¹ and their suggestion that the $\delta\delta$ and $\lambda\lambda$ combinations should be favored in *fac* coordination of the dien ligand seems to be supported by our observation. However, pca analyses of X-ray structures of complexes^{18,19} find that complexes have different chirality in the two rings more frequently. These analyses were supported by a more recent pca study²⁰ showing that 74 fragments had the $\delta\lambda$ chirality combination, 16 fragments had the $\lambda\delta$ chirality combination, 18 fragments had $\delta\delta$ and 18 enantiomeric fragments had the $\lambda\lambda$ chirality combination.

Table 4.3. Selected non-bonded distances (ppm) for $[\text{Re}(\text{CO})_3(\text{dien})]\text{PF}_6$ (**1a**), $[\text{Re}(\text{CO})_3(\text{dien})]\text{BF}_4$ (**1b**), $[\text{Re}(\text{CO})_3(N'\text{-Medien})]_4(\text{PF}_6)_3(\text{SO}_3\text{CF}_3)$ (**2**), $[\text{Re}(\text{CO})_3(N,N\text{-Me}_2\text{dien})]\text{PF}_6$ (**3**), *meso-exo*- $[\text{Re}(\text{CO})_3(N,N',N''\text{-Me}_3\text{dien})]\text{PF}_6$ (**meso-exo-4**), $[\text{Re}(\text{CO})_3(N,N,N',N'',N'''\text{-Me}_5\text{dien})]\text{OTf}$, $[\text{Re}(\text{CO})_3(\mu_3\text{-OH})]_4 \cdot 3.35\text{H}_2\text{O}$ (**5**) and $[\text{Re}(\text{CO})_3(\text{daes})]\text{PF}_6$ (**6**)

| Complex | Pucker | C5H-C6H | C5-C6 | C4H-C7H | C4-C7 | N1-N2 or N1-S | N2-N3 or N2-S |
|--|------------------|---------|-------|---------|-------|---------------|---------------|
| $[\text{Re}(\text{CO})_3(\text{dien})]\text{Br}$ | $\lambda\delta$ | 2.290 | 2.514 | 2.119 | 3.279 | 2.790 | 2.788 |
| 1a | $\lambda\lambda$ | 2.389 | 2.478 | 4.009 | 3.963 | 2.754 | 2.780 |
| 1b | $\lambda\delta$ | 2.296 | 2.524 | 2.080 | 3.281 | 2.787 | |
| 2 | $\delta\delta$ | 2.487 | 2.461 | 4.272 | 3.999 | 2.812 | 2.797 |
| 3 | $\lambda\lambda$ | 2.485 | 2.493 | 4.153 | 4.029 | 2.775 | 2.833 |
| meso-exo-4 | $\lambda\lambda$ | 2.419 | 2.458 | 4.011 | 3.937 | 2.840 | 2.826 |
| 5 | $\delta\delta$ | 2.390 | 2.459 | 4.128 | 4.054 | 2.890 | 2.902 |
| 6 | $\lambda\lambda$ | 2.616 | 2.683 | 3.945 | 4.010 | 3.070 | 3.032 |

4.3.1.4 $[\text{Re}(\text{CO})_3(N,N',N''\text{-Me}_3\text{dien})]^+$ Isomers. Three $[\text{Re}(\text{CO})_3(N,N',N''\text{-Me}_3\text{dien})]^+$ isomers are conceivable (Figure 4.4). The protons on the terminal amines can be *endo* (near the carbonyl ligands in the basal plane) or *exo* (away from the carbonyl ligands), giving the *meso-endo* isomer (in which both protons point near the carbonyl ligands), the *chiral* isomer (in which one methyl group points toward and the other away from the carbonyl ligands), and the *meso-exo* isomer (in which both protons point away from the carbonyl ligands). The synthesis afforded a mixture of the *meso-exo* (**meso-exo-4**) and the *chiral* (**chiral-4**) isomers, but only the *meso-exo* isomer was isolated in crystalline form and characterized by X-ray crystallography.

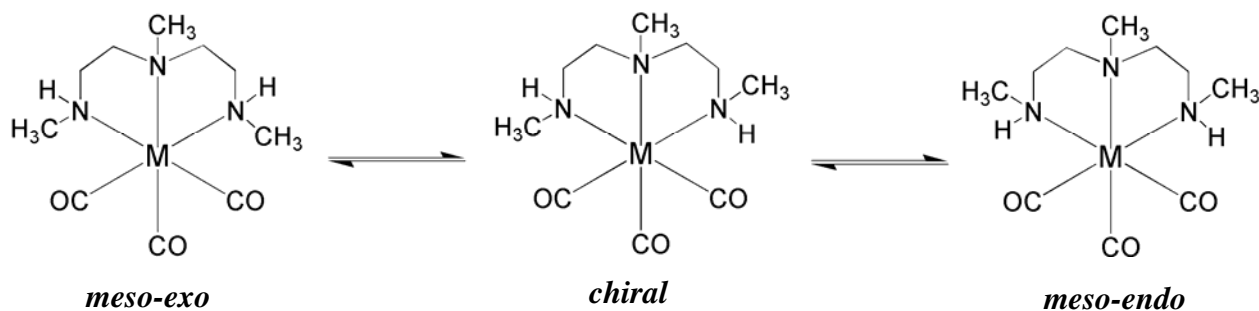


Figure 4.4. Possible isomers for $[\text{Re}(\text{CO})_3(\text{N},\text{N}',\text{N}''\text{-Me}_3\text{dien})]^+$.

4.3.2 NMR Spectroscopy

The $[\text{Re}(\text{CO})_3\text{L}]^+$ complexes reported here were characterized by NMR spectroscopy (Table 4.4) in different solvents (DMSO- d_6 , acetone- d_6 , acetonitrile- d_3). For a given solvent, the shifts of the respective terminal NH_2 and central NH signals were similar for all of these complexes. For complexes with terminal primary amino groups (**1**, **2**, **3**, and the previously reported $[\text{Re}(\text{CO})_3(\text{DNSH-dien})]^{10}$), the NH signals of this group have a chemical shift separation (Δ ppm) of 1 to 1.5 ppm in DMSO- d_6 . This separation is caused primarily by the fact that one of the NH signals is unusually upfield. The $[\text{Re}(\text{CO})_3(\text{chiral-LANH})]$ complex has two NH_2 groups; one group has NH signals with normal chemical shifts of 5.44 and 5.10 ppm (Δ ppm = 0.34) (similar to those of the $[\text{Re}(\text{CO})_3(\text{meso-LANH})]$ complexes), whereas the other NH_2 group has one unusually upfield (3.92 ppm) and one downfield (6.19 ppm) NH signal (Δ ppm = 2.2). In general, terminal amino groups in Pt and Pd complexes have two signals with a Δ ppm ranging from 0.1 to 0.4.^{29,30} Thus, in DMSO- d_6 the relatively downfield NH signal of the amino groups of **1** to **3** all fall in a normal shift range between 5.43 and 5.68 ppm, which is comparable to the shifts (5.11 to 5.66 ppm) of the respective NH signals of the NH_2 groups in $[\text{Pt}(\text{DNSH-dien})\text{Cl}]$ and $[\text{Pt}(\text{dien})\text{Cl}]\text{Cl}$.²⁹ Complexes **3** and **5**, which contain a dimethylamino group, have

two methyl signals with a separation of ~0.3 to 0.5 ppm in DMSO-*d*₆. In acetone-*d*₆ the separation of the methyl signals of **5** is 0.36 ppm, and both the chemical shift and the separation of the two methyl signals of the Me₅dien ligand were comparable to those of the [Pt(Me₅dien)I]₂Pt₂I₆ complex (Δ ppm = 0.17 ppm).³¹ The upfield shift effect appears to be generally limited to a particular type of NH group.

Table 4.4. Selected Chemical Shifts (ppm) for [Re(CO)₃(dien)]⁺ (**1**), [Re(CO)₃(*N'*-Medien)]₄(PF₆)₃(SO₃CF₃) (**2**), [Re(CO)₃(*N,N*-Me₂dien)]PF₆ (**3**), *meso-exo*-[Re(CO)₃(*N,N',N''*-Me₃dien)]PF₆ (**meso-exo-4**), *chiral*-[Re(CO)₃(*N,N',N''*-Me₃dien)]PF₆ (**chiral-4**), [Re(CO)₃(*N,N,N',N'',N''*-Me₅dien)]PF₆ (**5a**) and [Re(CO)₃(daes)]PF₆ (**6**) in various solvents

| <i>fac</i> -[Re(CO) ₃ L] ⁺ complex | | | | | | | |
|--|------|-----------------------|--------------------------------------|--|--|--|------|
| | dien | <i>N'</i> - Medien | <i>N,N</i> - Me ₂ dien | <i>N,N',N''</i> - Me ₃ dien <i>chiral</i> | <i>N,N',N''</i> - Me ₃ dien <i>meso-exo</i> | <i>N,N,N',N'',N''</i> - -Me ₅ dien | daes |
| DMSO- <i>d</i> ₆ | | | | | | | |
| <i>exo</i> -N1H/Me | 4.14 | 4.17 | 4.28/2.76 | 5.15/2.66 | 5.15 | 2.82 | 4.22 |
| <i>endo</i> -N1H/Me | 5.43 | 5.59 | 5.68/3.06 | 6.39/2.94 | 2.94 | 3.23 | 5.54 |
| N2H/Me | 6.98 | 3.13 | 7.02 | 3.15 | 3.18 | 3.19 | |
| acetone- <i>d</i> ₆ | | | | | | | |
| <i>exo</i> -N1H/Me | 4.40 | 4.37 | 4.27/3.01 | 4.74/2.99 | 5.02 | 3.08 | 4.41 |
| <i>endo</i> -N1H/Me | 5.22 | 5.42 | 5.54/3.30 | 6.03/3.21 | 3.21 | 3.44 | 5.43 |
| N2H/Me | 6.57 | 3.39 | 6.64 | 3.40 | 3.44 | 3.43 | |
| acetonitrile- <i>d</i> ₃ | | | | | | | |
| <i>exo</i> -N1H/Me | 3.35 | 3.39 | 3.25/2.73 | 3.85/2.72 | 4.06 | 2.84 | 3.39 |
| <i>endo</i> -N1H/Me | 4.32 | 4.43 | 4.58/3.13 | 5.04/3.02 | 3.03 | 3.27 | 4.37 |
| N2H/Me | 5.57 | 3.22 | 5.53 | 3.21 | 3.24 | 3.24 | |

4.3.2.1 *meso-exo*-[Re(CO)₃(*N,N',N''*-Me₃dien)]PF₆ (meso-exo-4**).** The isomerically pure *meso-exo*-[Re(CO)₃(*N,N',N''*-Me₃dien)]PF₆ salt in DMSO-*d*₆ has one set of ¹H NMR signals that included one relatively upfield NH signal (integrating to 2H) at 5.15 ppm (typical chemical shift

for secondary amine NH = ~7 ppm) and one methyl doublet (2.94 ppm). The spectrum remained unchanged even after two days. As mentioned above, a mixture of the *meso-exo* and the *chiral* isomer of $[\text{Re}(\text{CO})_3(\text{N},\text{N}',\text{N}''\text{-Me}_3\text{dien})]\text{PF}_6$ (ratio 1:1) was also isolated in the synthesis. The ^1H NMR spectrum ($\text{DMSO-}d_6$) of this mixture reveals a relatively downfield (6.39 ppm) small NH signal and a relatively upfield (5.15 ppm) large NH signal, which are respectively assigned to the *endo*-NH of *chiral*- $[\text{Re}(\text{CO})_3(\text{N},\text{N}',\text{N}''\text{-Me}_3\text{dien})]\text{PF}_6$ (***chiral-4***) and to overlapping signals of the *exo*-NH of ***chiral-4*** and the two *exo*-NH's of ***meso-exo-4***.

Sodium hydroxide was added to a $\text{DMSO-}d_6$ solution (5 mM, 600 μL) of the isolated *meso-exo*- $[\text{Re}(\text{CO})_3(\text{N},\text{N}',\text{N}''\text{-Me}_3\text{dien})]\text{PF}_6$ complex in order to catalyze isomerization at N1 or N3 of the *meso-exo* isomer (***meso-exo-4***) for conversion to other isomers. Upon addition of base ($\text{DMSO-}d_6/0.04\text{ M NaOH}$, 600 $\mu\text{L}/10\text{ }\mu\text{L}$, final $[\text{OH}^-] = 0.6\text{ mM}$), a new set of signals, belonging to a new isomer, appeared within minutes, and the NH signal of ***meso-exo-4*** shifted slightly downfield to 5.26 ppm. The intensities of the new signals continued to increase for ~2 h, and the final ratio of the signals of the new isomer to those of the *meso-exo* isomer was 1:2 (the sample was then monitored for 5 months and no further change was observed). The new set of signals included one downfield (6.39 ppm) and one relatively upfield (5.13 ppm) NH signal (for a secondary amine) and one relatively downfield (2.90 ppm) and one relatively upfield (2.66 ppm) methyl doublet signal. In a $^1\text{H-}^1\text{H}$ COSY NMR experiment (Appendix C), the relatively downfield NH signal gave a cross-peak to the relatively upfield methyl signal, while the relatively upfield NH signal gave a cross-peak to the relatively downfield methyl signal. These cross-peaks allowed the assignment of the new signals to the *chiral* isomer. By analogy to these assignments for the $[\text{Re}(\text{CO})_3(\text{N},\text{N}',\text{N}''\text{-Me}_3\text{dien})]^+$ isomers, we can assign the unusually upfield

NH signal in the spectra of complexes **1** to **3** to the *exo*-NH and the relatively downfield NH signal to the *endo*-NH.

Isomerization of a secondary amine group bound to a $\text{Re}(\text{CO})_3$ moiety at high pH was also observed for $[\text{Re}(\text{CO})_3(\text{ENDAC})]^-$.⁸ The terminal amine substituents are a proton and a dangling acetyl group (CH_2CO_2^-). Both isomers were isolated as the neutral $\text{Re}(\text{CO})_3(\text{ENDACH})$ complex. The NH signal of the *endo* isomer had a chemical shift at 5.84 ppm, whereas the *exo* isomer had an NH signal at 5.34 ppm in $\text{DMSO}-d_6$. Even though the difference in shift of the two signals is not so large as the difference in shift of the signals of **chiral-4**, the signal assignment is still consistent with our assignment that the *exo*-NH is the relatively upfield signal and the *endo*-NH is the relatively downfield signal.

As described above, upon addition of base to a $\text{DMSO}-d_6$ sample containing the pure *meso-exo* isomer of $[\text{Re}(\text{CO})_3(N,N',N''\text{-Me}_3\text{dien})]\text{PF}_6$ (**meso-exo-4**), the *exo*-NH signal of this starting **meso-exo-4** complex moved downfield, and isomerization at a terminal amine group occurred. When only H_2O was added to such a $\text{DMSO}-d_6$ sample, the **meso-exo-4** *exo*-NH signal did not shift. The effect of base was also studied with a $\text{DMSO}-d_6$ solution of the isolated non-crystalline mixture of $[\text{Re}(\text{CO})_3(N,N',N''\text{-Me}_3\text{dien})]\text{PF}_6$ (5 mM, 600 μL , **meso-exo-4** to **chiral-4** isomer ratio 1:1). Upon addition of base ($\text{DMSO}-d_6/0.1$ M NaOH, 600 $\mu\text{L}/10$ μL , final $[\text{OH}^-] = 1.7$ mM) only the *exo*-NH signal of **meso-exo-4** shifted downfield by ~ 0.5 ppm, whereas the NH signals of the **chiral-4** remained unchanged. In an essentially identical base addition experiment with $[\text{Re}(\text{CO})_3(\text{dien})]\text{PF}_6$, no NH signal shift change was observed.

The downfield shift observed for the *exo*-NH signal of the *meso-exo* isomer of $[\text{Re}(\text{CO})_3(N,N',N''\text{-Me}_3\text{dien})]\text{PF}_6$ upon addition of NaOH might be related to the fact that the two *exo*-NH groups of **meso-exo-4** project in the same direction and are relatively fixed in position

by the *endo*-Me groups. The **chiral-4** isomer has one *endo* and one *exo* NH and the NH's of $[\text{Re}(\text{CO})_3(\text{dien})]\text{PF}_6$ may not be at a fixed position because chelate rings are conformationally dynamic. These considerations lead us to suggest that the relatively selective shift effect for **meso-exo-4** could be the result of a hydroxo/water solvation cluster bridging the two NH's. In addition, the absence of such a cluster for the dien complex could be caused by the difference in solvation of the primary amines vs. the secondary amines in **meso-exo-4**.

4.3.2.2 Interaction of NH Protons with Cl^- Anion. Understanding the basis of the very different NH shifts of the *fac*- $[\text{Re}(\text{CO})_3\text{L}]$ complexes is a challenge. The shift difference we observe could arise from different exposure of the NH group to solvent. To test this possibility we added Cl^- to $\text{DMSO-}d_6$ solutions of representative complexes. This anion is known to form H-bonds in non-aqueous solvents. If any H-bonding occurs between NH and Cl^- , we would expect the NH signal to shift downfield.^{32,33}

Indeed, when Cl^- (1 to ~175 mM) was added to a solution of $[\text{Re}(\text{CO})_3(\text{dien})]^+$ (5 mM, $\text{DMSO-}d_6$), the upfield NH signal assigned to the *exo*-NH groups shifted downfield ($\Delta\delta \sim 1.2$ ppm) and reached a plateau at ~100 mM of Cl^- , whereas the downfield NH signals assigned to the *endo*-NH's and the central N2H remained relatively unchanged. Figure 4.5 shows the change in chemical shift ($\Delta\delta$) vs. the amount of Cl^- added. Even after the addition of more Cl^- , the *endo*-NH and the central N2H signals do not change significantly. In a similar experiment with $[\text{Re}(\text{CO})_3(\text{daes})]\text{PF}_6$ (**6**) (2.6 mM, $\text{DMSO-}d_6$), upon Cl^- addition the final $\Delta\delta$ observed was 0.9 ppm (at 100 mM) for the *exo*-NH signal giving a final shift of 5.13 ppm for the $[\text{Re}(\text{CO})_3(\text{daes})]^+$, Cl^- ion pair, a value relatively close to the 5.33 ppm observed for the *exo*-NH signal $[\text{Re}(\text{CO})_3(\text{dien})]^+$, Cl^- ion pair.

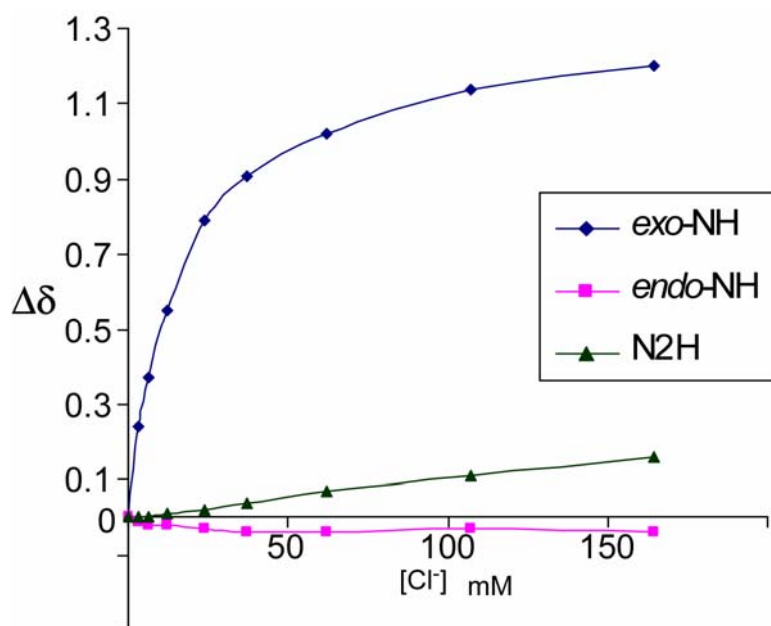


Figure 4.5. Change in chemical shift ($\Delta\delta$) of *exo*-NH, *endo*-NH and N2H signals of $[\text{Re}(\text{CO})_3(\text{dien})]\text{PF}_6$ upon addition of Cl^- in $\text{DMSO-}d_6$.

Behavior similar to that of $[\text{Re}(\text{CO})_3(\text{dien})]\text{PF}_6$ was observed when Cl^- (1 to ~175 mM) was added to a solution of an isomeric mixture of *meso-exo-4* and *chiral-4* (5 mM, $\text{DMSO-}d_6$). The *exo*-NH signal of *meso-exo-4* shifted downfield ($\Delta\delta$ between the final and initial chemical shifts ~1.5 ppm) and the relatively upfield *exo*-NH signal of *chiral-4* shifted downfield ($\Delta\delta \sim 1.1$ ppm). However, the relatively downfield *endo*-NH signal of *chiral-4* shifted downfield minimally ($\Delta\delta \sim 0.25$ ppm). Small changes were also observed in the CH signal of the ethylene chains.

Assuming that the final ion pair has a 1:1 ratio, we calculated from the data used to plot Figure 4.5 and figures in Appendix C equilibrium constants of $93 \pm 5 \text{ M}^{-1}$ for $[\text{Re}(\text{CO})_3(\text{dien})]^+, \text{Cl}^-$; $96 \pm 11 \text{ M}^{-1}$ for $[\text{Re}(\text{CO})_3(\text{daes})]^+, \text{Cl}^-$; and 56 ± 8 and $239 \pm 23 \text{ M}^{-1}$ for *chiral*- and *meso-exo*- $[\text{Re}(\text{CO})_3(N,N',N''\text{-Me}_3\text{dien})]^+, \text{Cl}^-$ ion pairs, respectively. The significantly higher binding constant for *meso-exo-4*, compared to those of **1** and *chiral*- $[\text{Re}(\text{CO})_3(N,N',N''\text{-}$

$\text{Me}_3\text{dien}]^+$ might be attributed to the fixed location of the *exo*-NH's of *meso-exo-4*, as discussed above.

In contrast to the above results, when Cl^- was added to solutions of complexes that have only one terminal NH_2 group, the *exo*-NH did not appear to interact strongly with Cl^- . Specifically, when as much as 80 mM Cl^- was added to 5 mM $\text{DMSO-}d_6$ solutions of $[\text{Re}(\text{CO})_3(\text{N,N-Me}_2\text{dien})]\text{PF}_6$ and of $\text{Re}(\text{CO})_3(\text{DNS-dien})$,¹⁰ no significant NH shift change was observed. Obviously, it is necessary to have at least one NH in each terminal amine group for H-bonding with Cl^- to occur. Only small changes in shift of the *endo*-NH, N2H and CH signals of **1**, *meso-exo-4*, and *chiral-4* were observed, and these are attributable to non-specific salt or ionic strength effects. On the other hand, the downfield shift by at least 1 ppm of the *exo*-NH signals of **1**, *meso-exo-4*, and *chiral-4*, attributable to NH - - Cl^- hydrogen bonding within the ion pair, correlates roughly with the magnitude of the equilibrium constant. These findings indicate that the Cl^- indeed interacts with the two *exo*-NH's in complexes **1**, *meso-exo-4*, and **6**, and are consistent with the ion pair model for H-bonding between Cl^- and the *exo*-NH's proposed in Figure 4.6. The distances of the Cl^- ion to N1 and N2, 3.258 and 3.289 Å, respectively, are very similar to the distances observed in the solid state for *fac*- $[\text{Pt}(\text{IV})(\text{dien})\text{Cl}_3]\text{Cl}$,³⁴ where the Cl^- counter ion was H-bonded to the two terminal NH_2 groups with Cl^- to N distances of 3.252 and 3.245 Å.

The effects of Cl^- addition were also examined for acetonitrile- d_3 solutions of $[\text{Re}(\text{CO})_3(\text{dien})]\text{PF}_6$ and a mixture of *meso-exo* and *chiral* $[\text{Re}(\text{CO})_3(\text{N,N',N''-Me}_3\text{dien})]\text{PF}_6$. However, a much lower concentration of Cl^- (20 mM) was necessary to reach the final downfield shifts. In this solvent, $\Delta\delta$ had a nearly linear dependence on Cl^- concentration (Appendix C); therefore, binding constants could not be calculated. The $\Delta\delta$ values for the *exo*-

NH signals of **1**, *meso-exo-4*, and *chiral-4* (~ 2.7 , 2.4 , and 2.7 ppm, respectively) in acetonitrile- d_3 were greater than in DMSO- d_6 and also greater than for the central N2H signal of $[\text{Re}(\text{CO})_3(\text{dien})]^+$ and the *endo*-NH signal of *chiral-4* ($\Delta\delta \sim 1.3$ and 1.4 ppm, respectively, in acetonitrile- d_3). The final "absolute" chemical shift values of these signals were similar in both DMSO- d_6 and acetonitrile- d_3 . This latter finding, combined with the observed larger $\Delta\delta$ values and apparently much larger binding constants for acetonitrile- d_3 , can be explained by the weaker hydrogen bonding of this solvent, an acetonitrile- d_3 property which allows better competition for the NH by Cl^- and which leads to a lower initial chemical shift for the NH signals.

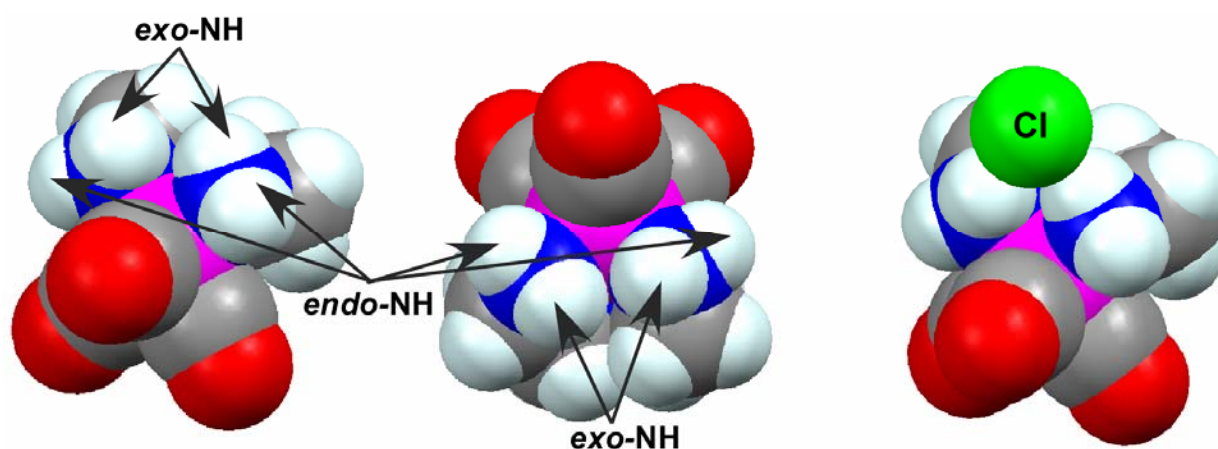


Figure 4.6. Space-filling model of **1a** showing the orientation of the *exo*-NH's and *endo*-NH's relative to the pocket formed by the ethylene chains of dien. Also shown (right) is the proposed positioning of the Cl^- ion for H-bonding between the *exo*-NH's.

To understand these interactions better, we examined dien complexes with the ligand coordinated in a meridional fashion. The ^1H NMR spectrum of $[\text{Pt}(\text{dien})\text{Cl}]\text{Cl}$ (DMSO- d_6 , 5 mM) exhibits two sets of three NH signals each: an upfield set for $[\text{Pt}(\text{dien})\text{Cl}]^+$ and a downfield set for $[\text{Pt}(\text{dien})(\text{Me}_2\text{SO}-d_6)]^{2+}$.²⁹ Upon Cl^- (~ 100 mM) addition to a such a solution, the $[\text{Pt}(\text{dien})(\text{Me}_2\text{SO})]^{2+}$ NH signals shifted downfield (from 6.43 and 6.52 ppm to 6.78 and 6.86

ppm, respectively, for the terminal NH₂ groups and from 7.10 to 8.66 ppm ($\Delta\delta \sim 1.6$ ppm) for the central NH group). In contrast, for [Pt(dien)Cl]⁺, the two terminal NH₂ signals (5.43 and 5.51 ppm) did not change, and only the central NH signal shifted (from 7.10 to 7.78 ppm, $\Delta\delta \sim 0.7$ ppm). The X-ray structure of [Pt(dien)Cl]Cl (meridional coordination of dien), (unpublished data) suggests that the central NH is somewhat shielded from the solvent by the two ethylene chains (*cf.* figure in Appendix C). Consequently, the central NH is not readily available to form H-bonds with DMSO-*d*₆. Upon Cl⁻ addition, we believe that the obstructed central NH forms H-bonds with the relatively small Cl⁻ ion (*vs.* the bulkier DMSO-*d*₆). In contrast, analysis of the X-ray structure of *fac*-[Re(CO)₃(dien)]⁺ suggests that the central NH will be relatively exposed to the solvent (the two ethylene chains project away from the central NH, *cf.* figure in Appendix C). Thus, the central NH is available for H-bonding with the solvent, disfavoring interaction with the Cl⁻ ion. The insignificant change in chemical shift of the terminal NH₂ signals in [Pt(dien)Cl]⁺ is attributed to the presence of the chloro ligand creating a localized negatively charged region inhibiting Cl⁻ ion interaction near the terminal NH₂ groups. Also, in [Pt(dien)(Me₂SO)]²⁺ the bulky Me₂SO ligand prevents strong interaction of the Cl⁻ ion with the terminal NH₂ groups. Thus, contrary to what is observed for the *fac*-[Re(CO)₃L] complexes, interaction of Cl⁻ ion at the central NH group of Pt(dien) complexes is more favorable than at the terminal amines.

From the locations of both the *endo*- and *exo*-NH protons of the terminal amine of the different *fac*-[Re(CO)₃L] structures, we believe that the *exo*-NH's are somewhat protected from the solvent, whereas the *endo*-NH's seem to be more exposed to the solvent. Space-filling models of the X-ray structures show that the *exo*-NH points slightly toward the pocket formed by the ethylene chains of L (Figure 4.6). In contrast, the *endo*-NH, which points toward the carbonyl ligands and away from any L bulk, appears to be more exposed to the solvent. The X-ray

structure of [Pt(dien)Cl]Cl (unpublished data) indicates that the *exo* and *endo* NH protons should have a similar exposure to solvent, explaining the much smaller difference in the chemical shift of the two NH signals compared to the difference observed for *fac*-[Re(CO)₃L] complexes.

4.4 Conclusions

The simple prototypical ligands studied here bind to the *fac*-Re(CO)₃ core in tridentate mode, giving cations of the *fac*-[Re(CO)₃L]⁺ type. Most complexes reported here have the same chirality in each chelate ring, a finding in accord with our observation that less severe steric clashes between rings would occur when both rings have the same chirality. However, our results are surprisingly in contrast in the light of literature surveys, which show that complexes of the *fac*-M(dien) type with different chirality occur more often. An interesting finding was the downfield shifting of the *exo*-NH's of the *meso-exo*-[Re(CO)₃(*N,N',N''*-Me₃dien)]PF₆ complex upon addition of base. This effect might be caused by the formation of a hydroxo/water solvation bridge between the two *exo*-NH's, which probably are in a relatively fixed position in this *meso-exo* isomer. Addition of Cl⁻ caused downfield shifting of the relatively upfield *exo*-NH's of [Re(CO)₃(dien)]⁺ and two isomers of [Re(CO)₃(*N,N',N''*-Me₃dien)]⁺, suggesting that hydrogen bonding occurs between the *exo*-NH's and the Cl⁻ ion. This finding indicates that the *exo*-NH's are protected from the solvent environment and therefore have relatively upfield chemical shifts compared to the *endo*-NH's. The interactions of the various ligand groups in tracer metal complexes influence biodistribution and must be understood in order to improve methods of targeting such tracers. NMR methods are among the best approaches for assessing interactions of tracer complexes in solution. The types of analysis that we have presented can be viewed as being in their infancies. Some of the unusual and as yet incompletely explained NMR shifts of Re analogues of ^{99m}Tc tracers very probably reflect differences in solvation of the various parts

of the bound ligands. We believe that more investigations of this type will be needed for rational design of tracers.

4.5 References

1. Alberto, R.; Schibli, R.; Egli, A.; Schubiger, P. A.; Abram, U.; Kaden, T. A. *J. Am. Chem. Soc.* **1998**, *120*, 7987-7988.
2. Alberto, R.; Schibli, R.; Schubiger, A. P.; Abram, U.; Pietzsch, H. J.; Johannsen, B. *J. Am. Chem. Soc.* **1999**, *121*, 6076-6077.
3. Alberto, R.; Schibli, R.; Waibel, R.; Abram, U.; Schubiger, A. P. *Coord. Chem. Rev.* **1999**, *192*, 901-919.
4. Schibli, R.; Alberto, R.; Abram, U.; Abram, S.; Egli, A.; Schubiger, P. A.; Kaden, T. A. *Inorg. Chem.* **1998**, *37*, 3509-3516.
5. Schibli, R.; La Bella, R.; Alberto, R.; Garcia-Garayoa, E.; Ortner, K.; Abram, U.; Schubiger, P. A. *Bioconjugate Chem.* **2000**, *11*, 345-351.
6. He, H.; Lipowska, M.; Xu, X.; Taylor, A. T.; Carlone, M.; Marzilli, L. G. *Inorg. Chem.* **2005**, *44*, 5437-5446.
7. He, H.; Lipowska, M.; Xu, X.; Taylor, A. T.; Marzilli, L. G. *Inorg. Chem.* **2007**, *46*, 3385-3394.
8. Lipowska, M.; Cini, R.; Tamasi, G.; Xu, X. L.; Taylor, A. T.; Marzilli, L. G. *Inorg. Chem.* **2004**, *43*, 7774-7783.
9. Mundwiler, S.; Candraia, L.; Hafliger, P.; Ortner, K.; Alberto, R. *Bioconjugate Chem.* **2004**, *15*, 195-202.
10. Christoforou, A. M.; Fronczek, F. R.; Marzilli, P. A.; Marzilli, L. G. *Inorg. Chem.* **2007**, *Accepted*.
11. Lazarova, N.; Babich, J. W.; Valliant, J.; Schaffer, P.; James, S.; Zubieta, J. *Inorg. Chem.* **2005**, *44*, 6763-6770.
12. Alves, S.; Paulo, A.; Correia, J. D. G.; Gano, L.; Smith, C. J.; Hoffman, T. J.; Santos, I. *Bioconjugate Chem.* **2005**, *16*, 438-449.
13. Alves, S.; Paulo, A.; Correia, J. D. G.; Domingos, A.; Santos, I. *J. Chem. Soc., Dalton Trans.* **2002**, 4714-4719.

14. Vitor, R. F.; Alves, S.; Correia, J. D. G.; Paulo, A.; Santos, I. *J. Organomet. Chem.* **2004**, *689*, 4764-4774.
15. Lipowska, M.; He, H.; Xu, X.; Taylor, A. T.; Marzilli, P. A.; Marzilli, L. G. **in preparation**.
16. Lipowska, M.; He, H.; Xu, X.; Marzilli, L. G.; Taylor, A. *J. Labelled Compd. Radiopharm.* **2005**, *48*, S258.
17. Banerjee, S. R.; Levadala, M. K.; Lazarova, N.; Wei, L.; Valliant, J. F.; Stephenson, K. A.; Babich, J. W.; Maresca, K. P.; Zubieta, J. *Inorg. Chem.* **2002**, *41*, 6417-6425.
18. Rodríguez, V.; Gutiérrez-Zorrilla, J. M.; Vitoria, P.; Luque, A.; Román, P.; Martínez-Ripoll, M. *Inorg. Chim. Acta* **1999**, *290*, 57-63.
19. Orpen, A. G. *Chem. Soc. Rev.* **1993**, *22*, 191-197.
20. Harris, S. E.; Pascual, I.; Orpen, A. G. *J. Chem. Soc., Dalton Trans.* **2001**, 2996-3009.
21. Schmidtke, H. H.; Garthoff, D. *Inorg. Chim. Acta* **1968**, *2*, 351-356.
22. Lipowska, M.; He, H. Y.; Malveaux, E.; Xu, X. L.; Marzilli, L. G.; Taylor, A. *J. Nucl. Med.* **2006**, *47*, 1032-1040.
23. Annibale, G.; Brandolisio, M.; Pitteri, B. *Polyhedron* **1995**, *14*, 451-453.
24. Otwinowski, Z.; Minor, W. *Macromolecular crystallography, part A*; New York Academic Press: New York, 1997; Vol. 276.
25. Sheldrick, G. M. In *Program for Crystal Structure Solution and Refinement*; University of Gottingen: Gottingen, Germany, 1997.
26. Egli, A.; Hegetschweiler, K.; Alberto, R.; Abram, U.; Schibli, R.; Hedinger, R.; Gramlich, V.; Kissner, R.; Schubiger, A. P. *Organometallics* **1997**, *16*, 1833-1840.
27. Britten, J. F.; Lock, C. J. L.; Pratt, W. M. C. *Acta Crystallogr., Sect. B: Struct. Sci.* **1982**, *B38*, 2148-2155.
28. Bondi, A. *J. Phys. Chem.* **1964**, *68*, 441-451.
29. Christoforou, A. M.; Marzilli, P. A.; Marzilli, L. G. *Inorg. Chem.* **2006**, *45*, 6771-6781.
30. Alul, R.; Cleaver, M. B.; Taylor, J.-S. *Inorg. Chem.* **1992**, *31*, 3636-3646.
31. Cini, R.; Intini, F. P.; Maresca, L.; Pacifico, C.; Natile, G. *Eur. J. Inorg. Chem.* **1998**, 1305-1312.

32. Marzilli, L. G.; Chang, C.-H.; Caradonna, J. P.; Kistenmacher, T. J. *Adv. Mol. Relax. Interact. Processes* **1979**, *15*, 85-101.
33. Chang, C.-H.; Marzilli, L. G. *J. Am. Chem. Soc.* **1974**, *96*, 3656-3657.
34. Britten, J. F.; Lock, C. J. L. *Acta Crystallogr., Sect. B: Struct. Sci.* **1980**, *B36*, 2958-2963.

CHAPTER 5. CONCLUSIONS

In general the sulfonamide ligands proved to be excellent ligands for both the Pt(II) and *fac*-Re(CO)₃ metal centers. The DNSH-dienH ligand can act as a bidentate, tridentate, or quadridentate ligand in Pt(II) complexes, and the tmbSO₂-dien and tmbSO₂-dipn ligands can act as bidentate or tridentate in *fac*-[Re(CO)₃L] complexes. In general high pH is necessary for the sulfonamide group to deprotonate and bind to the metal center, whereas in low pHs only the amine groups of the tridentate ligand bind.

We achieved the synthesis of a new Pt(II) complex, Pt(DNSH-dien)Cl, which increases the reactivity toward 5'-GMP relative to that toward met. Therefore, such a complex might act as a model for the development of a new class of Pt(II) drugs with lower reactivity toward S-containing biomolecules and consequently less toxicity than cisplatin.

The sulfonamido group in the *fac*-[Re(CO)₃L] (L = sulfonamide ligands) complexes can act as a potential anchor for bioconjugation, while giving complexes with neutral net charge, indicating that this class of tridentate ligands should be useful in the development of radiopharmaceuticals with a ^{99m}Tc(CO)₃ label.

The NMR investigation of *fac*-[Re(CO)₃L] complexes with the simple NNN and NSN prototypical ligands provided insight into the basis of the existence of one unusual NH signal in several *fac*-[Re(CO)₃L] complexes with terminal amino groups. We were able to assign the relatively upfield NH signal to the *exo*-NH proton and we believe that this unusual upfield chemical shift might be attributed to its limited exposure to the solvent environment.

APPENDIX A. *fac*-[Re(CO)₃L] COMPLEXES CONTAINING TRIDENTATE MONOANIONIC LIGANDS (L⁻) HAVING A TERMINAL AMIDO AND TWO AMINE LIGATING GROUPS*

A.1 Introduction

Technetium-99m (^{99m}Tc) is the most widely used diagnostic radionuclide in nuclear medicine.¹⁻⁴ The [^{99m}Tc(V)O]³⁺ core has been used most predominantly, but recently the development of the advantageous [^{99m}Tc(CO)₃(H₂O)₃]⁺ precursor has opened new directions for radiolabeling.⁵⁻⁷ Schibli et al. showed that agents with the *fac*-^{99m}Tc(I)(CO)₃⁺ core bearing a tridentate coordinated ligand are more robust and have better pharmacokinetic profiles than agents bearing bidentate ligands.⁸ Frequently used chelating ligands contain N, O, or S donor atoms in groups such as carboxyls,⁹ amines,^{10,11} nitrogen heterocycles,¹² and thioethers.^{13,14} A neutral metal-containing label is most useful in the development of small (~5 kDa) metal nuclide radiopharmaceuticals for bioconjugation to hormones, small peptides, etc. because such neutral labels are most likely to preserve the biological properties of the tagged species.¹⁵ Complexes made from the non-radioactive *fac*-[Re(CO)₃(H₂O)₃]⁺ analogue of *fac*-[^{99m}Tc(CO)₃(H₂O)₃]⁺ generally provide the necessary background to define the chemistry of the ^{99m}Tc agents.¹³ A neutral labeling unit can best be achieved by using monoanionic tridentate ligands. The most common negative donor, the carboxyl group, does not allow bioconjugation, however. We recently reported a series of *fac*-[Re(CO)₃(NNN)] complexes of monoanionic tridentate ligands with three nitrogen donors (NNN) containing the seldom-used sulfonamido group.¹⁶ In the names of the NNN ligands (**LH**) used here (*cf.* caption of Figure 4.1), the **H**'s designate the sulfonamide and amide NH proton that is absent in the facially coordinated deprotonated bound

* Submitted to the Journal of Chemical Crystallography: Christoforou, A. M., Marzilli, P. A., Fronczek, F. R., Marzilli, L. G., "*fac*-Re(CO)₃L Containing Tridentate Monoanionic Ligands (L⁻) Having a Terminal Amido Group and Two Amine Ligating Groups"

L^- . The sulfonamido group offers diverse chemistry and allows bioconjugation through the terminal ligating group. The amido group is very commonly used in bioconjugation chemistry because of its significance in peptides. Although the amido group has been widely used as a ligating group in $M(V)O^{3+}$ radiopharmaceuticals,¹⁷ very little use of this group has been made for $fac\text{-}^{99m}\text{Tc}(\text{I})(\text{CO})_3$ agents, especially as a terminal ligating group.¹⁸ Herein, we describe the $fac\text{-}[\text{Re}(\text{CO})_3\text{L}]$ complexes formed by $fac\text{-}[\text{Re}(\text{CO})_3(\text{H}_2\text{O})_3]^+$ with $\text{tmbCO-}N,N\text{-Me}_2\text{dienH}$ and tmbCO-dienH , containing the monoanionic deprotonated amido ligand bound in a tridentate fashion. Because all compounds described herein have a facial arrangement of the three carbonyls, hereafter the *fac* designation will be used only in referring to general types of compounds and will be omitted when referring to specific compounds.

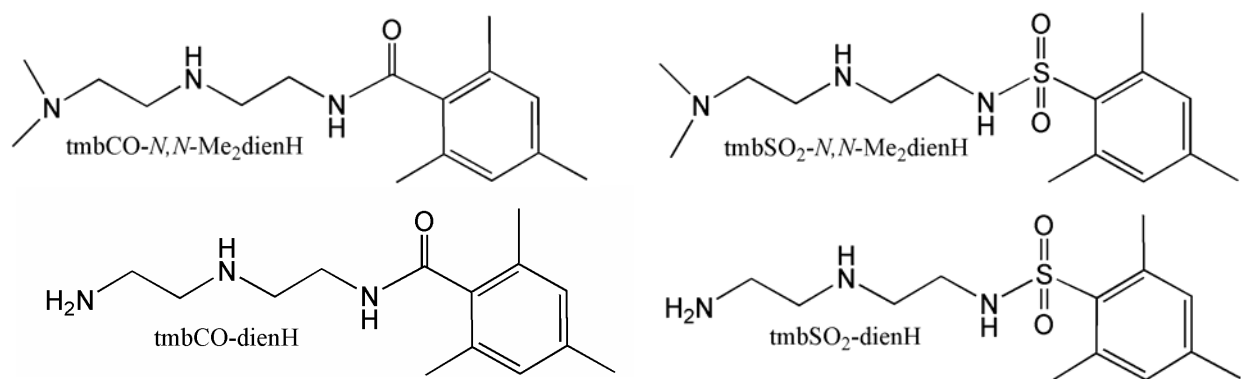


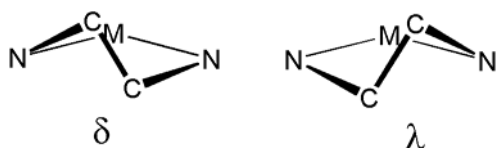
Figure A.1. Ligands used in this study: *N*-[2-(2-dimethylaminoethylamino)-ethyl]-2,4,6-trimethylbenzamide ($\text{tmbCO-}N,N\text{-Me}_2\text{dienH}$); and *N*-[2-(2-aminoethylamino)-ethyl]-2,4,6-trimethylbenzamide (tmbCO-dienH) and ligands referred to in the text: *N*-[2-(2-dimethylaminoethylamino)-ethyl]-2,4,6-trimethylbenzenesulfonamide ($\text{tmbSO}_2\text{-}N,N\text{-Me}_2\text{dienH}$) and *N*-[2-(2-aminoethylamino)-ethyl]-2,4,6-trimethylbenzenesulfonamide ($\text{tmbSO}_2\text{-dienH}$). The H's in the ligand names designate a sulfonamide/amide proton lost upon Re binding.

In $fac\text{-}[^{99m}\text{Tc}(\text{CO})_3\text{L}]$ agents, the bioconjugation emanates from an atom of one chelate ring of the tridentate ligand. Because chelate ring atoms act as a fulcrum, the configuration of asymmetric centers, the shape, and the conformation of the rings can have a large effect on the

overall shape of the agent, and hence on its biological activity. Therefore, it is clearly important to understand how the ligand pucker depends on the various components that can influence it (donor atoms, chains linking these atoms, exocyclic substituents, etc.).

Although chelate ring pucker and factors affecting pucker have not been thoroughly examined for radiopharmaceuticals, extensive structural information exists for a large number of complexes with other metals containing chelate rings with an ethylene group bridge between ligating atoms. Many of these structures have been analyzed by using principal component analysis (pca) and other methods.¹⁹⁻²⁶ When diethylenetriamine-type ligands bind to a metal center in a tridentate fashion, the two five-membered chelate rings can have either δ or λ chirality (Chart 1), leading to four possible combinations of chelate ring chirality: $\delta\lambda$, $\lambda\delta$, $\lambda\lambda$ and $\delta\delta$.

Chart A.1



Pca studies on X-ray structures from the Cambridge Structural Database (CSD) of M(dien) structures¹⁹⁻²¹ showed that the $\delta\lambda$ and $\lambda\delta$ conformation combinations were found much more frequently than those with the $\lambda\lambda$ and $\delta\delta$ pucker chirality.

A.2 Experimental Section

A.2.1 Starting Materials. *N,N*-dimethyldiethylenetriamine (*N,N*-Me₂dien) from Ames Laboratories, 2,4,6-trimethylbenzoyl chloride (tmbCOCl) from Alfa Aesar, diethylenetriamine (dien) and Re₂(CO)₁₀ from Aldrich were all used as received. The [Re(CO)₃(H₂O)₃]OTf¹³ (OTf = trifluoromethanesulfonate) precursor was prepared by known methods.

A.2.2 NMR Spectroscopy. ^1H NMR spectra were recorded on either a 300 MHz or 400 MHz spectrometer. Peak positions are relative to TMS or solvent residual peak, with TMS as reference. All NMR data were processed with XWINNMR and Mestre-C software.

A.2.3 X-ray Data Collection and Structure Determination. All single crystals suitable for X-ray crystallography were obtained by slow evaporation from acetone or methanol. Single crystals were placed in a cooled nitrogen gas stream at 90 K on a Nonius Kappa CCD diffractometer fitted with an Oxford Cryostream cooler with graphite-monochromated Mo $K\alpha$ (0.71073 Å) radiation. Data reduction included absorption corrections by the multi-scan method, with HKL SCALEPACK.²⁷ All X-ray structures were solved by direct methods and difference Fourier techniques and refined by full-matrix least squares techniques using SHELXL97.²⁸ All non-hydrogen atoms were refined anisotropically. All hydrogen atoms were visible in difference maps, but were placed in idealized positions. A torsional parameter was refined for each methyl group.

A.2.4 Synthesis of *fac*-[Re(CO)₃L]. The crude ligands, **LH**, were synthesized by a slight modification of Krapcho's method.²⁹ A solution of the acyl chloride (tmbCOCl) (~5 mmol, 100 mL of dioxane) was added dropwise over the course of about 2 h to a solution of the amine (~50 mmol, 100 mL of dioxane). The reaction mixture was stirred at RT for 10 h. The dioxane was completely removed under vacuum, and water (50 mL) was added. The product was extracted into CH_2Cl_2 (2 × 100 mL), and the solvent was removed under rotary evaporation. The oil thus obtained was used to synthesize the *fac*-[Re(CO)₃L] complexes as follows: an aqueous solution of $[\text{Re}(\text{CO})_3(\text{H}_2\text{O})_3]^+$ (10 mL, 0.1 mmol) was treated with a methanol (5 mL) solution of the ligand (0.1 mmol). The pH was adjusted to ~5 and the reaction mixture was heated at reflux for 10 h, then allowed to cool at RT, and the pH was increased to ~ 7. The resulting white solid that

precipitated was collected on a filter, washed with water, and dried under vacuum. This procedure succeeded with **LH** having an amide group, but the procedure was less reliable than for the analogues with the sulfonamide group.

A.2.4.1 [Re(CO)₃(tmbCO-*N,N*-Me₂dien)] (1). The general method, with 1 g of tmbSO₂Cl and 6 mL of *N,N*-Me₂dien, afforded the crude tmbCO-*N,N*-Me₂dienH ligand (650 mg, 45% yield). ¹H NMR (ppm) in CDCl₃: 6.82 (s, 2H), 6.50 (b, 1H, NH), 3.52 (t, 2H, CH₂), 2.84 (t, 2H, CH₂), 2.68 (t, 2H, CH₂), 2.35 (t, 2H, CH₂), 2.29 (s, 3H, CH₃), 2.26 (s, 6H, CH₃), 2.28 (s, 3H, CH₃), 2.15 (s, 6H, NCH₃). Treatment of [Re(CO)₃(H₂O)₃]⁺ (0.1 mmol) with tmbCO-*N,N*-Me₂dienH (27 mg) as described above afforded [Re(CO)₃(tmbCO-*N,N*-Me₂dien)] as a white powder, (12 mg, 22% yield). Crystals obtained by slow evaporation from acetone were characterized by single-crystal X-ray crystallography. ¹H NMR (ppm) spectrum in acetone-*d*₆: 6.78 (s, 1H), 6.75 (s, 1H), 6.14 (b, 1H, N2H), 3.47 (m, 1H, CH₂), 3.25 (m, 3H, CH₂), 3.12 (m, 2H, CH₂), 3.12 (s, 3H, NCH₃), 2.97 (s, 3H, NCH₃), 2.87 (m, 2H, CH₂), 2.21 (s, 3H, CH₃), 2.18 (s, 3H, CH₃), 2.13 (s, 3H, CH₃).

A.2.4.2 [Re(CO)₃(tmbCO-dien)] (2). The general method, with tmbCOCl (1 g) and dien (5 mL), yielded the crude tmbCO-dienH ligand (650 mg, 45% yield). ¹H NMR (ppm) in CDCl₃: 6.80 (s, 2H), 6.27 (b, 1H, NH), 3.53 (t, 2H, CH₂), 2.85 (t, 2H, CH₂), 2.77 (t, 2H, CH₂), 2.67 (t, 2H, CH₂), 2.28 (s, 3H, CH₃), 2.26 (s, 6H, CH₃). Treatment of [Re(CO)₃(H₂O)₃]⁺ (0.1 mmol) with tmbCO-*N*Me₂dienH (25 mg) as described above afforded [Re(CO)₃(tmbCO-*N*Me₂dien)] as a white powder (15 mg, 29% yield). Crystals obtained by slow evaporation from acetone were characterized by single-crystal X-ray crystallography. ¹H NMR (ppm) spectrum in acetone-*d*₆: 6.79 (s, 1H), 6.75 (s, 1H), 6.16 (b, 1H, N2H), 4.86 (b, 1H, N1H), 4.52 (b, 1H, N1H), 3.31 (m,

1H, CH₂), 3.16 (m, 1H, CH₂), 3.08-2.94 (m, 5H, CH₂), 2.67 (m, 1H, CH₂), 2.20 (s, 3H, CH₃), 2.18 (s, 6H, CH₃).

A.3 Results and Discussion

A.3.1 X-Ray Characterization. Both complexes reported here (Figure A.2) have a distorted octahedral structure, with the three carbonyl ligands coordinated facially. The remaining coordination sites are occupied by two sp³ N amines and one sp² N from an amido group. Typically, the Re–C(3) bonds, involving the CO group trans to the amido group, are not different from those of the other Re–CO bonds or the respective Re–C(3) bonds of the relevant sulfonamido complexes.¹⁶ Crystal data and structural refinement details are summarized in Table A.1 for **1** and **2**. Although we found that the aromatic rings facilitated our efforts to obtain crystals, these rings generally were not stacked.

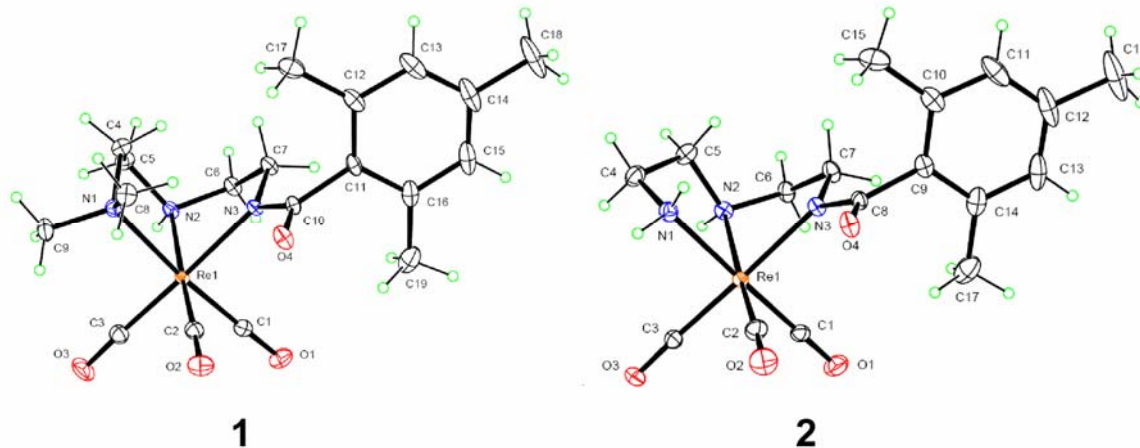


Figure A.2. Perspective drawings of the S configuration of [Re(CO)₃(tmbCO-*N,N*-Me₂dien)] (**1**) and [Re(CO)₃(tmbCO-dien)] (**2**). Thermal ellipsoids are drawn with 50% probability.

A.3.2 Bond Lengths and Bite Angles. The average Re–N bond length of ~2.2 Å (Table A.2) found in the amido complexes is consistent with distances found in relevant fac-[Re(CO)₃L] complexes.^{11,14,16} The Re–N1 bond (N1Me₂ group) in [Re(CO)₃(tmbCO-*N,N*-

Me₂dien)] (**1**) is longer than the other Re–N bonds of **1** and **2**. This lengthening is attributed to the bulkiness of the two methyl groups on N1 (for **1**) compared to the smaller H group in **2**. Similar results, were observed for the respective bonds of fac-[Re(CO)₃L] (L = tmb-sulfonamido ligands) complexes.

Table A.1. Crystal Data and Structural Refinement for [Re(CO)₃(tmbCO-*N,N*-Me₂dien)] (**1**), and [Re(CO)₃(tmbCO-dien)] (**2**)

| | <i>fac</i> -[Re(CO) ₃ L] complex | |
|--|--|---|
| | 1 | 2 |
| empirical formula | C ₁₉ H ₂₆ N ₃ O ₄ Re | C ₁₇ H ₂₂ N ₃ O ₄ Re•H ₂ O |
| fw | 546.63 | 536.59 |
| crystal system | monoclinic | monoclinic |
| space group | <i>P</i> 2 ₁ / <i>c</i> | <i>C</i> 2/ <i>c</i> |
| <i>a</i> (Å) | 19.5793 (15) | 36.861 (7) |
| <i>b</i> (Å) | 7.4239 (5) | 7.3990 (10) |
| <i>c</i> (Å) | 14.8071 (10) | 14.933 (3) |
| β (°) | 104.425 (5) | 102.145 (8) |
| <i>V</i> (Å ³) | 2084.4 (3) | 3981.6 (12) |
| <i>T</i> (K) | 90 | 90 |
| <i>Z</i> | 4 | 8 |
| ρ_{calc} (mg/m ³) | 1.742 | 1.790 |
| μ (mm ⁻¹) | 5.857 | 6.135 |
| transm. coeff. | 0.387-0.474 | 0.373-0.837 |
| $2\theta_{\text{max}}$ (°) | 73.8 | 65.2 |
| <i>R</i> indices ^a | 0.027 | 0.032 |
| wR2 = [<i>I</i> > 2 σ (<i>I</i>)] ^b | 0.060 | 0.077 |
| data/param | 9895/253 | 7003/245 |
| resid. dens. (Å ⁻³) | 1.39, -2.14 | 1.78, -1.88 |

Table A.2. Selected Bond and Atom Distances (Å) and Angles (deg) for [Re(CO)₃(tmbCO-*N,N*-Me₂dien)] (**1**), and [Re(CO)₃(tmbCO-dien)] (**2**)

| <i>fac</i> -[Re(CO) ₃ L] complex | | |
|---|-------------|-------------|
| | 1 | 2 |
| bond distances | | |
| Re–N1 | 2.2738 (19) | 2.216 (3) |
| Re–N2 | 2.2087 (19) | 2.207 (3) |
| Re–N3 | 2.1744 (17) | 2.185 (3) |
| bond angles | | |
| N1–Re–N2 | 79.37 (7) | 77.87 (10) |
| N2–Re–N3 | 76.10 (7) | 74.26 (10) |
| N1–Re–N3 | 85.81 (7) | 90.16 (10) |
| N2–Re–C2 | 172.33 (9) | 170.10 (13) |
| non-bonded distances | | |
| N1 to N2 | 2.863 | 2.779 |
| N2 to N3 | 2.702 | 2.651 |
| C4 to C7 | 3.308 | 4.169 |
| C4H to C7H | 2.299 | 4.621 |
| C5 to C6 | 2.510 | 2.468 |
| C5H to C6H | 2.283 | 2.586 |

It is known that the sp² N donors can form shorter Re–N bonds than the sp³ N donors.^{12,30} The Re–N3 sp² bond of the amido group in both **1** and **2** is statistically shorter than the respective Re–N1 and Re–N2 bonds (which are Re–sp³N bonds). The shorter Re–N3 sp² bond compared to the Re–N sp³ bonds was also observed in similar *fac*-[Re(CO)₃L] (L = tmb-sulfonamido ligands) complexes.¹⁶ The effect of the hybridized sp² N3 should also be seen in the

N3–C7 bond. Indeed, the N3–C7 bond is numerically (but not significantly) shorter than the other sp^3 N–C bonds (N1–C4, N2–C5, and N2–C6). Typical Re– sp^2 N bond lengths range from 2.14 to 2.18 Å, as measured in a several Re structures containing Re–N bonds (aromatic sp^2 N, e.g., in pyridyl ligands), whereas a typical Re– sp^3 N bond length is ~ 2.2 Å.¹²⁻¹⁴ The sp^2 hybridized N3 should affect the C–N3–C7, C–N3–Re, and C7–N3–Re angles. However, the differences between molecules, while generally consistent with expectations for Re– sp^2 N vs. Re– sp^3 N centers, are small and thus are masked by steric and solid state effects. The N–Re–N bite angles in the amido complexes are between 74.2 and 79.3°. The N2–Re–N3 bite angle (ring containing the amido group) is smaller ($\sim 75^\circ$) than the N1–Re–N2 bite angle ($\sim 78^\circ$), as found for the related angles in *fac*-[Re(CO)₃L] (L = tmb-sulfonamido ligands) complexes.¹⁶ The N1 to N2 and N2 to N3 non-bonded distances within five-membered chelate rings in **1** and **2** have a narrow range of values (Table A.2) and are similar to those of relevant *fac*-[Re(CO)₃L] complexes,¹⁶ as well as those of complexes with higher valent metal centers.³¹

A.3.3 Chelate Ring Chirality. As mentioned in the Introduction, chelate ring shape and conformation affect the overall shape of the bioconjugated agent. In accordance with other relevant compounds,^{20,21} and our findings for *fac*-[Re(CO)₃L] sulfonamido complexes,¹⁶ **1** has different chirality in each ring pucker; $\lambda\delta$ for the S configuration at Re (The Re configuration is S for structures shown in Figure A.2).¹⁶ In contrast, both chelate rings have the same chirality in complex **2** (both δ for the S configuration), a finding we attribute to two strong intermolecular hydrogen bonds from the NH₂ to two waters of crystallization (N...O 2.924(4) at x,y,z and 2.941(4) Å at 1-x, 1-y, 1-z). The fact that complex **2** has the same chirality in both rings is an unusual but not unprecedented finding.^{16,19-21} The non-bonded distances between the chelate rings agree with our previous study¹⁶ finding that C5 to C6 (Table A.2) and C5H to C6H

distances are not very different whether the pucker chirality of the two chelate rings is the same or different, whereas the C4 to C7 and C4H to C7H distances (*cf.* Figure A.2 for the atom numbering) are larger than when the chirality is different.

We compared the position of the pendant group and the shape and chirality of the ring pucker of complex **1** with its relevant sulfonamido complex.¹⁶ An overlay of the structure of complex **1** and the $[\text{Re}(\text{CO})_3(\text{tmbSO}_2\text{-}N,N\text{-Me}_2\text{dien})]$ complex (Figure A.3) illustrates that even though the dien backbone of the ligand has a very good fit, the location of the pendant tmb group is significantly different. These comparisons indicate that the change from an amido to a sulfonamido ligating group does not affect the backbone structure, but the change in the nature of the linkage of the tmb group to the coordinated nitrogen influences the position of the pendant group.

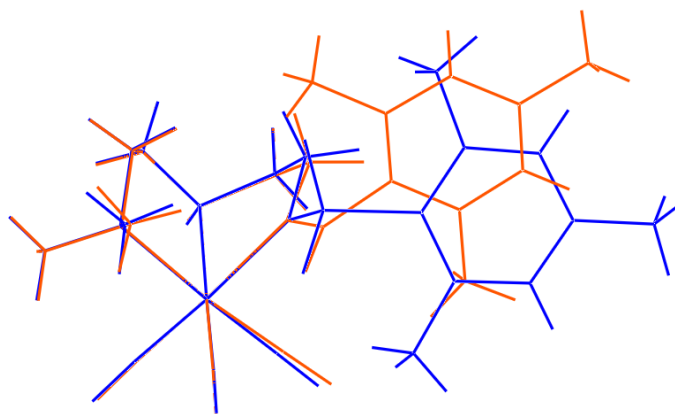


Figure A.3. Overlay of the $[\text{Re}(\text{CO})_3(\text{tmbCO-}N,N\text{-Me}_2\text{dien})]$ (red) and $[\text{Re}(\text{CO})_3(\text{tmbSO}_2\text{-}N,N\text{-Me}_2\text{dien})]$ (blue) complexes (RMS = 0.026 Å from overlaying the Re, N1, N2, and N3 atoms).

A.3.4 Trimethylbenzyl Group Rotation. In the X-ray structures of **1** and **2** (Figure A.2), the 3 and 5 protons and the 2 and 6 methyl groups of the tmbSO₂ group are not equivalent. Indeed, in the ¹H NMR spectra of complexes **1** and **2**, the signals of the magnetically

inequivalent two aromatic protons and two methyl groups of the tmbCO group have similar shifts (see Experimental Section) but are fully resolved. The signals do not merge when the spectrum in acetone- d_6 is recorded at 40 °C. In contrast, for *fac*-[Re(CO) $_3$ L] complexes with a sulfonamido group instead of an amido group, these signals are combined for the aromatic and for the methyl protons, indicating fast rotation on the NMR time scale.¹⁶

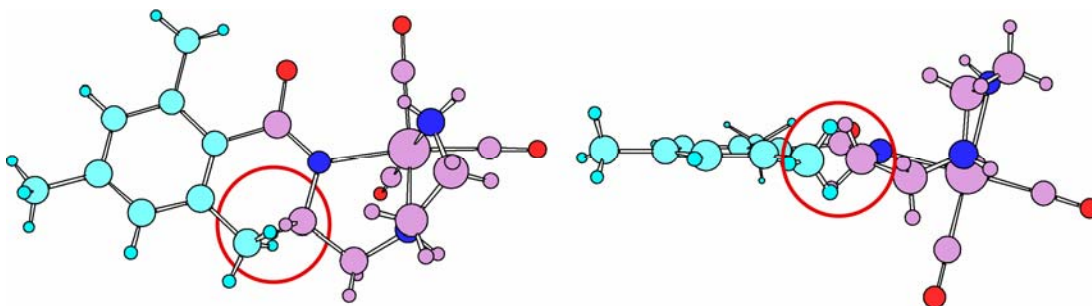


Figure A.4. Two views illustrating the possible steric clashes leading to restricted rotation around the C (amido group)–C (tmb group) bond for **2**.

In the X-ray structures of **1** and **2**, the amido N3–C–O group is planar. Therefore, it can adopt only two orientations with the oxygen facing away or towards the coordination face; in both orientations serious clashes are observed when the tmb group is rotated around the C–C(tmb) bond (with the help of modeling software). The conformer with the oxygen facing towards the coordination face seems to be unfavorable because the tmb group is placed very close to the carbonyl group and rotation of the tmb group would overlap with the carbonyl group. In the second conformer (which is observed in the X-ray structures of **1** and **2**) clashes of the methyl group (of tmb) with the ethylene chain of dien appear to hinder rotation around the C(amido)–C(tmb) bond. Similar clashes were observed also in the relevant *fac*-[Re(CO) $_3$ L] (L = tmb-sulfonamido complexes) complexes¹⁶ during rotation the around the C(sulfonamido)–C(tmb)

bond. The sulfonamido group S atom is part of longer bonds (N–S and S–C) bonds and a more acute N3–S–C angle compared to the respective bonds (N3–C ~1.32 Å and C–C ~1.51 Å) and angle (N3–C–C ~120°) of the amido group in the [Re(CO)₃(tmbCO-dien)] and [Re(CO)₃(N,N-Me₂tmbCO-dien)] complexes. The equivalence of the tmb signals of the sulfonamido complexes despite the inequivalence in the X-ray structure¹⁶ was attributed to the relatively faster rotation of the tmb group about the S(sulfonamido)–C(tmb) bond of the sulfonamido group compared to the C(amido)–C(tmb) bond of the amido group,³² and that synchronous rotations about the longer N–S and S–C bonds can explain the relatively free rotation of the tmb group for sulfonamido complexes.¹⁶ We believe that for the *fac*-[Re(CO)₃L] amido complexes (**1** and **2**) the combination of the presence of only one favorable conformer, the short bonds and slow rotation of the amido group result in hindered rotation around the C(amido)–C (tmb) bond, from clashes of the methyl group (of tmb) with the ethylene chain (Figure A.4).

A.3.5 NMR Characterization of [Re(CO)₃L] (L⁻ = tmbCO-*N,N*-Me₂dien⁻ and tmbCO-dien⁻). The *fac*-[Re(CO)₃L] complexes were characterized by NMR spectroscopy in DMSO-*d*₆, as well as in acetone-*d*₆ (Table A.3). The [Re(CO)₃(tmbCO-dien)] (**2**) complex has a terminal NH₂ group with one NH *exo* and one NH *endo* to the tricarbonyl face, which give rise to a relatively upfield *exo*-NH signal (3.94 ppm) and a relatively downfield *endo*-NH signal (4.99 ppm) in DMSO-*d*₆. These shifts (Table A.3) are roughly comparable to those for the terminal NH₂ group of relevant *fac*-[Re(CO)₃L] (L⁻ = tmb-sulfonamido ligands) complexes (3.30 to 3.54 ppm for upfield NH signal and 5.21 to 5.26 ppm for downfield NH signal).¹⁶ The *exo*-NH signal of [Re(CO)₃(tmbSO₂-dien)] is ~0.5 ppm more upfield compared to that of **2**, a difference that might be attributed to the different distance of the *exo*-NH protons to the nearest oxygens of the sulfonamido/amido group. The distance of the *exo*-NH of **2** to the oxygen of the CO group is 3.5

Å, whereas the respective distance for the $[\text{Re}(\text{CO})_3(\text{tmbSO}_2\text{-dien})]$ complex is 2.8 Å. The explanation for the relatively upfield shift of the *exo*-NH signal is unclear, but such a signal appears to be a general finding for *fac*- $[\text{Re}(\text{CO})_3\text{L}]$ complexes with an *exo*-NH group. One possibility is that steric effects obstruct formation of H-bonds with the solvent and therefore the downfield shift effect of NH H-bonding to solvent is decreased.

Table A.3. Selected Chemical Shifts (ppm) of $[\text{Re}(\text{CO})_3(\text{tmbCO-}N,N\text{-Me}_2\text{dien})]$ (**1**), and $[\text{Re}(\text{CO})_3(\text{tmbCO-dien})]$ (**2**)

| | 1 | 2 |
|--------------------------------|----------|----------|
| DMSO- <i>d</i> ₆ | | |
| <i>exo</i> -N1H/Me | 2.79 | 3.94 |
| <i>endo</i> -N1H/Me | 3.02 | 4.99 |
| N2H | 6.72 | 6.69 |
| acetone- <i>d</i> ₆ | | |
| <i>exo</i> -N1H/Me | 2.97 | 4.53 |
| <i>endo</i> -N1H/Me | 3.12 | 4.86 |
| N2H | 6.14 | 6.17 |

A.4 Conclusions

In our studies we find that the *fac*- $[\text{Re}(\text{CO})_3\text{L}]$ amido complexes are much more difficult to synthesize, compared to the related sulfonamido complexes, consistent with the scarcity of related amido complexes in the literature. An inner coordination sphere with a neutral charge is achieved upon binding of the tridentate monoanionic amido ligands in the *fac*- $[\text{Re}(\text{CO})_3(\text{NNN})]$ complexes studied here. The dangling tmb group connected through the amido bond experiences hindered rotation on the NMR time scale, due to the rigidity of the amido group (compared to the

more flexible sulfonamido group). Complex **1** has different chirality in each chelate ring, as commonly found in the literature, whereas complex **2** has same chirality in each chelate ring. The pendant tmb group has very different positions in $[\text{Re}(\text{CO})_3(\text{tmbCO-}N,N\text{-Me}_2\text{dien})]$ and $[\text{Re}(\text{CO})_3(\text{tmbSO}_2\text{-}N,N\text{-Me}_2\text{dien})]$. Therefore, the different linker components (CO and SO₂) lead to different overall shapes.

A.5 References

1. Schwochau, K. *Angew. Chem., Int. Ed. Engl.* **1994**, *33*, 2258-2267.
2. Schibli, R.; Schubiger, P. A. *Eur. J. Nucl. Med. Mol. Imaging* **2002**, *29*, 1529-1542.
3. Jurisson, S. S.; Lydon, J. D. *Chem. Rev.* **1999**, *99*, 2205-2218.
4. Bandoli, G.; Tisato, F.; Dolmella, A.; Agostini, S. *Coord. Chem. Rev.* **2006**, *250*, 561-573.
5. Alberto, R.; Schibli, R.; Schubiger, A. P.; Abram, U.; Pietzsch, H. J.; Johannsen, B. *J. Am. Chem. Soc.* **1999**, *121*, 6076-6077.
6. Alberto, R.; Schibli, R.; Egli, A.; Schubiger, P. A.; Abram, U.; Kaden, T. A. *J. Am. Chem. Soc.* **1998**, *120*, 7987-7988.
7. Schibli, R.; Alberto, R.; Abram, U.; Abram, S.; Egli, A.; Schubiger, P. A.; Kaden, T. A. *Inorg. Chem.* **1998**, *37*, 3509-3516.
8. Schibli, R.; La Bella, R.; Alberto, R.; Garcia-Garayoa, E.; Ortner, K.; Abram, U.; Schubiger, P. A. *Bioconjugate Chem.* **2000**, *11*, 345-351.
9. Lipowska, M.; Hansen, L.; Marzilli, L. G.; Taylor, A. *J. Nucl. Med.* **2001**, *42*, 259P-259P.
10. Lipowska, M.; Cini, R.; Tamasi, G.; Xu, X. L.; Taylor, A. T.; Marzilli, L. G. *Inorg. Chem.* **2004**, *43*, 7774-7783.
11. Mundwiler, S.; Candreia, L.; Hafliger, P.; Ortner, K.; Alberto, R. *Bioconjugate Chem.* **2004**, *15*, 195-202.
12. Wei, L.; Babich, J. W.; Ouellette, W.; Zubieta, J. *Inorg. Chem.* **2006**, *45*, 3057-3066.
13. He, H.; Lipowska, M.; Xu, X.; Taylor, A. T.; Carlone, M.; Marzilli, L. G. *Inorg. Chem.* **2005**, *44*, 5437-5446.

14. He, H.; Lipowska, M.; Xu, X.; Taylor, A. T.; Marzilli, L. G. *Inorg. Chem.* **2007**, *46*, 3385-3394.
15. Taylor, A.; Eshima, D.; Fritzberg, A. R.; Christian, P. E. *J. Nucl. Med.* **1986**, *27*, 795-803.
16. Christoforou, A. M.; Fronczek, F. R.; Marzilli, P. A.; Marzilli, L. G. *Inorg. Chem.* **2007**, *Accepted*.
17. Lipowska, M.; Hansen, L.; Xu, X.; Marzilli, P. A.; Taylor, A.; Marzilli, L. G. *Inorg. Chem.* **2002**, *41*, 3032-3041.
18. Alberto, R.; Schibli, R.; Waibel, R.; Abram, U.; Schubiger, A. P. *Coord. Chem. Rev.* **1999**, *192*, 901-919.
19. Harris, S. E.; Pascual, I.; Orpen, A. G. *J. Chem. Soc., Dalton Trans.* **2001**, 2996-3009.
20. Rodríguez, V.; Gutiérrez-Zorrilla, J. M.; Vitoria, P.; Luque, A.; Román, P.; Martínez-Ripoll, M. *Inorg. Chim. Acta* **1999**, *290*, 57-63.
21. Orpen, A. G. *Chem. Soc. Rev.* **1993**, *22*, 191-197.
22. Schmidtke, H. H.; Garthoff, D. *Inorg. Chim. Acta* **1968**, *2*, 351-356.
23. Konno, M.; Marumo, F.; Saito, Y. *Acta Crystallogr., Sect. B: Struct. Sci.* **1973**, *B 29*, 739-744.
24. Kobayashi, A.; Marumo, F.; Saito, Y. *Acta Crystallogr., Sect. B: Struct. Sci.* **1972**, *28*, 3591-3595.
25. Bond, A. M.; Hambley, T. W.; Snow, M. R. *Inorg. Chem.* **1985**, *24*, 1920.
26. Okiyama, K.; Sato, S.; Saito, Y. *Acta Crystallogr., Sect. B: Struct. Sci.* **1979**, *35*, 2389-2392.
27. Otwinowski, Z.; Minor, W. *Macromolecular crystallography, part A*; New York Academic Press: New York, 1997; Vol. 276.
28. Sheldrick, G. M. In *Program for Crystal Structure Solution and Refinement*; University of Gottingen: Gottingen, Germany, 1997.
29. Krapcho, A. P.; Kuell, C. S. *Synth. Commun.* **1990**, *20*, 2559-2564.
30. Correia, J. D. G.; Domingos, A.; Santos, I.; Alberto, R.; Ortner, K. *Inorg. Chem.* **2001**, *40*, 5147-5151.

31. Britten, J. F.; Lock, C. J. L.; Pratt, W. M. C. *Acta Crystallogr., Sect. B: Struct. Sci.* **1982**, *B38*, 2148-2155.

32. Lyapkalo, I. M.; Reissig, H. U.; Schafer, A.; Wagner, A. *Helv. Chim. Acta* **2002**, *85*, 4206-4215.

APPENDIX B. SUPPLEMENTARY MATERIAL FOR CHAPTER 3

B.1 Synthesis and Crystal Data and Structural Refinement for $\text{Re}(\text{CO})_3(\text{DNS-dien})^1$

B.1.1 Synthesis of $\text{Re}(\text{CO})_3(\text{DNS-dien})$ (4). Treatment of 0.1 mmol of $[\text{Re}(\text{CO})_3(\text{H}_2\text{O})_3]^+$ with 33.2 mg of DNS-dienH^2 as described for $\text{Re}(\text{CO})_3\text{L}$ afforded $\text{Re}(\text{CO})_3(\text{DNS-dien})$ as a white powder (35 mg, 58% yield). Crystals obtained by slow evaporation from methanol were characterized by single-crystal X-ray crystallography. ^1H NMR spectrum ($\text{acetone-}d_6$) (ppm): 8.66 (d, 1H), 8.40 (d, 1H), 8.12 (d, 1H), 7.49 (q, 2H), 7.20 (d, 1H), 6.23 (b, 1H, N1H), 4.77 (b, 1H, N1H), 4.09 (b, 1H, N1H), 3.67 (m, 1H, CH_2), 3.32-2.94 (m, 5H, CH_2), 2.92 (m, 1H, CH_2), 2.85 (s, 6H, CH_3).

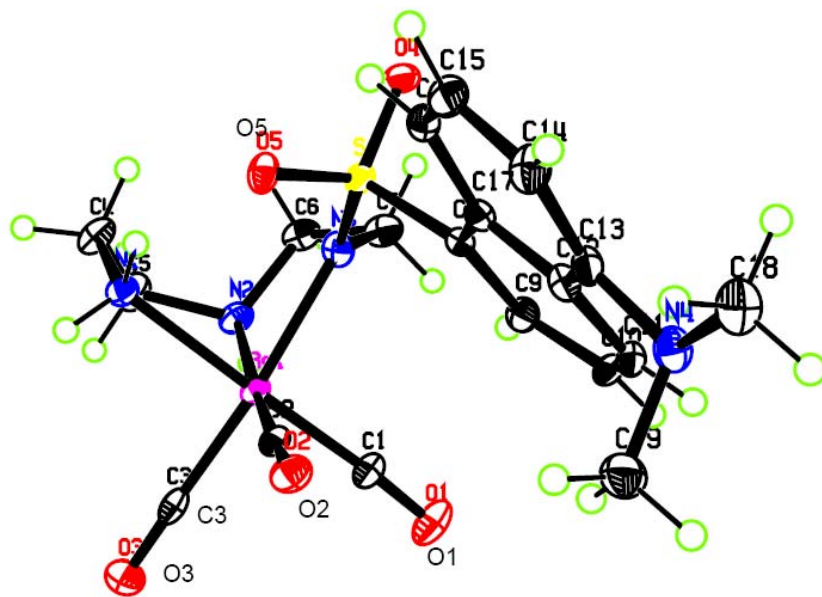


Figure B.1. Perspective drawings of the S configuration of $\text{Re}(\text{CO})_3(\text{DNS-dien})$ (4).¹ Thermal ellipsoids are drawn with 50% probability.

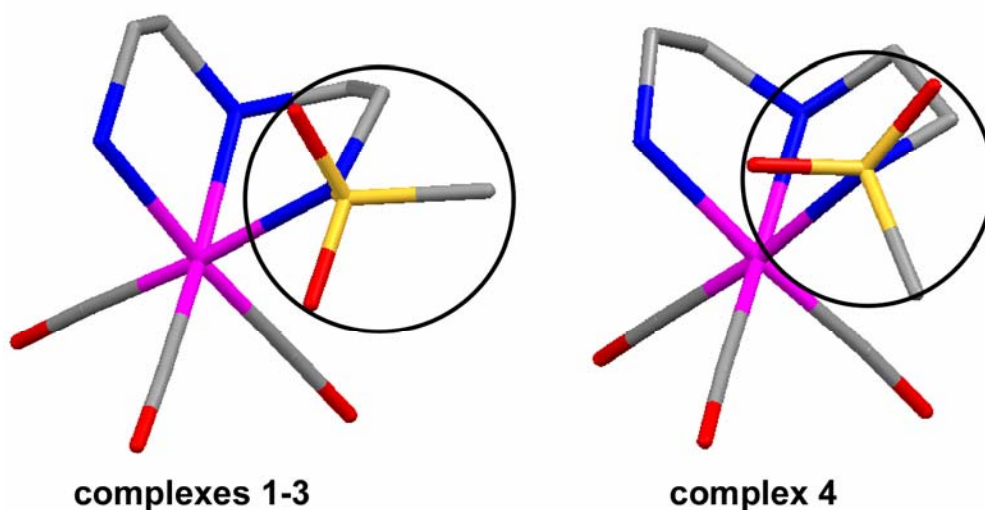


Figure B.2. Orientation of the SO₂ group in complexes **1-4**.

Table B.1. Crystal Data and Structural Refinement for Re(CO)₃(DNSH-dien) (**4**)

| | Re(CO) ₃ (DNSH-dien) | | Re(CO) ₃ (DNSH-dien) | |
|----------------------|---|---|---------------------------------|--|
| empirical formula | C ₁₉ H ₂₃ N ₄ O ₅ ReS | γ (°) | 90.0 | |
| fw | 605.67 | V (Å ³) | 2164.8 (8) | |
| crystal system | monoclinic | T (K) | 110 | |
| space group | $P2_1/c$ | Z | 4 | |
| unit cell dimensions | | ρ_{calc} (g/cm ³) | 1.858 | |
| a (Å) | 12.527 (3) | abs coeff (mm ⁻¹) | 5.748 | |
| b (Å) | 13.934 (3) | $2\theta_{\text{max}}$ (°) | 61 | |
| c (Å) | 12.603 (2) | R indices ^a | 0.036 | |
| α (°) | 90.0 | wR2 = $[I > 2\sigma(I)]^b$ | 0.082 | |
| β (°) | 100.249 (9) | data/param | 6591/273 | |

$${}^a R = (\sum ||F_o| - |F_c||) / \sum |F_o|; {}^b \text{wR2} = [\sum [w(F_o^2 - F_c^2)^2] / \sum [w(F_o^2)^2]]^{1/2}$$

B.2 Comparison of Metric Information and Structural Features of Complexes 1-5

B.2.1 Distances of the ethylene chain carbons to the N–Re–N plane. The distances between the carbons of the ethylene chains to the N–Re–N plane are listed in Table 3. For complexes **1-4** in the sulfonamido-containing ring both C6 and C7 are below (away from the triangular face of L^-) the N2–Re–N3 plane (Figure 4). In contrast, in the terminal amine ring C4 is above and C5 is below the N1–Re–N2 plane for complexes **1-3**. In **4**, C5 is also below the plane but C4 is almost in the N1–Re–N2 plane (Table S2, Figure 4)

Table B.2. Distances of Ethylene Chain Carbons to the N–Re–N Plane (Sign Denotes if the C is Above (Positive) and Toward the Ligand Coordinated Face or Below (Negative) and Away From the Ligand Trigonal Face)

| Re(CO) ₃ L complex | | | | |
|-------------------------------|---------------|----------|----------|----------|
| | 1 | 2 | 3 | 4 |
| C4 to N1–Re–N2 | 0.526/0.546 | 0.462 | 0.375 | -0.026 |
| C5 to N1–Re–N2 | -0.104/-0.074 | -0.145 | -0.251 | -0.652 |
| C6 to N2–Re–N3 | -0.750/-0.771 | -0.697 | -0.683 | -0.294 |
| C7 to N2–Re–N3 | -0.249/-0.235 | -0.148 | -0.125 | -0.836 |

Table B.3. Selected Torsion Angles (deg) for complexes **2-5** Used to Assign the NH₂ ¹H NMR Signals

| Re(CO) ₃ L complex | | | | |
|-------------------------------|----------|----------|----------|----------|
| | 2 | 3 | 4 | 5 |
| H1B–N1–C4–H4A | 41.5 | 39.0 | 25.9 | 56.2 |
| H1B–N1–C4–H4B | 77.5 | 80.2 | 92.7 | 173.9 |
| H1A–N1–C4–H4A | 159.8 | 157.0 | 143.1 | 58.1 |
| H1A–N1–C4–H4B | 40.6 | 37.69 | 24.5 | 59.6 |

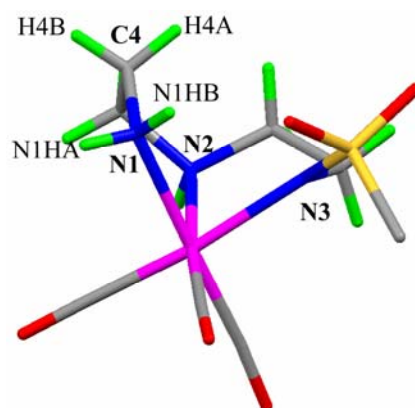


Figure B.3. Drawing of $\text{Re}(\text{CO})_3\text{L}$, showing the torsion angle between N1H and C4H.

B.3 IR Spectroscopy.

The IR spectra of acetone solutions of complexes **1-5** exhibit three bands attributed to CO stretching of the *fac*- $\text{Re}(\text{CO})_3$ moiety (Table S4); a sharp, strong band in the 2010-2027 cm^{-1} region and two broad bands in the 1860-1920- cm^{-1} region. These values are in a similar range of those of relevant $\text{Re}(\text{CO})_3$ complexes containing amine chelate ligands³ as well those of the $[\text{Re}(\text{CO})_3(\text{NH}_3)_3]^+$ complex.⁴

Table B.4. CO-stretching Absorptions (cm^{-1}) in the IR Spectra of Acetone Solutions of **1-5**

| Re(CO) ₃ L complex | | | | |
|-------------------------------|----------|----------|----------|----------|
| 1 | 2 | 3 | 4 | 5 |
| 2015 | 2027 | 2019 | 2010 | 2010 |
| 1907 | 1920 | 1906 | 1888 | 1889 |
| 1877 | 1884 | 1883 | 1875 | 1860 |

B.4 References.

1. Marzilli, L. G.; Christoforou, A. M.; Maheshwari, V.; Adams, K. M.; Fronczek, F. R.; Marzilli, P. A. In *Technetium, Rhenium, and Other Metals in Chemistry and Nuclear Medicine*; Mazzi, U., Ed.; SGEEditoriali: Padova, 2006; Vol. 7, pp 3-8.
2. Corradini, R.; Dossena, A.; Galaverna, G.; Marchelli, R.; Panagia, A.; Sartor, G. *J. Org. Chem.* **1997**, *62*, 6283-6289.
3. Wei, L.; Babich, J. W.; Ouellette, W.; Zubieta, J. *Inorg. Chem.* **2006**, *45*, 3057-3066.
4. Angelici, R. J.; Blacik, L. J. *Inorg. Chem.* **1972**, *11*, 1754-1758.

APPENDIX C. SUPPLEMENTARY MATERIAL FOR CHAPTER 4

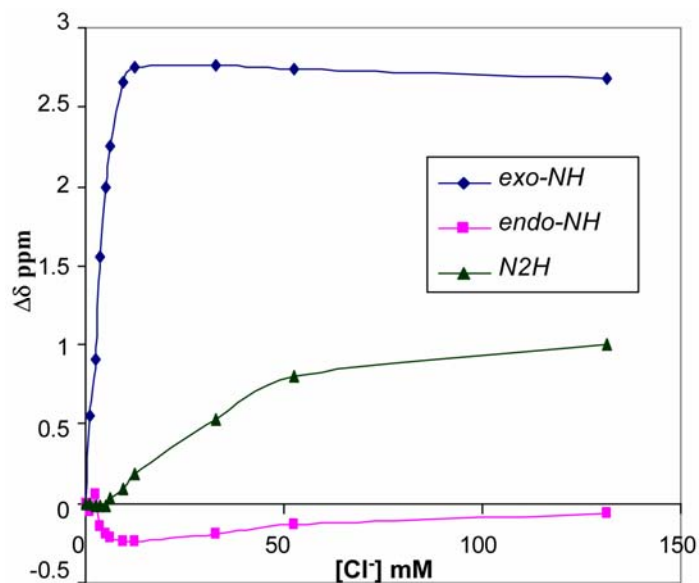


Figure C.1. Change in chemical shift ($\Delta\delta$) of *exo-NH*, *endo-NH* and *N2H* signals of $[\text{Re}(\text{CO})_3(\text{dien})]\text{PF}_6$ upon addition of Cl^- in acetonitrile- d_3 .

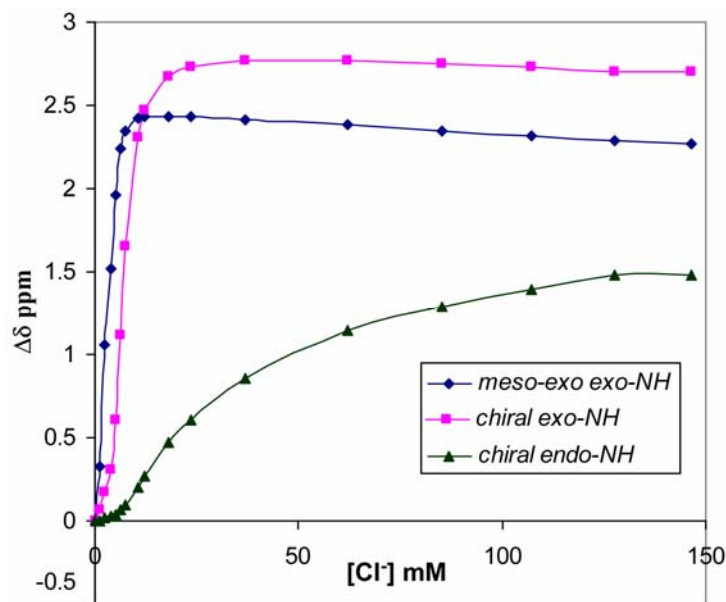


Figure C.2. Change in chemical shift ($\Delta\delta$) of *exo-NH* signal of *meso-exo-4* and *exo-NH* and *endo-NH* signals of *chiral-4* upon addition of Cl^- in acetonitrile- d_3 .

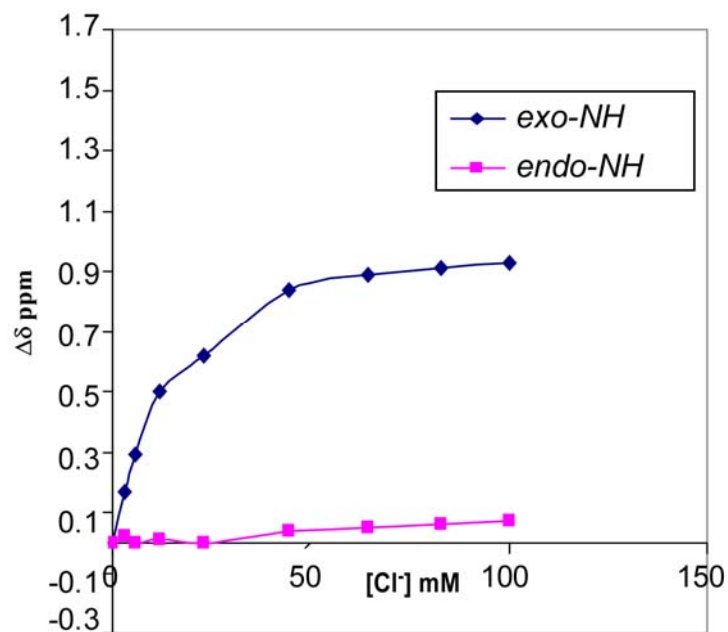


Figure C.3. Change in chemical shift ($\Delta\delta$) of *exo*-NH and *endo*-NH signals of $[\text{Re}(\text{CO})_3(\text{daes})]\text{PF}_6$ upon addition of Cl^- in $\text{DMSO-}d_6$.

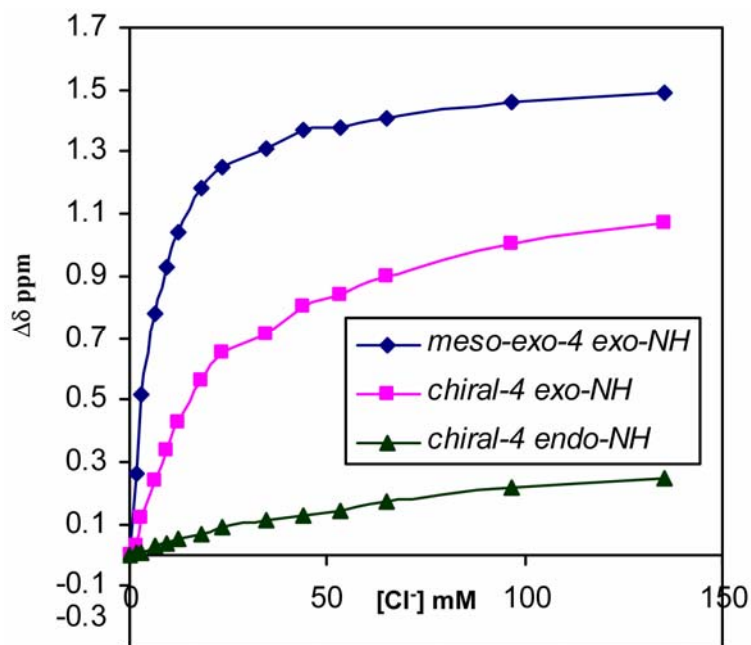


Figure C.4. Change in chemical shift ($\Delta\delta$) of *exo*-NH signal of *meso-exo-4* and *exo*-NH and *endo*-NH signals of *chiral-4* upon addition of Cl^- in $\text{DMSO-}d_6$.

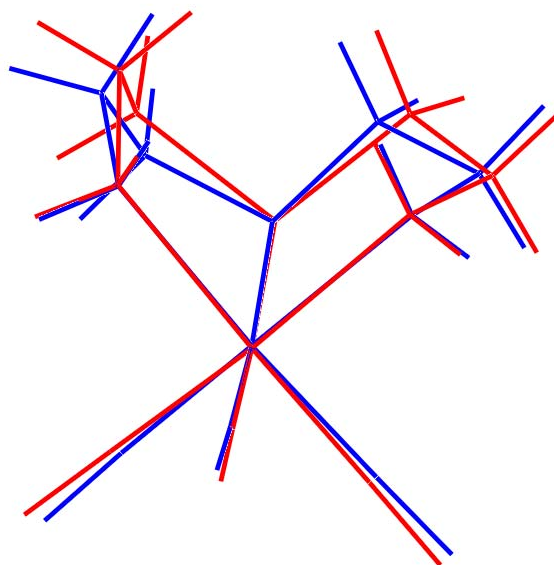


Figure C.5. Overlay illustration of complexes **6** (red) and **2** (blue) (RMS value = 0.125 from overlaying the Re, N1, N2/S, and N2/N3 atoms). The N2-CH₃ group of **2** is omitted for clarity.

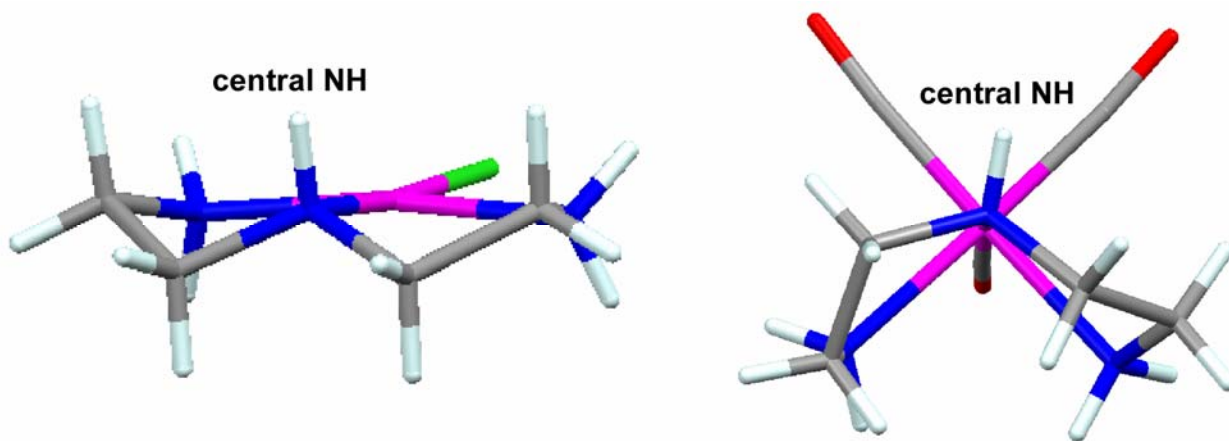


Figure C.6. Orientation of central NH in [Pt(dien)Cl]Cl (left) and Re(CO)₃(dien)]PF₆ (right). Counter ions are omitted for clarity.

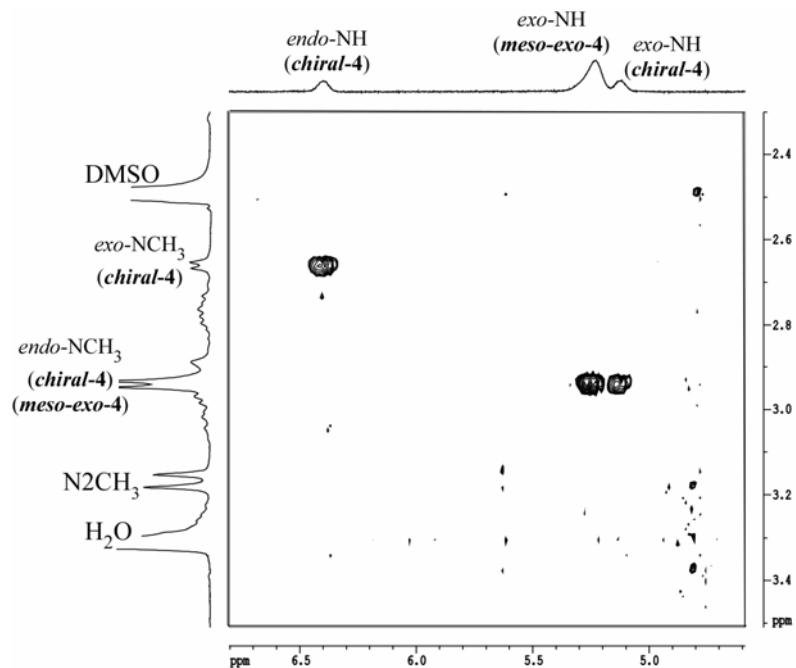


Figure C.7. ^1H - ^1H COSY NMR spectrum of *meso-exo-4* and *chiral-4* (mixture obtained upon isomerization with base) in $\text{DMSO-}d_6/0.04\text{ M NaOH}$, $600\ \mu\text{L}/10\ \mu\text{L}$.

APPENDIX D. CRYSTALLOGRAPHIC AND SPECTROSCOPIC DATA FOR MISCELLANEOUS PLATINUM(II)-SULFONAMIDO COMPLEXES

Two types of ligands based on 2-aminopyridine (2-amp), diethylenetriamine (dien) or ethylenediamine (en) with a 2,4,6-trimethylbenzoyl (tmbSO₂) or methyl (CH₃) group through a sulfonamide group were used in this study. Treatment of *cis*-Pt(Me₂SO)₂Cl₂ with the sulfonamide ligands gave the neutral complexes Pt(2-ampSO₂CH₃)(Me₂SO)Cl, Pt(2-ampSO₂tmb)(Me₂SO)Cl, Pt(tmbSO₂-en)(Me₂SO)Cl, and Pt(tmbSO₂-*N,N*-Me₂dien)Cl. X-ray crystallographic and NMR analyses confirm that in both the solid and solution states the ligands based on 2-amp or en are bound to Pt(II) in a bidentate fashion with the sulfonamido group being deprotonated. The coordination sphere is completed with a Cl ligand (trans to the sulfonamido N) and a Me₂SO ligand (trans to the pyridine N). The tmbSO₂-*N,N*-Me₂dienH ligand is bound in tridentate fashion with the sulfonamido group being deprotonated.

D.1 Experimental Section

D.1.1 Starting Materials. 2-aminomethylpyridine, methanesulfonyl chloride (CH₃SO₂Cl) and 2-mesitylenesulfonyl chloride (tmbSO₂Cl) from Aldrich were all used as received. *cis*-Pt(Me₂SO)₂Cl₂, tmbSO₂-*N,N*-Me₂dien and tmbSO₂-en were synthesized as described elsewhere.^{1,2}

D.1.2 NMR Spectroscopy. ¹H NMR spectra were recorded on either a 300 MHz or 400 MHz spectrometer. Peak positions are relative to TMS or solvent residual peak, with TMS as reference. All NMR data were processed with XWINNMR and Mestre-C software.

D.1.3 X-ray Data Collection and Structure Determination. All single crystals suitable for X-ray crystallography were obtained by slow evaporation from acetone or methanol. Single crystals were placed in a cooled nitrogen gas stream at ~100 K on a Nonius Kappa CCD diffractometer fitted with an Oxford Cryostream cooler with graphite-monochromated Mo K α

(0.71073 Å) radiation. Data reduction included absorption corrections by the multi-scan method, with HKL SCALEPACK.³ All X-ray structures were determined by direct methods and difference Fourier techniques and refined by full-matrix least squares techniques, by using SHELXL97.⁴ All non-hydrogen atoms were refined anisotropically. All hydrogen atoms were visible in difference maps, but were placed in idealized positions. A torsional parameter was refined for each methyl group. Mercury Software was used for measuring torsion angles.

D.2 Pt(II) Complexes of 2-Aminopyridine-Sulfonamide Ligands.

D.2.1 Synthesis of 2-ampSO₂R (R = CH₃ or tmb)

A solution of the sulfonyl chloride (tmbSO₂Cl or CH₃SO₂Cl) (~5 mmol, 100 mL of dioxane) was added dropwise over the course of about 0.5 h to a solution of 2-amp (~10 mmol, 100 mL of dioxane). The reaction mixture was stirred at RT overnight. A white solid was present in the reaction mixture at the end of the reaction. The dioxane was completely removed under vacuum, and water (50 mL) was added. The product was extracted into CH₂Cl₂ (2 × 100 mL), and the solvent was removed under rotary evaporation. The oil thus obtained was used to synthesize the Pt(2-ampSO₂R)(Me₂SO)Cl complexes as follows.

D.2.1.1 Synthesis of 2-ampSO₂CH₃ (1). The general method, with CH₃COCl (0.56 g) and 2-amp (1.08 g), yielded the 2-ampSO₂CH₃ ligand (1.18 g, 65% yield). Crystals obtained from CDCl₃ were characterized by single-crystal X-ray crystallography. ¹H NMR (ppm) in CDCl₃: 8.56 (d, 1H), 7.73 (t, 1H), 7.36 (t, 1H), 7.26 (d, 1H), 6.13 (b, 1H, NH), 4.47 (d, 2H, CH₂), 2.91 (s, 3H, CH₃).

D.2.1.2 Synthesis of 2-ampSO₂tmb (2). The general method, with tmbCOCl (1.02 g) and 2-amp (1.08 g), yielded the 2-ampSO₂CH₃ ligand (1.68 mg, 58 % yield). Crystals obtained from slow evaporation of a CH₂Cl₂ solution were characterized by single-crystal X-ray

crystallography ^1H NMR (ppm) in CDCl_3 : 8.47 (d, 1H), 7.56 (t, 1H), 7.15 (m, 2H), 6.89 (s, 2H, tmb), 6.00 (b, 1H, NH), 4.16 (d, 2H, CH_2), 2.67 (s, 6H, CH_3), 2.26 (s, 3H, CH_3).

D.2.2 Synthesis of $\text{Pt}(\text{2-ampSO}_2\text{R})(\text{Me}_2\text{SO})\text{Cl}$ ($\text{R} = \text{CH}_3$ or tmb)

A methanol solution (20 mL) of *cis*- $\text{Pt}(\text{Me}_2\text{SO})_2\text{Cl}_2$ (0.5 mmol) and 2-ampSO₂R ($\text{R} = \text{CH}_3$ or tmb) (0.5 mmol) in the presence of triethylamine (500 μL) was heated at 60 °C for 2 h. The reaction mixture was allowed to stir at RT overnight. The yellow solid that precipitated was collected, washed with diethyl ether and dried in vacuo.

D.2.2.1 Synthesis of $\text{Pt}(\text{2-ampSO}_2\text{CH}_3)(\text{Me}_2\text{SO})\text{Cl}$ (3). Treatment of *cis*- $\text{Pt}(\text{Me}_2\text{SO})_2\text{Cl}_2$ (0.211 g) with 2-ampSO₂CH₃ (146 mg) afforded $\text{Pt}(\text{2-ampSO}_2\text{CH}_3)(\text{Me}_2\text{SO})\text{Cl}$ (158 mg, 52 % yield) as a yellow solid. Crystals obtained from slow evaporation of the reaction filtrate were characterized by single-crystal X-ray crystallography. ^1H NMR (ppm) in $\text{DMSO-}d_6$: 8.92 (d, 1H), 8.15 (t, 1H), 7.80 (d, 1H), 7.59 (t, 1H), 4.56 (d, 2H, CH_2), 2.59 (s, 3H, CH_3).

D.2.2.2 Synthesis of $\text{Pt}(\text{2-ampSO}_2\text{tmb})(\text{Me}_2\text{SO})\text{Cl}$ (4). Treatment of *cis*- $\text{Pt}(\text{Me}_2\text{SO})_2\text{Cl}_2$ (0.211 g) with 2-ampSO₂CH₃ (94 mg) afforded $\text{Pt}(\text{2-ampSO}_2\text{CH}_3)(\text{Me}_2\text{SO})\text{Cl}$ (114 mg, 46 % yield) as a yellow solid. Crystals obtained from slow evaporation of the reaction filtrate were characterized by single-crystal X-ray crystallography. ^1H NMR (ppm) in $\text{DMSO-}d_6$: 8.61 (d, 1H), 7.91 (t, 1H), 7.58 (d, 1H), 7.36 (t, 1H), 6.73 (s, 2H, tmb), 4.36 (d, 2H, CH_2), 2.73 (s, 6H, tmb- CH_3), 2.08 (s, 3H, tmb- CH_3).

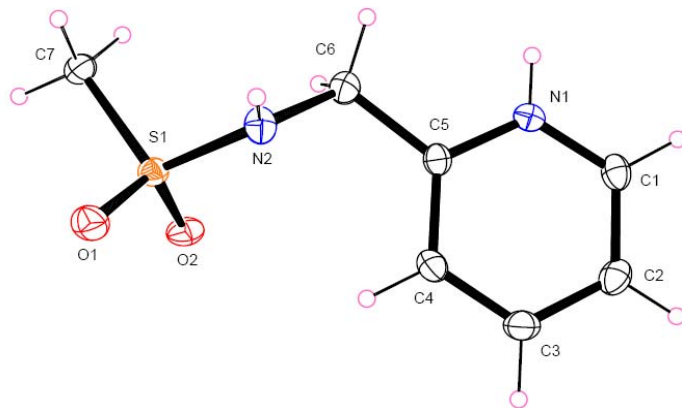


Figure D.1. Perspective drawing of 2-ampSO₂CH₃ (**1**). Thermal ellipsoids are drawn with 50% probability.

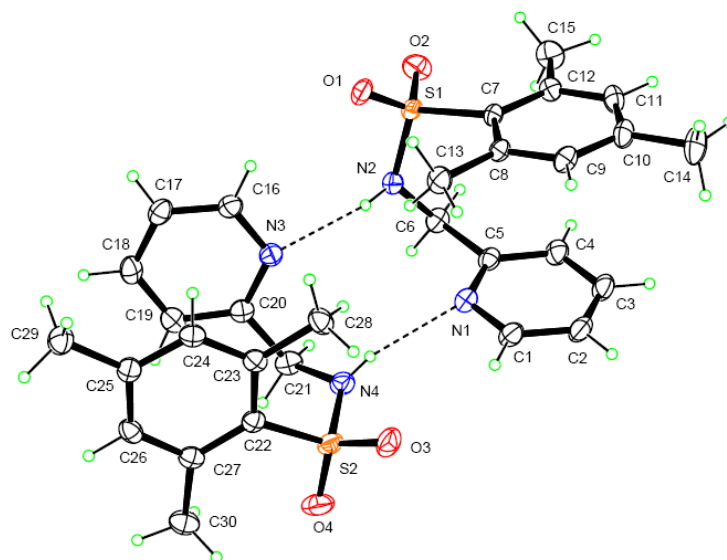


Figure D.2. Perspective drawing of 2-ampSO₂CH₃ (**2**). Hydrogen bonds observed in solid state are depicted. Thermal ellipsoids are drawn with 50% probability.

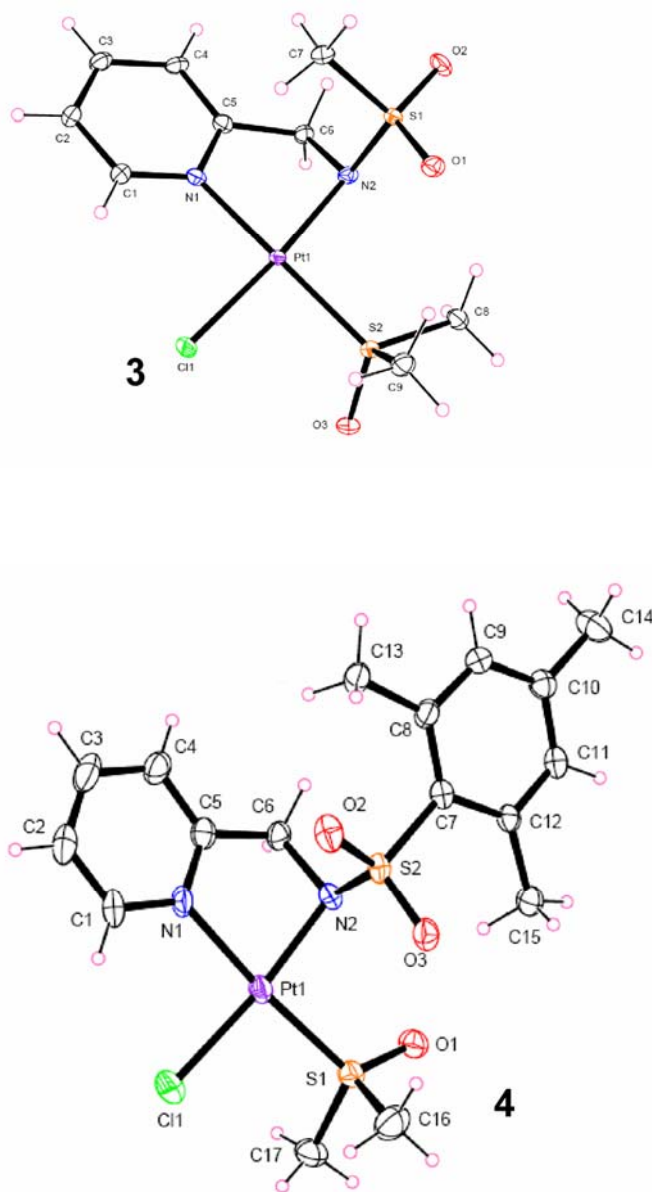


Figure D.3. Perspective drawings of $\text{Pt}(2\text{-ampSO}_2\text{CH}_3)(\text{Me}_2\text{SO})\text{Cl}$ (**3**) and $\text{Pt}(2\text{-ampSO}_2\text{tmb})(\text{Me}_2\text{SO})\text{Cl}$ (**4**). Thermal ellipsoids are drawn with 50% probability.

Table D.1. Crystal Data and Structural Refinement for 2-ampSO₂CH₃ (**1**), 2-ampSO₂tmb (**2**), Pt(2-ampSO₂CH₃)(Me₂SO)Cl (**3**), and Pt(2-ampSO₂tmb)(Me₂SO)Cl (**4**)

| | 1 | 2 | 3 | 4 |
|---|--|---|---|---|
| Chemical formula | C ₇ H ₁₀ N ₂ O ₂ S·HCl | C ₁₅ H ₁₈ N ₂ O ₂ S | C ₉ H ₁₅ ClN ₂ O ₃ PtS ₂ | C ₁₇ H ₂₃ ClN ₂ O ₃ PtS ₂ ·CH ₄ O |
| M_r | 222.69 | 290.37 | 493.89 | 630.08 |
| Cell setting | Monoclinic | Monoclinic | Monoclinic | Monoclinic |
| space group | $P2_1/c$ | $P2_1/c$ | $P2_1/c$ | $P2_1/n$ |
| Temperature (K) | 110 | 100 | 90 | 115 |
| a (Å) | 7.332 (2) | 13.6863 (15) | 14.7137 (17) | 9.2130 (10) |
| b (Å) | 14.067 (4) | 11.5328 (12) | 8.6927 (10) | 21.591 (3) |
| c (Å) | 9.474 (3) | 18.838 (2) | 10.5988 (15) | 11.1716 (15) |
| β (°) | 91.898 (11) | 104.933 (4) | 98.935 (7) | 100.777 (7) |
| V (Å ³) | 976.6 (5) | 2873.0 (5) | 1339.2 (3) | 2183.0 (5) |
| Z | 4 | 8 | 4 | 4 |
| D_x (Mg m ⁻³) | 1.515 | 1.343 | 2.450 | 1.917 |
| μ (mm ⁻¹) | 0.57 | 0.23 | 10.99 | 6.77 |
| No. of measured, independent and observed reflections | 18808, 2972, 2403 | 46928, 10432, 8039 | 30404, 5269, 4819 | 30100, 6696, 5494 |
| R_{int} | 0.028 | 0.025 | 0.021 | 0.033 |
| θ_{max} (°) | 30.5 | 32.6 | 33.7 | 30.8 |
| $R[F^2 > 2s(F^2)], wR(F^2), S$ | 0.036, 0.081, 1.06 | 0.043, 0.110, 1.02 | 0.026, 0.064, 1.09 | 0.058, 0.136, 1.24 |
| No. of relections | 2972 reflections | 10432 reflections | 5269 reflections | 6696 reflections |
| No. of parameters | 125 | 374 | 167 | 259 |
| $(\Delta/\sigma)_{\text{max}}$ | 0.001 | 0.001 | 0.003 | 0.002 |
| $\Delta\rho_{\text{max}}, \Delta\rho_{\text{min}}$ (e Å ⁻³) | 0.42, -0.43 | 0.43, -0.45 | 1.58, -2.49 | 3.91, -3.93 |
| Extinction coefficient | | 0.0007 (2) | 0.00150 (13) | |

Table D.2. Selected Bond and Atom Distances (Å) and Angles (deg) for Pt(2-ampSO₂CH₃)(Me₂SO)Cl (**3**) and Pt(2-ampSO₂tmb)(Me₂SO)Cl (**4**).

| | 3 | 4 |
|----------|----------------|-----------|
| | bond distances | |
| Pt–N1 | 2.045 (3) | 2.058 (7) |
| Pt–N2 | 2.029 (3) | 2.039 (7) |
| | bond angles | |
| N1–Pt–N2 | 80.85 (11) | 80.9 (3) |
| N1–Re–S | 172.86 (8) | 173.8 (2) |
| N1–Re–Cl | 94.68 (8) | 93.1 (2) |

D.3 Pt(II) Complexes of Ethylenediamine- and Diethylenetriamine-Sulfonamide Ligands

D.3.1 Synthesis of Pt(tmbSO₂-*N,N*-Me₂dien)Cl (**5**).

A methanol solution (20 mL) of *cis*-Pt(Me₂SO)₂Cl₂ (0.5 mmol, 211 mg) was treated with tmbSO₂-*N,N*-Me₂dien (0.5 mmol, 156 mg) in the presence of triethylamine (500 μL). The reaction mixture was allowed to stir at RT overnight. The yellow solid that precipitated was collected, washed with diethyl ether and dried in vacuo; yield, 132 mg (48 %). Crystals obtained from slow evaporation of the reaction filtrate were characterized by single-crystal X-ray crystallography. ¹H NMR (ppm) in DMSO-*d*₆: 6.88 (s, 2H), 6.61 (b, NH), 3.03 (m, 4H, CH₂), 2.84 (m, 4H, CH₂), 2.81 (s, 3H, CH₃), 2.73 (s, 3H, CH₃), 2.73 (s, 6H, CH₃), 2.19 (s, 3H, CH₃).

D.3.2 Synthesis of Pt(tmbSO₂-en)(Me₂SO)Cl (**6**).

A methanol solution (20 mL) of *cis*-Pt(Me₂SO)₂Cl₂ (0.25 mmol, 105 mg) was treated with tmbSO₂-en (0.25 mmol, 61 mg) in the presence of triethylamine (500 μL). The reaction mixture was allowed to stir at RT overnight. The yellow solid that precipitated was collected, washed with diethyl ether and dried in vacuo; yield, 57 mg (42 %). Crystals obtained upon

addition of acetonitrile to the reaction filtrate were characterized by single-crystal X-ray crystallography. ¹H NMR (ppm) in DMSO-*d*₆: 6.95 (s, 2H), 5.77 (s, 2H), 2.76 (b, 2H, CH₂), 2.72 (s, 6H, CH₃), 2.23 (s, 3H, CH₃), 2.01 (b, 2H, CH₂).

Table D.3. Crystal Data and Structural Refinement for Pt(tmbSO₂-*N,N*-Me₂dien)Cl (**5**) and Pt(tmbSO₂-en)(Me₂SO)Cl (**6**)

| | 5 | 6 |
|--|---|--|
| Chemical formula | C ₁₅ H ₂₆ ClN ₃ O ₂ PtS | C ₁₃ H ₂₃ ClN ₂ O ₃ PtS ₂ |
| <i>M_r</i> | 542.99 | 549.99 |
| Cell setting | Monoclinic | Monoclinic |
| space group | <i>P</i> 2 ₁ / <i>c</i> | <i>P</i> 2 ₁ / <i>c</i> |
| Temperature (K) | 90 | 90 |
| <i>a</i> (Å) | 15.075 (3) | 19.7581 (15) |
| <i>b</i> (Å) | 13.191 (3) | 7.5133 (5) |
| <i>c</i> (Å) | 9.6030 (15) | 11.8480 (10) |
| β (°) | 105.167 (13) | 91.003 (5) |
| <i>V</i> (Å ³) | 1843.1 (6) | 1758.5 (2) |
| <i>Z</i> | 4 | 4 |
| <i>D_x</i> (Mg m ⁻³) | 1.957 | 2.077 |
| μ (mm ⁻¹) | 7.88 | 8.38 |
| No. of measured, independent and observed reflections | 26111, 6660, 4340 | 54939, 11293, 9138 |
| <i>R</i> _{int} | 0.057 | 0.025 |
| θ _{max} (°) | 32.6 | 41.4 |
| <i>R</i> [<i>F</i> ² > 2σ(<i>F</i> ²)], <i>wR</i> (<i>F</i> ²), <i>S</i> | 0.044, 0.093, 1.03 | 0.030, 0.075, 1.06 |
| No. of reflections | 6660 reflections | 11293 reflections |
| No. of parameters | 212 | 205 |
| (Δ/σ) _{max} | 0.001 | 0.002 |
| Δρ _{max} , Δρ _{min} (e Å ⁻³) | 4.01, -2.09 | 2.41, -3.00 |
| Extinction coefficient | 0.00053 (11) | 0.00213 (13) |

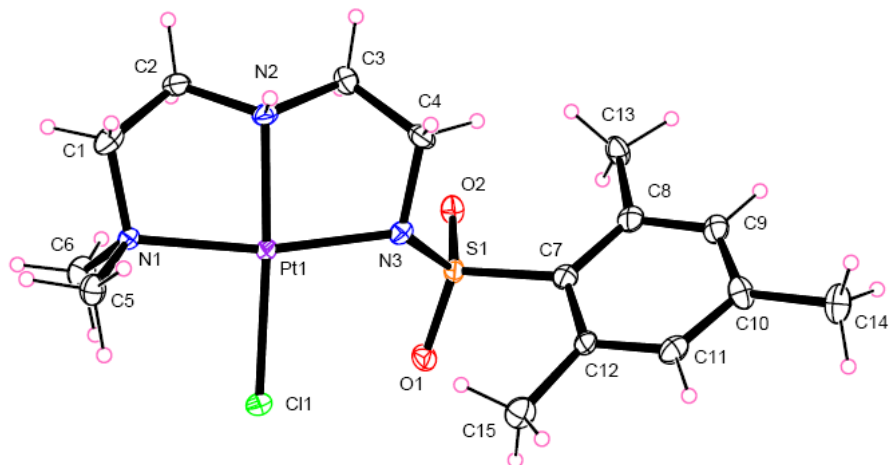


Figure D.4. Perspective drawings of Pt(tmbSO₂-*N,N*-Me₂dien)Cl (**5**). Thermal ellipsoids are drawn with 50% probability.

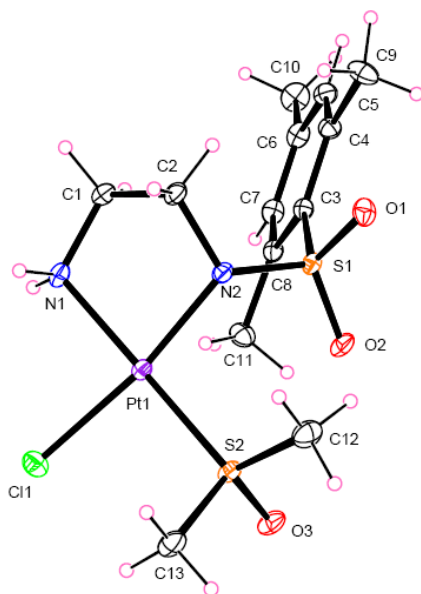


Figure D.5. Perspective drawings of Pt(tmbSO₂-en)(Me₂SO)Cl (**6**). Thermal ellipsoids are drawn with 50% probability.

D.4 References

1. Price, J. H.; Schramm, R. F.; Wayland, B. B.; Williams, A. *Inorg. Chem.* **1972**, *11*, 1280-1284.
2. Christoforou, A. M.; Fronczek, F. R.; Marzilli, P. A.; Marzilli, L. G. *Inorg. Chem.* **2007**, *in press*.
3. Otwinowski, Z.; Minor, W. *Macromolecular crystallography, part A*; New York Academic Press: New York, 1997; Vol. 276.
4. Sheldrick, G. M. In *Program for Crystal Structure Solution and Refinement*; University of Gottingen: Gottingen, Germany, 1997.

APPENDIX E. PERMISSION LETTERS



American Chemical Society

Publications Division
Copyright Office

1155 Sixteenth Street, NW
Washington, DC 20036
Phone: (1) 202-872-4368 or -4367
Fax: (1) 202-776-8112 E-mail: copyright@acs.org

VIA FAX: 225-578-3458 DATE: June 12, 2007

TO: Anna Maria Christoforou, Department of Chemistry, Louisiana State University
Rm. 232, Baton Rouge, LA 70803

FROM: C. Arleen Courtney, Copyright Associate *C. Arleen Courtney*

Thank you for your request for permission to include **your** paper(s) or portions of text from **your** paper(s) in your thesis. Permission is now automatically granted; please pay special attention to the implications paragraph below. The Copyright Subcommittee of the Joint Board/Council Committees on Publications approved the following:

Copyright permission for published and submitted material from theses and dissertations

ACS extends blanket permission to students to include in their theses and dissertations their own articles, or portions thereof, that have been published in ACS journals or submitted to ACS journals for publication, provided that the ACS copyright credit line is noted on the appropriate page(s).

Publishing implications of electronic publication of theses and dissertation material

Students and their mentors should be aware that posting of theses and dissertation material on the Web prior to submission of material from that thesis or dissertation to an ACS journal may affect publication in that journal. Whether Web posting is considered prior publication may be evaluated on a case-by-case basis by the journal's editor. If an ACS journal editor considers Web posting to be "prior publication", the paper will not be accepted for publication in that journal. If you intend to submit your unpublished paper to ACS for publication, check with the appropriate editor prior to posting your manuscript electronically.

* If your paper has not yet been published by ACS, we have no objection to your including the text or portions of the text in your thesis/dissertation in **print and microfilm formats**; please note, however, that electronic distribution or Web posting of the unpublished paper as part of your thesis in electronic formats might jeopardize publication of your paper by ACS. Please print the following credit line on the first page of your article: "Reproduced (or 'Reproduced in part') with permission from [JOURNAL NAME], in press (or 'submitted for publication'). Unpublished work copyright [CURRENT YEAR] American Chemical Society." Include appropriate information.

If your paper has already been published by ACS and you want to include the text or portions of the text in your thesis/dissertation in **print or microfilm formats**, please print the ACS copyright credit line on the first page of your article: "Reproduced (or 'Reproduced in part') with permission from [FULL REFERENCE CITATION.] Copyright [YEAR] American Chemical Society." Include appropriate information.

Submission to a Dissertation Distributor: If you plan to submit your thesis to UMI or to another dissertation distributor, you should not include the unpublished ACS paper in your thesis if the thesis will be disseminated electronically, until ACS has published your paper. After publication of the paper by ACS, you may release the entire thesis (**not the individual ACS article by itself**) for electronic dissemination through the distributor; ACS's copyright credit line should be printed on the first page of the ACS paper.

Use on an Intranet: The inclusion of your ACS unpublished or published manuscript is permitted in your thesis in print and microfilm formats. If ACS has published your paper you may include the manuscript in your thesis on an intranet that is not publicly available. Your ACS article cannot be posted electronically on a publicly available medium (i.e. one that is not password protected), such as but not limited to, electronic archives, Internet, library server, etc. The only material from your paper that can be posted on a public electronic medium is the article abstract, figures, and tables, and you may link to the article's DOI or post the article's author-directed URL link provided by ACS. This paragraph does not pertain to the dissertation distributor paragraph above.

06/07/06

Copyright Transfer Statement



The copyright to this article is transferred to Springer (respective to owner if other than Springer and for U.S. government employees: to the extent transferable) effective if and when the article is accepted for publication. The author warrants that his/her contribution is original and that he/she has full power to make this grant. The author signs for and accepts responsibility for releasing this material on behalf of any and all co-authors. The copyright transfer covers the exclusive right to reproduce and distribute the article, including reprints, translations, photographic reproductions, microform, electronic form (offline, online) or any other reproductions of similar nature.

An author may self-archive an author-created version of his/her article on his/her own website and his/her institution's repository, including his/her final version; however he/ she may not use the publisher's PDF version which is posted on www.springerlink.com. Furthermore, the author may only post his/her version provided acknowledgement is given to the original source of publication and a link is inserted to the published article on Springer's website. The link must be accompanied by the following text: "The original publication is available at www.springerlink.com".

Please use the appropriate DOI for the article (go to the Linking Options in the article, then to OpenURL and use the link with the DOI). Articles disseminated via www.springerlink.com are indexed, abstracted, and referenced by many abstracting and information services, bibliographic networks, subscription agencies, library networks, and consortia.

After submission of this agreement signed by the corresponding author, changes of authorship or in the order of the authors listed will not be accepted by Springer.

VITA

Anna Maria Christoforou was born in Nicosia, Cyprus, and is a graduate of the Ethnomartyra Kyprianou High School in Nicosia, Cyprus. She received her Bachelor of Sciences degree in chemistry. After working for one year in Medisell Co, she enrolled in the doctoral program of chemistry at Louisiana State University. She is a candidate for the Degree of Doctor of Philosophy during the Summer Commencement 2007.